DISCLAIMER:

This document does not meet the
current format guidelines of
the Graduate School at
The University of Texas at Austin.

It has been published for
informational use only.

The Dissertation Committee for Carly Frances Sakumura
certifies that this is the approved version of the following dissertation:

The Framework for Satellite Gravity Data Assimilation into Land Surface Models

Committee:

Srinivas Bettadpur, Supervisor

Clint Dawson

Wallace Fowler

Byron Tapley

Zong-Liang Yang

The Framework for Satellite Gravity Data Assimilation into Land Surface Models

by

Carly Frances Sakumura, B.S.E., M.S.E.

DISSERTATION

Presented to the Faculty of the Graduate School of
The University of Texas at Austin
in Partial Fulfillment
of the Requirements
for the Degree of

DOCTOR OF PHILOSOPHY

The University of Texas at Austin
May 2016

Acknowledgments

First and foremost I would like to thank my adviser, Srinivas Bettadpur, for his advice, support, and leadership over the past six years. His commitment to my growth in knowledge and as a researcher has been an amazing part of my graduate school experience. He was instrumental in creating the wonderful opportunities I've had and the professional skills and confidence I've developed while at UT and CSR and I am deeply appreciative. I am also grateful for the chance to work at and be a part of the Center for Space Research. I would like to thank the researchers and staff at CSR for their willingness and excitement to help and fully answer any questions from administrative matters to in-depth subject matter. I'd like to acknowledge and thank my entire dissertation committee for their direction and advice over the years to produce this work. In particular, Zong-Liang Yang, who welcomed me into his research group and expanded my research knowledge into land surface modeling and land/atmosphere dynamics from my aerospace background. I'd further like to acknowledge his entire LEAD group for accepting me into their fold, I greatly enjoyed learning from and working with them all.

My fellow graduate students were an incredible component of this process. Both personally - making my time in Austin more enjoyable and fun - and through collaboration on coursework, studying together for qualifying exams, and discussing our research. Especially to my research buddy, Christopher

McCullough, who was always ready to discuss any issues, help work through any problem, or just take a break and chat, thanks. Finally I'd like to thank my family for their support, putting up with me when I was stressed out, still trying to understand what I do, and always helping to put things in perspective. Looking back over the past six years, I've had an amazing experience throughout my PhD and am incredibly grateful for everyone who was a part of it.

The Framework for Satellite Gravity Data Assimilation into Land Surface Models

by

Carly Frances Sakumura, Ph.D.
The University of Texas at Austin, 2016
SUPERVISOR: Srinivas Bettadpur

The Gravity Recovery and Climate Experiment (GRACE) mission has provided an unprecedented global, homogeneous observational dataset of the time variation in terrestrial water storage (TWS) since 2002. This product has seen widespread use in the study of processes in hydrology, oceanography, the cryosphere, and is particularly critical to inform, improve, and validate computational models of the Earth system. Assimilation of the GRACE TWS fields into current land surface models can correct model deficiencies due to errors in the model structure, atmospheric forcing datasets, parameters, etc. However, the assimilation process is complicated by spatial and temporal resolution discrepancies between the model and observational datasets, characterization of the error in each, and requires tuning to the unique characteristics of satellite gravity data. This study establishes a framework for hydrological data assimilation of terrestrial water storage data from GRACE, closes the loop between GRACE product development and its scientific use, and analyzes the

assimilated results for use with current GRACE products and future satellite gravity missions. The framework fuses the strengths of the observational and land surface model datasets into an assimilated product representative of the signal strength and large scale structures of the GRACE dataset effectively downscaled to the high resolution land surface dynamics.

The data assimilation framework was developed through a comprehensive analysis of the deficiencies and potential improvements of the satellite data products, the assimilation procedures and error characterization, and the assimilation effectiveness over time. This analysis motivated the development of a higher frequency GRACE dataset more representative of the hydrometeorological signal content with reduced temporal aliasing of the TWS signal. Three innovations were implemented in the product development: regularization, sliding windows, and mascon basis functions, to develop a high-fidelity daily gravity field product (RSWM). The signal and error profile of the RSWM product was comprehensively analyzed via an end-to-end simulation analysis of the GRACE mission. The simulation analysis developed an error covariance representative of the magnitude, correlation, and spatial pattern of error in the RSWM dataset available for use in the data assimilation system. The assimilation algorithms and tools were advanced to optimally incorporate the GRACE TWS data and error covariance information.

Daily assimilation was performed globally at the one degree gridcell level, significantly reducing spatial and temporal smoothing of the assimilation update from previous basin-scale assimilation of the monthly mean GRACE datasets. Framework elements additionally defined the mechanisms of the as-

similation process: (i) the Gaspari-Cohn localization radius to spatially smooth the coarser resolution GRACE data, (ii) the necessary assimilation update rate to balance assimilation performance and computational efficiency, and (iii) open-loop error growth after assimilation has conditioned the system to advise data latency requirements. The GRACE data assimilation framework is versatile and adaptable to other land surface models, different formulations of data from the current GRACE mission, and future satellite gravity datasets.

Table of Contents

List of Tables

List of Figures

Chapter 1

Introduction

1.1 The Gravity Recovery and Climate Experiment

The Gravity Recovery and Climate Experiment (GRACE) is a joint scientific satellite mission between the National Aeronautics and Space Administration (NASA) and Deutsches Zentrum für Luft und Raumfahrt (DLR). Currently in its fifteenth year of operation, GRACE was launched in March 2002 with a nominal five-year mission plan to track and model the Earth's static and time-varying gravitational field on an unprecedented scale. The GRACE mission consists of two identical satellites flying in tandem in low Earth orbit approximately 220 km apart [79]. To ensure global coverage, the satellites are in a near-polar orbit with an inclination of 89.0 degrees and at an initial altitude of approximately 500 km that has been allowed to naturally decay over time. The two satellites experience orbit perturbations due to the non-uniformity of the gravitational field as well as non-gravitational accelerations. Because of their along-track separation, as the satellites approach a gravity disturbance the leading satellite will be affected first and then the trailing satellite causing a continuous change in the inter-satellite range. Accurate tracking of the inter-satellite range and the orbital evolution of the two satellites can then be used to determine variations in the Earth's gravitational

field.

In order to accurately capture this range variation and precisely determine the orbit of the two satellites, three key measurements are taken. First, the inter-satellite range is measured to the micron level using a K-Band microwave ranging (KBR) system [21]. Each satellite is also equipped with BlackJack Global Positioning System (GPS) receivers for absolute position determination and relative timing [21]. Finally, SuperSTAR high-precision accelerometers measure the non-gravitational accelerations imparted upon each satellite (ACC) [84]. The KBR, GPS, and ACC data are used in a least-squares analysis process to determine the best estimate of the gravitational potential of the Earth.

The process by which gravitational information is obtained from the GRACE measurements can be described as "Science by Omission", illustrated in Figure 1.1. The new scientific information from GRACE lies in the difference between the GRACE measurements and the current best measured and modeled state of the Earth's gravitational field. The process proceeds as follows: the satellite measurements described previously (KBR, GPS, and ACC) represent the flight data. The KBR and GPS information is used to precisely calculate the observed state of the satellites. A background gravity field is created using a high-fidelity static gravity model of the Earth in combination with well-understood and well-modeled time-varying components of the gravitational field. These time-varying signal models represent perturbations to the satellite's orbit due to solid earth tides, ocean tides, atmospheric and oceanic variability, N-body perturbations, and general relativistic perturbations [6].

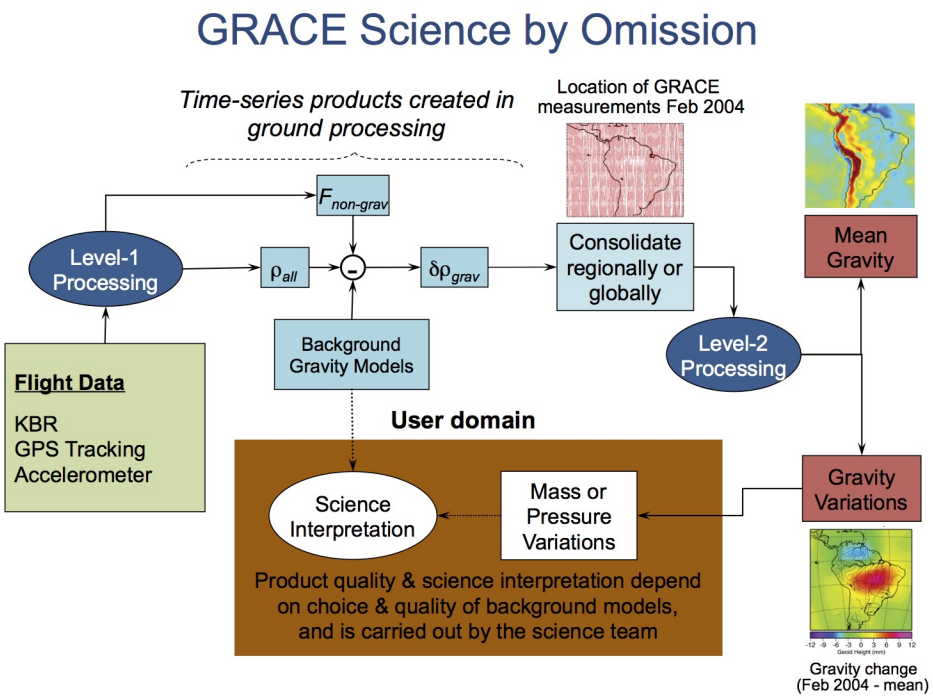

Figure 1.1: Extraction of time-variable gravity signals from the GRACE measurements

Using apriori initial conditions of the satellites, the background gravity model, and the measured non-gravitational accelerations from the ACC data, the expected orbital path of the satellite is calculated. The residual of the observed and calculated orbit, $\delta\rho_{grav}$, contains the contributions of the errors in the previously unmodeled, or "omitted", component of the gravitational field.

The new information represented in $\delta\rho_{grav}$ is then consolidated and used to calculate an update to that best modeled gravitational field. Two types of fields can then be calculated: short-term time-variations in the global

gravitational field (TVG) or a mean (static) gravity field. The variational field is calculated from a specific window of observational data. TVG fields can be produced at daily to monthly frequencies and capture gravitational variations on a variety of physically and socially informative timescales. These gravitational variations can be converted into a number of analysis fields: time-variations in equivalent water height, geoid, gravity anomalies, among others to aid in various scientific endeavors. From a long time series of measurements a high-resolution static gravity field can be determined that improves upon previous static gravity models by more than an order of magnitude [79].

The precise global models of the Earth's time-varying gravitational field available from GRACE yield a unique insight into the complex evolution of our planet. The gravitational field represents the mass distribution of the planet. It is constantly shifting as mass is redistributed within and above the surface of our planet due to variations in the solid earth, the exchange of mass between land, ocean, and atmosphere, tidal forces, etc. A time-series of TVG products will show long-term secular trends as well as seasonal and sub-seasonal variations in global mass transport. GRACE therefore offers the unprecedented ability to homogeneously and continuously track changes in surface water movement, groundwater storage, ocean heat storage, currents, polar ice accumulation and sea level rise across the entire planet [60]. Within oceanography, GRACE data has been used to validate models, study ocean circulation, tides, and currents [12], [13], [35]. In cryosphere studies GRACE data has been used to quantify the rate, location, and total mass lost from ice sheet melt [70], [4], [87]. The application of GRACE to hydrology will be

the focus of this study. The variation of water over land is one of the most evident signals in the GRACE data and this information offers new insight into seasonal and long term variations in terrestrial water storage [80].

1.2 Scientific Application and Data Assimilation of GRACE

The GRACE product over land represents the time-variation in terrestrial or total water storage (TWS), a vertically integrated measure of the water column encompassing groundwater, soil moisture, surface water, snow, and ice. TWS is a fundamental component of the Earth system, interacting with the climate energy and water balance on an array of scales and fronts [25]. Accurate knowledge of terrestrial water storage is thus very important for understanding and characterizing the Earth's climate system. However, prior to the GRACE mission little was known about global continental water storage as in-situ measurements are costly and difficult to maintain with limited spatial applicability and previous remote sensing missions were limited to surface or near-surface water storage [60].

Each component of the TWS measurement plays an integral part of the water cycle in various ways and at various scales in time and space. Soil moisture and snow represent key components of climate modeling on seasonal to annual time scales. They act as a boundary condition for land-atmosphere interaction, control the partitioning of land surface heat fluxes and thermal properties of the soil, and act as a driver for vegetation [19]. In contrast, groundwater storage is indicative of longer term mechanisms and, as such, has a longer memory in land surface processes. Anthropogenic effects are partic-

ularly impactful on groundwater resources as it is a crucial source of drinking water and irrigation for many regions of the world [24]. However, these effects are difficult to predict and characterize in models and groundwater is poorly monitored globally. Thus the direct global measurement from GRACE offers a wealth of information for monitoring and tracking all levels of the global hydrological cycle.

The GRACE information has many applications within hydrology - for drought and flood monitoring and prediction [46], [36], [10], for analysis of land use such as groundwater pumping for irrigation [83], as well as for model evaluation and improvement [93], [31]. GRACE has been featured prominently in the news for its use in the quantification of ice mass loss and the recent extreme droughts in Texas and California. While surface water storage and soil moisture stores can more easily recover from drought, GRACE's ability to measure groundwater change gives a more complete picture of the impact of these extreme events on a region. Improvements to the current GRACE product and improved accuracy from future missions will increase the range and application to which this knowledge can be applied.

Global hydrological models were previously the primary source of terrestrial water storage information. However, due to errors in the model physics, parameters, initial conditions, atmospheric forcing and other input data the models still fall short of accurate global characterization of the water cycle [31]. While relatively good agreement can be found between many hydrological models and the GRACE measurements, the GRACE dataset has much to offer for validation, calibration, and direct improvement of these models

through data assimilation. With enhanced models, we can improve drought and flood forecasting, weather prediction, aid in environmental planning, and provide tangible information to local water planners about the rate of groundwater depletion, drought, or floods in a region.

The GRACE assimilation problem, however, also contains many challenges and departures from typical data assimilation processes. The source of these challenges lies in the form of the GRACE measurement as well as the interaction of the data assimilation methods with the observational and model data. Most techniques for assimilation into geophysical models were originally developed for atmospheric systems with high-frequency, high-resolution datasets. In comparison, GRACE has a coarser resolution in time and space than land surface models as well as anisotropic and correlated error patterns. The operational GRACE product is a monthly mean field that has been smoothed and filtered to reduce error and thus has an effective resolution in equatorial regions of approximately 300 km in radius. The coarse spatial and temporal resolution of these GRACE fields in comparison to the model spatio-temporal resolution has required that the calculated model update be smoothed in space and time in the assimilation process.

These challenges have been evident in previous investigation with GRACE data assimilation. Zaitchik et. al. (2008) first assimilated basin-averaged GRACE TWS fields into the Catchment Land Surface Model (CLSM) for the Mississippi River Basin. This study had promising results for GRACE assimilation, showing improvements in correlation and decreased root mean square error between measured and simulated groundwater, improved simulation of

variability in hydrology, and improved correlation in runoff. GRACE measurements have since been assimilated into the National Drought Monitor [36] and snow-dominated basins [27], [74], among others. These studies have generally used an Ensemble Kalman Filter to assimilate basin scale, monthly mean TWS observations with a fixed error variance. All showed improved results through assimilation, however with a limited effect. Improvement and specialization of the GRACE fields to be closer to the model resolution in time and space, better defined for assimilation space, and assimilation algorithms and methods tuned to address these GRACE-specific issues will improve the effectiveness of such an analysis.

1.3 Motivation and Approach

This investigation will establish a framework for GRACE data assimilation, close the loop between the GRACE product development and its scientific use, and analyze these results for use with current operational products and for future geodetic remote sensing missions. Assimilation of GRACE data presents a unique set of challenges, primarily because the GRACE products are calculated from a global inversion of the observations rather than by taking a direct measurement of a component of the system. The fields thus have anisotropic and correlated errors, the spatial and temporal distribution of which is difficult to characterize as there is no true validation dataset for GRACE. Existing data assimilation techniques require tuning to account for the nature of these fields. In addition, the current GRACE products require smoothing in space and time in the assimilation process to account for the

relatively coarse temporal and spatial resolution of GRACE data. In order to address these problems and improve both the GRACE product for hydrological applications as well as the data assimilation methods for GRACE, this study proposes to:

1. Design a new GRACE product which increases the spatial and temporal signal content of the GRACE terrestrial water storage information via the use of sliding windows, regularization, and mascons in the estimation process.

2. Fully define the signal and error profile of the new product for data assimilation.

3. Specialize the data assimilation algorithms and parameters for use with GRACE.

These new GRACE fields, error characterization, and assimilation algorithms are the foundation of the GRACE assimilation framework. This framework will be tested by assimilating the newly developed GRACE TWS products into the Community Land Model (CLM) via the Data Assimilation Research Testbed (DART). Rigorous analysis of the product signal and error profile informs the assimilation algorithm development and determination of DA parameters. This assimilation framework is designed to apply to the new product, but also extend to future products from GRACE, the GRACE-FO mission, and future remote sensing missions.

Three key innovations are introduced to create an improved daily GRACE product: sliding windows, regularization, and mascons. Each component will be presented in detail in Chapter 2, however, all aim to increase the spatio-temporal resolution and accuracy of the GRACE fields. Sliding windows allow the GRACE fields to be produced on shorter time scales by optimizing the frequency characteristics of the observations and solution formation [7]. Regularization and representation in mascon basis functions uses our knowledge of the system to better inform the estimation process, reduce error in the GRACE fields, and improve the signal placement and amplitude retention [65] [68]. The regularized sliding window mascon (RSWM) fields do not require post-processing techniques that often further degrade the spatial resolution of GRACE and can dampen geophysical signals [45]. These new fields increase the range and power of signals obtained from GRACE and advance the product and methods for assimilation into land surface models.

Part of the challenge of data assimilation with GRACE is a misunderstanding of the product itself. In order to address this, the full signal and error profile of the new RSWM product is analyzed. Analysis of the signal profile shows the GRACE resolution in time and space and the scales and sizes of processes which are observable. A comprehensive simulation of the GRACE mission is performed to simulate the size, structure, and sources of error in the new product. The resulting error profile is constructed to better inform the data assimilation process and accurately reflect the spatial and temporal error patterns present in the data. The effect of the various error sources on gravity field retrieval is quantified, highlighting areas of improvement for future work

or satellite missions, and the areas in which the new product excels. The improved error profile is critical for data assimilation of GRACE as an accurate representation of both the LSM and observational error has been found to be critical for optimal results [53].

Data assimilation commonly employs the Ensemble Kalman Filter (EnKF), a statistical method for data assimilation. The EnKF does not explicitly model the adjoint and covariance of the LSM, but uses an ensemble of model states representative of the uncertainty in the model and input atmospheric forcing data to estimate a statistical covariance. This statistical covariance is used to measure the LSM error and map the observation update to the model state variables. This reduces the computational requirements and has been shown in many cases to outperform methods such as 4-D VAR which explicitly model these parameters [11]. This method, however, only takes the error variance of the observation into account in calculation of the optimal state update. Due to correlated errors persistent in GRACE fields from the gravitational field estimation it is important that the full covariance be considered in the data assimilation process. Therefore, a hybrid EnKF is developed that reads in many realizations of the GRACE error variance generated from the full covariance. Additional data assimilation techniques such as localization, sampling error, and inflation are used to ensure that correlations between adjacent observations are taken into account, statistical errors do not grow in the data, and the model spread does not collapse.

These innovations to the GRACE product and data assimilation process are all used to extract the maximum amount of useful information from the

GRACE mission. This study approaches GRACE data assimilation from both sides by combining our knowledge of estimation, orbital mechanics, geodesy, and mission design as well as the hydrological processes and needs of hydrologists and modelers to create new time-variable gravity fields from GRACE and construct the framework by which they can best inform land surface models. Accurate knowledge of terrestrial water storage is critical to understanding the Earth climate system and a full understanding of the motivations and needs of this community allow for a more informative and efficient product to be generated. Both the new GRACE fields and model-assimilated results will be validated and analyzed so that scientists and engineers generating and using time-variable gravity data from GRACE and future missions can continue to make incredible discoveries and improve our understanding of our planet.

1.4 Contributions

This study establishes a framework for optimal, efficient assimilation of time-variable gravity field products from the GRACE mission into land surface models. Accurate and effective assimilated results combine the best characteristics of each data source to create a more accurate picture of global mass transport that aids in environmental prediction, planning, and assessment. The GRACE product is quite unique and thus traditional data assimilation techniques must be analyzed and adapted for GRACE. In addition, the GRACE product must be formulated and analyzed to blend well with the specifications of the assimilation algorithm and land surface model. Three key contributions are developed in this work to establish, support, and advance the

GRACE assimilation framework: (1) the regularized sliding window mascon GRACE product development and analysis, (2) specification of the new product signal profile and the end-to-end error simulations creating an accurate and reliable GRACE covariance and error estimates, and (3) specification of assimilation algorithms and parameters for assimilation of the GRACE data into land surface models.

The regularized sliding window mascon product is the first daily GRACE-only time-variable gravitational dataset. This new dataset offers a wealth of high-frequency information along with reduced noise due to the innovations in estimation and processing techniques. Sub-monthly variability, flooding events, and many other short-term processes can now be identified and studied. Additionally, the new product offers great advances for assimilation of GRACE data into land surface models. The model can be updated daily and with lower-latency than traditional GRACE monthly mean fields and temporal smoothing of the update is not required.

The calculation of each update is improved with the enhanced GRACE error and covariance information along with GRACE-specific assimilation algorithms and parameter definition. Accurate knowledge of observational error is critical to the assimilation process and the covariance information further informs the data assimilation algorithms about the full nature of GRACE error. Tuning of the assimilation parameters to address the idiosyncrasies of the model and observational data is additionally critical in calculation of the model update. For example, ensemble inflation is used to counteract filter divergence, however, if done incorrectly can cause the model spread to collapse in

some areas while growing too high in others. Thus some regions will ignore the GRACE information entirely while others will allow unrealistically large updates that can upset the global water balance. The covariance-informed error clones, ensemble inflation, Gaspari-Cohn localization, and other assimilation parameters greatly impact the size and location of the DA process.

This framework will be analyzed and verified for its ability to continuously and effectively improve the assimilated LSM results, downscale the coarse resolution GRACE product to the higher spatio-temporal model resolution, and calibrate the model for forecast runs. The framework is designed to be flexible and extensible to different formulations of the current GRACE product as well as future geodetic observing products. Future lower latency products could be assimilated in near real time to improve short to medium range model forecasts, and longer time series of TWS products could be used in climate forecasting. Therefore, the rigorously tested datasets, parameters, and algorithms presented in this work will clarify, specialize, and advance data assimilation with GRACE, GRACE Follow-On, and future geodetic observational data.

1.5 Dissertation Organization

The process of forming the GRACE gravity field estimate will be discussed in Chapter 2. The new fields presented in this work implement several modifications to the traditional estimation and post-processing of the observational data. In order to fully understand this new product and what it represents, this chapter will go through the full process and theory of estimat-

ing the global gravity field from the satellite observations, what improvements the innovations add, and the representation of the gravity field. These new fields will be assessed and compared with independent datasets for validation.

Chapter 3 will explore characterization of the error in the solution. The sources of error in the GRACE data and end product will be discussed and the error characterized through an end to end simulation of the GRACE mission and error sources. An error covariance profile of the new product is established, and broken down so the component error sources and relative magnitudes can be quantified.

The new products were developed with the intent to improve the GRACE product for scientific use and data assimilation (DA). In order to assess the products a case study was performed assimilating the new fields into the Community Land Model 4.0 (CLM) . Chapter 4 will introduce land surface modeling and CLM as well as the data assimilation algorithms developed for the GRACE data. The new techniques in the assimilation algorithms, an analysis of the sensitivity and necessary tuning of these routines, and the data assimilation software used will be described in detail.

In Chapter 5 the assimilated results will be analyzed and validated. The effectiveness of the new products at informing the model to correct signal amplitude, seasonal phases, and the effectiveness of the model in downscaling the GRACE signal will be assessed. This will be done through comparison with in-situ data as well as with high-fidelity regional models. The use of data assimilation for model calibration and the effect to which data latency affects

the model will be analyzed as well.

Finally, conclusions and recommendations for future study will be presented in Chapter 6. Additional background information on the GRACE measurement and geophysical principles are included in the appendices.

Chapter 2

Increasing the Spatio-Temporal Resolution of the Gravity Field

2.1 The GRACE Science Data Product

Three centers were identified as components of the GRACE Science Data System (SDS): GeoForschungsZentrum (GFZ), the Jet Propulsion Laboratory (JPL) and the University of Texas Center for Space Research (CSR). While other research institutions also produce GRACE data products, these three centers have the primary responsibility for processing the GRACE observational data to produce the project validated estimates of the Earth's time-varying gravitational field. The data products are defined at 4 levels in the processing schematic. The Level 0 data products are collected by the GRACE Raw Data Center at DLR in Neustrelitz and are the result of the telemetry data reception, collection, and decommutation. This includes the KBR, GPS, ACC, star camera (SCA), satellite timing, and other housekeeping data. [9]. The Level 0 data is then processed and reformatted into Level 1A Data after application of the sensor calibration factors, checking time tags, and adding editing and quality control flags. Additional processing is applied to both the Level 1A and 0 data to form the Level 1B data made available to the scientific community [9]. The primary science data product from the

GRACE mission is the Level 2 Data: monthly mean estimates of spherical harmonic coefficients for the Earth's gravitational potential along with orbital data for the two GRACE spacecrafts. The monthly fields ensure sufficient global coverage and a stable time series of high-quality solutions. The current SDS solutions are the fifth release (RL05) and contain a low level of error and a long history of use in a wide range of scientific fields.

The typical GRACE product uses approximately thirty equally weighted days of data to estimate a monthly mean gravity field with 300+ km resolution. The coarse spatio-temporal resolution of this typical GRACE solution, however, has limited scientific analysis to primarily broad scale seasonal and longer term processes. Many hydrometeorological processes, particularly natural hazards such as floods, tropical cyclones, hurricanes, etc., will not be captured in this product. Information about the extent and duration of terrestrial water storage variations at these shorter temporal scales is critical for environmental planning and prediction. By implementing three innovations in the gravity field estimation methodology - sliding windows, regularization, and representation in mascon basis functions - this study has developed a new GRACE data product with improved temporal and spatial resolution to measure transient and high frequency hydrometeorological signals.

The new time series, a regularized sliding window mascon (RSWM) time-variable gravity field, is the first gravity time series at daily resolution using purely GRACE information. Implementation of a differentially weighted sliding window function reduces aliasing and increases the filter bandwidth to improve the temporal resolution. Regularization and representation in mascon

basis functions better condition the estimation process to reduce noise and improve signal retention. The daily RSWM product expands opportunities for scientific analysis, data assimilation, and practical use of observations from GRACE, GRACE Follow-On, and future satellite gravity missions.

This chapter will discuss the processing methods at CSR to estimate the Level 2 time-variable gravity field product and the formulation, effect, and implementation of the three innovations to the GRACE processing scheme to create the new product. The signal and frequency content of the RSWM product is then rigorously analyzed on a global and regional scale. Two focus regions with contrasting hydrological profiles, Texas and Bangladesh, are examined in detail to evaluate and validate the product. This assessment makes use of several datasets to rigorously intercompare and validate the new solution. These include the GRACE RSWM product defined in this chapter, the monthly operational GRACE products, data from the NOAH and CLM land surface models, as well as an in-situ total water volume storage dataset over the country of Bangladesh.

The GRACE, model, and in situ datasets are all represented in TWS, or equivalent water height (EWH), representing the vertical integration of near-surface water storage. TWS from GRACE is calculated from estimates of time variation in the Earth's gravitational field. It is assumed that the time variation is concentrated in a thin layer near the Earth's surface. Following the method of [*Wahr*, 1998], the change in surface density ($\Delta\sigma$) at a geographic location (θ, ϕ) is defined as the radial integral of the variation in density ($\Delta\rho$)

through the near surface layer as:

$$\Delta\sigma(\theta,\phi) = a_e\rho_w \sum_{l=0}^{\infty}\sum_{m=0}^{l} \bar{P}_{lm}(cos\theta)(\Delta\hat{C}_{lm}cos(m\phi) + \Delta\hat{S}_{lm}sin(m\phi)) \quad (2.1)$$

$\Delta\hat{C}_{lm}$ and $\Delta\hat{S}_{lm}$ are the Stokes coefficients representing the time-variation in the Earth's gravitational field, ρ_w is the density of water, l and m are the spherical harmonic degree and order respectively. The variation in surface mass over the gridcell is defined as the change in surface density divided by the density of water, $\frac{\Delta\sigma}{\rho_w}$, and is represented in TWS as the overall change in water height over the gridcell area. The GRACE TWS field is therefore representative of the sum total of the water column in a land surface model gridcell: soil moisture, snow, and groundwater or aquifer storage (where applicable). Unless otherwise specified all satellite and model data will be expressed in millimeters of equivalent water height over the defined gridcell or basin.

Data Product	Time Frame	Data Frequency	Gridcell Size	Units
RSWM	2002-2014	Daily	0.5 x 0.5 degree	mm
RL05	2002-2014	Monthly	1.0 x 1.0 degree	mm
NLDAS	2005-2008	Daily	0.125 x 0.125 degree	mm
CLM	2003-2010	Daily	0.9 x 1.25 degree	mm
Bangladesh	2004-2010	Weekly	0.25 x 0.25 degree	mm

Table 2.1: Terrestrial Water Storage Datasets

The CSR operational monthly mean fields are post-processed with the anisotropic DDK-2 filter [43] and will be referred to as RL05. The sum of soil moisture and snow water equivalent estimates over North America form the TWS field from the NOAH land surface model implementing the North American Land Data Assimilation System (NLDAS) atmospheric forcing data

[52]. Groundwater is notably absent from this dataset, as it is not explicitly modeled in by the NOAH land surface model. The Community Land Model (CLM) does contain an unconfined aquifer model and its TWS estimate is composed of the aquifer, soil moisture, and snow water equivalent fields. For this study, CLM is run in offline mode using a bias-corrected Community Atmosphere Model ensemble atmospheric forcing dataset [59]. The in-situ total water volume dataset of [*Steckler*, 2010] over the country of Bangladesh is derived from 304 stream gauges.

2.2 Estimation of the Regularized Sliding Window Mascon Product

The RSWM fields use the same estimation structure as the RL05 CSR monthly fields whereby a least squares procedure is implemented with Q-R factorization to solve for the time-variation in the global gravity field as described in [*Bettadpur*, 2012]. The Level 1B (L1B) input data products are those described in [*Case et. al.*, 2010], composed of the processed satellite measurements and other housekeeping data. Atmospheric and oceanic dealiasing is performed with the AOD1B product as described in [*Flechtner et. al.*, 2015]. The additional force models, reference systems, and measurement models are outlined in [*Bettadpur*, 2012]. This section will describe the general gravity field estimation process as well as the theoretical foundation and advancements from the use of sliding windows, regularization, and mascon representation to form the RSWM product.

2.2.1 The Estimation Process for GRACE RL05

The mathematical foundation for determination of the gravity field from the satellite measurement residuals is as follows. The satellite measurements and model residuals are accumulated over an *arc* of typically one day, defined by a new set of initial conditions. CSR's Multi-Satellite Orbit Determination program (MSODP) precisely computes the satellite trajectories and subsequently predict observations over each arc. The satellite K-band range-rate (KBR), double-differenced GPS, accelerometer (ACC) and star camera attitude measurements inform an "observed" satellite state estimate. The differences between the observations and their predicted values are accumulated into a residual vector, $\mathbf{y}$. A matrix, H, of the observation partials is determined by the CSR Multi-Satellite Orbit Determination Program (MSODP) [62] which linearly maps the observation deviations to the estimation state vector, $\mathbf{x}$ through the relation:

$$\mathbf{y}_i = H_i\mathbf{x} + \epsilon \tag{2.2}$$

Where the subscript i indicates the arc and $\mathbf{x}$ includes the satellite state, dynamical model parameters, geopotential parameters, and observation parameters. The noise in the system is represented by ϵ.

The state update is calculated from the observation residuals according to the methods presented in [*Tapley et. al.*, 2004a], designed to minimize the sum of the square of the error while retaining the maximum possible amount of signal. To accomplish this, the cost function, J, to be minimized is defined

as:

$$J = (\mathbf{y}_i - H_i\mathbf{x})^T W (\mathbf{y}_i - H_i\mathbf{x}) \tag{2.3}$$

Where W is a diagonal matrix of observation weights [*Rim*, 1992]. QR factorization is implemented by inserting an orthogonal matrix, Q, into the cost function as:

$$J = (\mathbf{y}_i - H_i\mathbf{x})^T W^{1/2} Q^T Q W^{1/2} (\mathbf{y}_i - H_i\mathbf{x}) = ||QW^{1/2}(\mathbf{y}_i - H_i\mathbf{x})||^2 \tag{2.4}$$

Q is chosen such that:

$$QW^{1/2}H = \begin{bmatrix} R_i \\ 0 \end{bmatrix} \tag{2.5}$$

$$QW^{1/2}\mathbf{y}_i = \begin{bmatrix} \mathbf{b}_i \\ \mathbf{e} \end{bmatrix} \tag{2.6}$$

Where R is an upper-triangular matrix of rank n, 0 is a null matrix, $\mathbf{b}$ is a column vector of length n, and $\mathbf{e}$ is column vector of length m-n. Substituting these into Equation 2.4:

$$J = || \begin{bmatrix} R_i \\ 0 \end{bmatrix} \mathbf{x} - \begin{bmatrix} \mathbf{b}_i \\ \mathbf{e} \end{bmatrix} ||^2 = ||R_i\mathbf{x} - \mathbf{b}_i||^2 + ||\mathbf{e}||^2 \tag{2.7}$$

$||\mathbf{e}||$ represents the vector of observation residuals - the misfit between the observations and least squares solution. It is the minimum value of the performance index as it is independent of $\mathbf{x}$. The condition for the optimal state update $\mathbf{x}$ that minimizes J is therefore:

$$R_i\hat{\mathbf{x}} = \mathbf{b}_i \tag{2.8}$$

The estimation problem as formulated thus far is very unstable as the observations contained in a single arc are insufficient to estimate a well conditioned

global gravity field. This instability is addressed by accumulating multiple arcs of data in the solution process to compute each estimate. We can illustrate the combination of multiple days of observational data into a single gravity field solution with the geometric normal equation estimation method [81]. The optimal state update $\hat{\mathbf{x}}$ is defined as:

$$\hat{\mathbf{x}} = N^{-1}M \tag{2.9}$$

This is a clear analog to Equation 8 with N = R_i and M = b_i. To form a solution $\hat{\mathbf{x}}$ using S arcs of data N and M will thus be formulated as:

$$N = \sum_{i=1}^{S} w_i R_i \quad M = \sum_{i=1}^{S} w_i b_i \tag{2.10}$$

The weight, w_i, applied to each arc defines the solution window and will be discussed further in Section 2.3. The full calculations for $\hat{\mathbf{x}}$ are computationally intensive and are performed using the Advanced Estimation Solver for Parallel Systems (AESoP) [32].

2.2.2 Mascons and Regularization of the GRACE Data

Unconstrained estimates of the global gravity field retain a relatively high level of error, primarily evident as north-south stripes due to imperfect background models, measurement noise, and the ill-posedness of the GRACE estimation problem [65]. It is necessary to post-process the unconstrained solutions to reduce these correlated error patterns by filtering or destriping and smoothing the gravity field. These processes tend to degrade the spatial resolution of the estimate and damp signal amplitudes. The GRACE gravity

estimation problem is ill-posed primarily because of downward continuation and ground coverage. The strength of a gravity field exhibits a wavelength-dependent decay as the distance from the source increases; therefore short-wavelength signals are more strongly attenuated at satellite altitudes. The ill-posedness will also amplify the noise that is particularly prevalent at shorter wavelengths. This inability of the observations to capture short-wavelength anomalies along with the ground coverage, or spatial placement of the satellite ground tracks, give rise to observability problems in the estimation process [65].

In order to address these issues in the new solutions, the techniques developed by [*Save et. al.* (2012), (2015)] are applied to regularize the estimation problem and represent the gravity field in mass concentrations. Save et. al. (2012) developed the methodology for GRACE gravity field estimation based on Tikhonov regularization using the L-curve method in combination with orthogonal transforms. The process will be briefly described here but a full description can be found in [*Save*, 2009] and [*Save et. al.*, 2012]. Tikhonov regularization improves the conditioning of the system by adding pseudo-information into the estimation process. This pseudo-information is informed by our knowledge of the problem and the nature of expected errors. Thus the cost function originally defined in Equation 2.4 is now modified as:

$$J = ||H\mathbf{x} - \mathbf{y}||^2 + \mu||M\mathbf{x}||^2 \tag{2.11}$$

Estimation of the gravitational field in mascon basis functions rather than spherical harmonics requires a linear transform to convert the spherical harmonic representation in $\mathbf{x}$ to a mass grid, $\mathbf{z}$ through the transformation

matrix, T:

$$\mathbf{x} = T\mathbf{z} \tag{2.12}$$

The CSR Mascon solution is computed on a geodesic grid composed of 40,692 equal area hexagons [68]. Each cell has an area of approximately 12,400 km^2 with an average distance of 120 km between cell centers. Inputting the above transformation into Equation 2.11 leads to the new cost function:

$$J = ||HT\mathbf{z} - \mathbf{y}||^2 + \mu||M\mathbf{z}||^2 = ||\bar{H}\mathbf{z} - \mathbf{y}||^2 + \mu||M\mathbf{z}||^2 \tag{2.13}$$

Where $\bar{H}$ = HT. Pseudo-information is added in the form of the regularization operator, M, and the regularization parameter μ (≥ 0). M was designed by Save et. al. (2015) to vary over the GRACE mission duration following an analysis of long term statistics of the regularized spherical harmonic solutions from GRACE [67]. Additionally, M is formulated to be diagonal, to prevent land-ocean correlation, and is independent of earth system models or other outside information. The regularization parameter, μ, determines the weight given to the pseudo-information, defining the level of constraint applied in the estimation process. The optimal μ for each solution is determined from computation of the L-curve via Lanczos bidiagonalization - an efficient way to visualize the value of μ that optimizes the balance of signal and error in each regularized solution. Minimizing the cost function J, in the same manner as previously described leads to the following estimate:

$$\hat{\mathbf{z}}_\mu = (\bar{H}^T\bar{H} + \mu M^T M)^{-1}\bar{H}^T\mathbf{b} \tag{2.14}$$

The resulting mascon fields are then resampled to a 0.5^o grid for analysis. This addition of pseudo information in the estimation process to improve the

conditioning of the system reduces noise and leakage and increases the spatio-temporal signal content of the GRACE data.

2.2.3 Improved Frequency Retention via a Sliding Window

The GRACE mission is limited in its ability to capture high frequency information by observability; a minimum of eight days of observational data is required to estimate a well-conditioned global solution [7]. As discussed in section 2.2, each individual gravity field solution is formed from a combination of arcs, shown in Equations 2.9 and 2.10, with a defined weighting scheme, or *window*. The operational GRACE products [*Bettadpur*, 2012] aggregate approximately 30 days of equally weighted arcs into a 30 day boxcar solution representative of the mean monthly total water storage. The 30 day boxcar window will, however, alias the day to day variability into the 30 day solution. To reduce these errors and improve the high frequency signal capture, in this section we introduce an improved window design and implement a sliding window method to increase the sampling rate of the gravity field. The use of sliding windows for estimation of GRACE gravity field solutions was investigated in depth by [*Bonin*, 2010], and that document serves as a basis for the sliding window theory used in this analysis.

Estimation of a single gravity field solution from multiple data arcs has a natural low pass filtering effect and will suppress high frequency information in the estimated time series. While this low pass filtering effect is beneficial in the reduction of high-frequency noise due to instrumentation and process error, signal is also attenuated or aliased into lower frequencies. The ideal fil-

ter will boost the gain in the low-frequency range (1-12 cycles per year) where the larger amplitude geophysical signals reside while lowering the gain at high frequencies that are more dominated by noise in the data and vulnerable to a lack of observability. As the window width decreases in the time domain the low frequency gain characteristics improve. However, if the window becomes too narrow it may not meet the observability requirements of the gravity solution. The sliding window must therefore be designed to meet this observability requirement while maximizing the signal frequency retention attainable from the GRACE data.

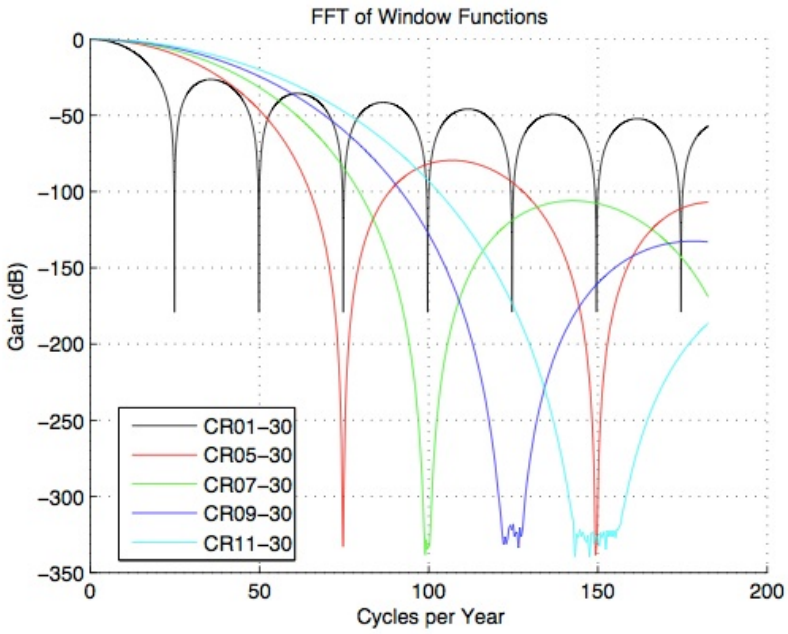

Figure 2.1: 30 day CRN windows with different numbers of self-convolutions in the frequency domain

McCullough (2013) analyzed a number of window functions (boxcar,

Gaussian, CRN, spline, flat-top, and Blackman) for their ability to preserve signals in frequency range of 4 to 12 cpy while simultaneously attenuating high, noise-dominated frequencies in the GRACE data. The CRN filter exhibited the best frequency domain characteristics and gain ripple reduction [82]. The CRN windowing function is derived from N self-convolutions of a rectangular time-domain window function. As the number of self-convolutions increases the window width narrows and reduces the effective size of the information content. The information content, or the number of effective days in each solution, is calculated as the integral of the window in the time domain. The sidelobes of the Fourier transform of the the window function decrease as well with increasing self-convolutions, as shown in Figure 2.1.

The preferred frequency characteristics of the window therefore improve with increasing number of convolutions: the gain remains close to one at lower frequencies and is significantly attenuated in the high frequency range. The number of convolutions selected for the CRN filter is a compromise between these observability and frequency retention characteristics. The selected window undergoes 9 self-convolutions of a 47-day rectangular window function. This window is then "chopped" so only the middle 21 weighted values are included, giving it an effective size of approximately 10 days of observational data and is referred to as CR09-47C21 [49]. Chopping the window has a minimal effect on its frequency retention ability (the weights assigned to the chopped days are very small) while reducing the GRACE observational data requirements and decreasing the latency at which solutions can be produced.

The CR09-47C21 window has an increased bandwidth, higher gain at

low frequencies, and requires fewer arcs of observational data than the 30 day boxcar window. The CR09-47C21 window cutoff frequency, defined as the frequency at which the filter gain drops below 0.5, is approximately 20 cpy, in comparison to 7 cpy for the 30 day boxcar window. The next section will explore the impact of this updated windowing function on the retrieval of higher frequency periodic geophysical signals and transient extreme events.

2.3 Effect of the Sliding Window on TWS Capture

The RSWM product was primarily designed to improve the temporal resolution of the GRACE product in order to observe transient events, sub-monthly variability, and higher frequency periodic signals. This section reports the impact of the CR9-47C21 and 30 day boxcar windows on retrieval of geophysical signals. Specifically, we measure the ability of the window to capture the frequency range, signal amplitude, and power of a terrestrial water storage time series. In addition, the time-correlation properties of the CRN window and RSWM product are quantified and compared to land surface model estimates.

2.3.1 TWS Signal Retention

To establish the effect of windowing a time series, the RSWM and RL05 windowing methods are applied to a CLM one degree global gridded dataset for 2006. In this synthetic experiment, the original CLM dataset is defined as a truth field, and the difference between the windowed and original day will be representative of signal damping, smoothing, or aliasing due to the

window. A CRN filtered CLM gridded time series (CRN/CLM) for 2006 is created by applying the CR9-47C21 window to each CLM gridcell for 2006 - along with the last ten days of 2005 and the first ten days of 2007. Thus the day labeled January 1, 2006 in the CRN filtered CLM time series is a weighted average of the CLM daily fields from December 22, 2005 to January 11, 2006. This process is continued through the year until December 31, 2006 of the new time series is composed of CLM data from December 21, 2006 through January 10, 2007. The same process is repeated with a 30 day boxcar window (Boxcar/CLM) for comparison to the current GRACE windowing strategy.

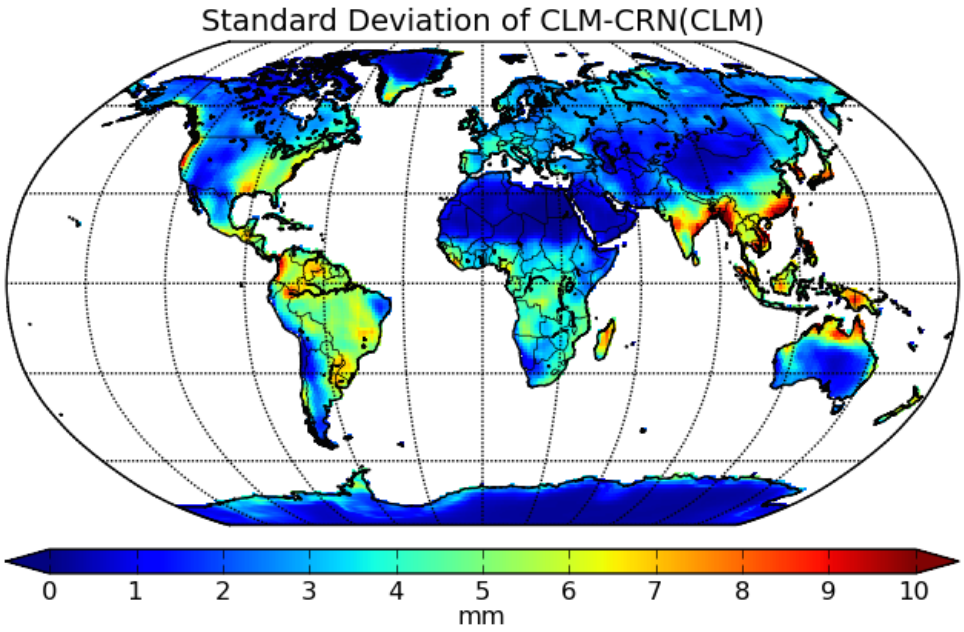

Figure 2.2: Global standard deviation between the CLM and CRN filtered CLM time gridded products

Figure 2.2 shows the global standard deviation of the difference between the original CLM series and the CRN/CLM gridded time series. The

	Mean Difference	Standard Deviation	Max Difference
Global	1.48 mm	2.94 mm	120 mm
Texas	-0.03 mm	3.21 mm	14.0 mm
Bangladesh	-.002 mm	9.2 mm	53.0 mm

Table 2.2: Effect of the CRN Filter on global and regional signals. Each region (Global, Texas, Bangladesh) is representative of the difference between the original CLM TWS time series and the CRN filtered CLM time series.

differences are less than 1 cm for all but very specific regional signals with a mean global difference over the year of 1.5 mm and mean standard deviation of 2.9 mm, (Table 2.2). Regions exhibiting greater signal variation with the CR9-47C21 window applied include the land areas surrounding the Gulf of Carpentia in Australia, Southeast Asia, Madagascar, and Western Amazon River Basin. It can be reasonably assumed that these larger variations are due to signal damping from the low-pass filter effect of the CR9-47C21 window.

The CLM, CRN/CLM, and Boxcar/CLM time series are analyzed in further detail for two regions, Texas and Bangladesh, which show the range of response to windowing. Texas exhibits a rather typical level of change due to application of the CR9-47C21 window with a mean standard deviation of 3.2 mm. Bangladesh, in contrast, shows a significantly higher effect from windowing; the difference between the CLM and CRN/CLM time series has a mean standard deviation of 9.2 mm.

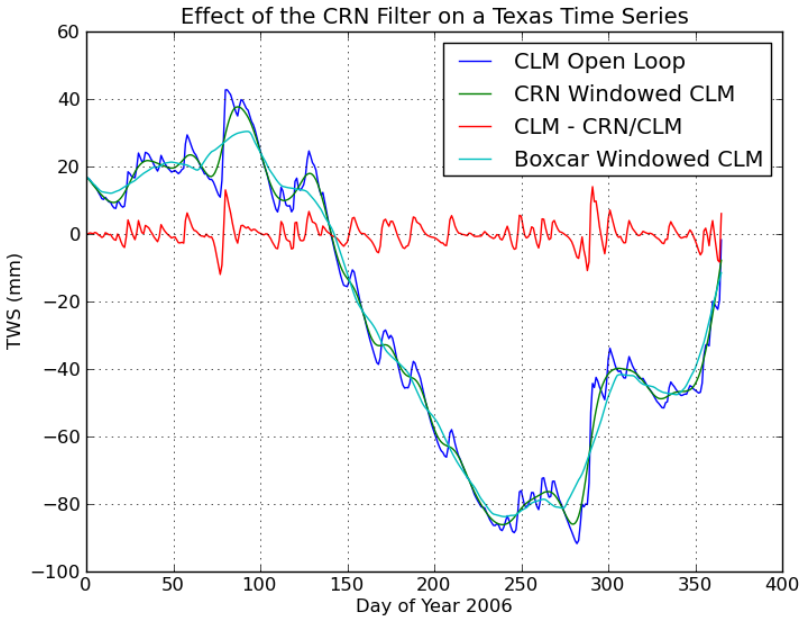

(a) 2006 Texas TWS

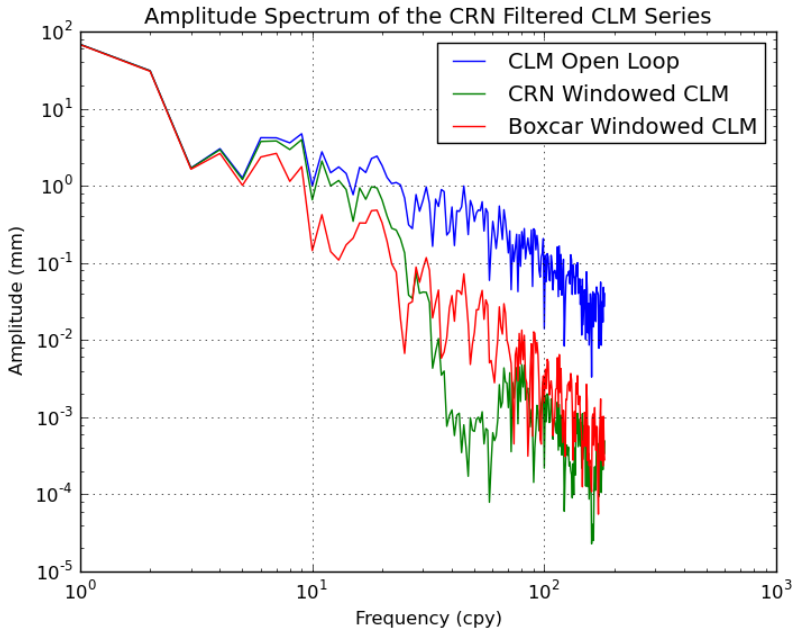

(b) Amplitude Spectrum

Figure 2.3: Signal and frequency profile of Texas 2006 terrestrial water storage

The comparison of the CLM, CRN/CLM, and Boxcar/CLM time series in Texas for 2006 (a) and the amplitude spectral density for each (b) in Figure 2.3 shows that the CRN window better captures the signal in the desired pass-band for geophysical signals, therefore better retrieving the signal amplitude and variation in time than the 30 day boxcar. The signal attenuation with the CRN filter is very small - the difference stays within one centimeter (-9.5 mm to 8.9 mm to be exact). This is within the error estimate for current products from the GRACE mission. The two show nearly identical power at low frequencies and the effect of the CR9-47C21 window becomes evident at frequencies above 20 cpy. In contrast, the 30 day boxcar window attenuates the signal at frequencies above 7 cpy, but exhibits less attenuation than the CRN window at higher, more noise-prone frequencies in the GRACE data. The CRN window is therefore fulfilling its design requirements - improved retention (increased signal gain) in the 4-12 cpy signal range and increased damping of noise dominated, very high frequency data.

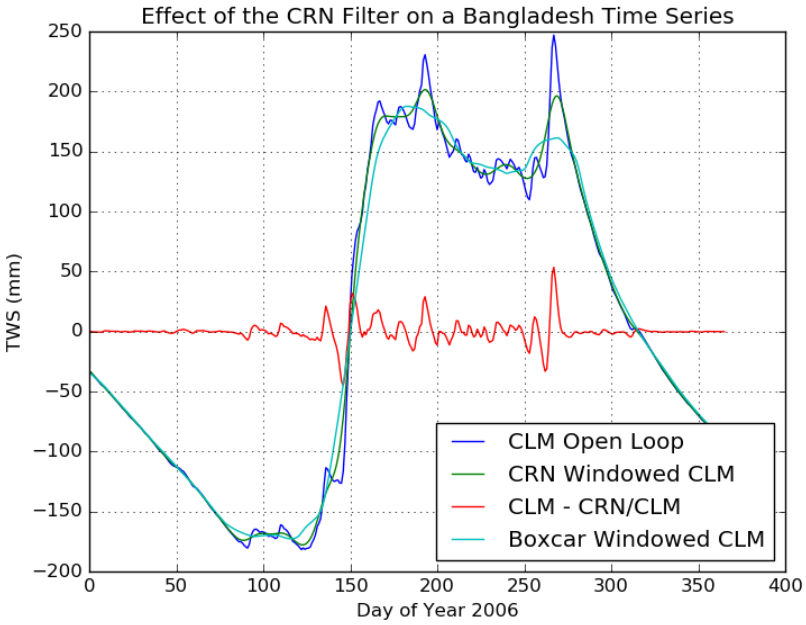

(a) 2006 Bangladesh TWS

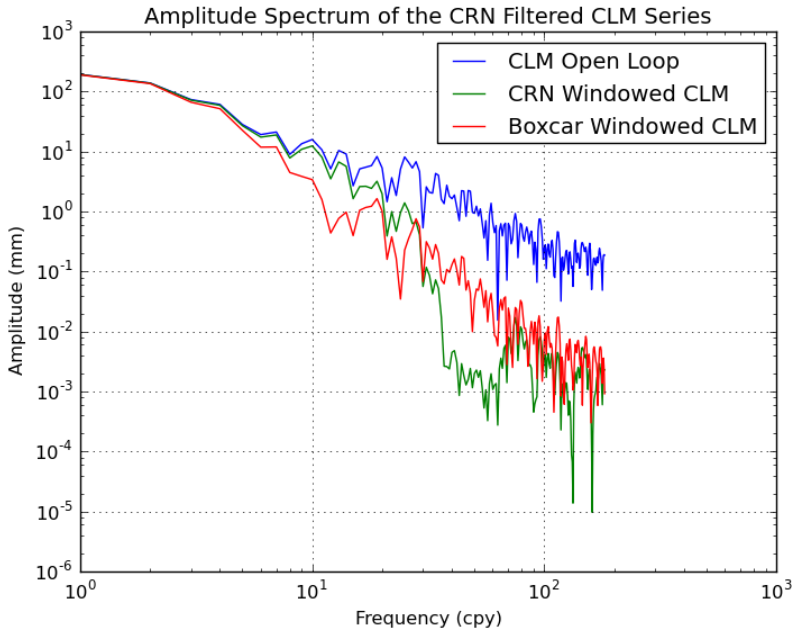

(b) Amplitude Spectrum

Figure 2.4: Signal and frequency profile of Bangladesh 2006 terrestrial water storage

The CRN filtered CLM time series in Bangladesh again better captures the signal content than the boxcar windowed CLM time series in the signal and frequency domains, as seen in Figure 2.4. Both window designs capture the seasonal signal, but the CRN/CLM time series also captures rapid fluctuations in TWS. The CRN/CLM time series in Bangladesh does show some significant (>2 cm) signal attenuation for very short period high-amplitude events. The amplitude spectrum in Figure 2.4 (b) shows the expected high-frequency damping from the windowing. Again, it acts primarily on low amplitude signals at frequencies greater than 20 cpy. Therefore, although there will be a slight amount of signal attenuation for high-amplitude, short period events, the size of signal lost is minimal - generally below the GRACE resolution - while the frequency retrieval is greatly improved in comparison to the monthly RL05 solutions.

2.3.2 Transient Event Capture

The operational RL05 product has a well-established ability to capture the seasonal cycle and processes operating over longer time scales, however, transient events are aliased into the monthly mean solutions. At best, bi-monthly variability is measured in the product and hydrological processes are not tied to calendar months. Due to an increased sampling frequency and improved filter design the RSWM product is able to capture sub-monthly variability and transient events with minimal signal smoothing.

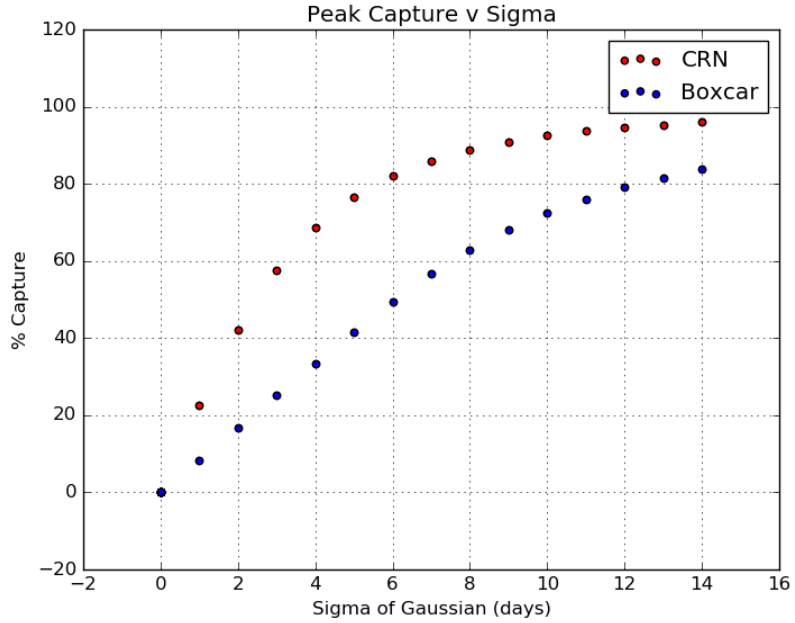

(a) Signal Amplitude Damping

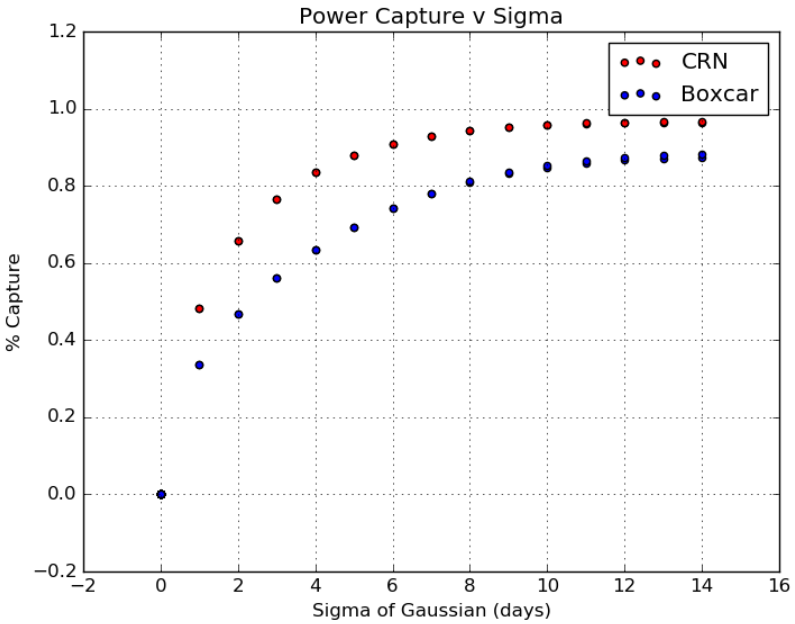

(b) Power Capture

Figure 2.5: Amount of signal damping and power capture from windowing a transient event with the CR9-47C21 and 30 day boxcar windows

The amount of signal amplitude damping and total power loss from the CR9-47C21 and 30 day boxcar windows is examined in Figure 2.5. Transient extreme events are modeled as a Gaussian function of varying width defined by the variance (σ). The CRN window shows significantly less signal damping and greater overall power retrieval in comparison to the 30 day boxcar. While the shape of particularly short term events is altered - they are generally temporally smoothed to a wider, lower amplitude shape - the CR9-47C21 window captures 50 percent of the power for events on the scale of 3 days and greater than 80 percent of the power at time scales of 9 days and longer. In comparison a daily 30-day boxcar filter would capture 10-20 % less power, show 15-30% greater signal damping. Signals at these time scales would be completely unobservable in the monthly RL05 products.

To illustrate this in practice, recall the comparison of the windowed CLM Bangladesh time series in Section 4.1. The largest difference between the CLM and CRN/CLM time series is examined more closely in Figure 2.6. The two peaks in the CLM series are smoothed into one peak in the CRN/CLM series with some signal attenuation, but the CRN time series captures 98% of the power of this event. Short term, high amplitude events must be carefully analyzed but can clearly now be captured with GRACE. This analysis will continue in Section 5 with comparison of the RSWM product to model time series and in situ data.

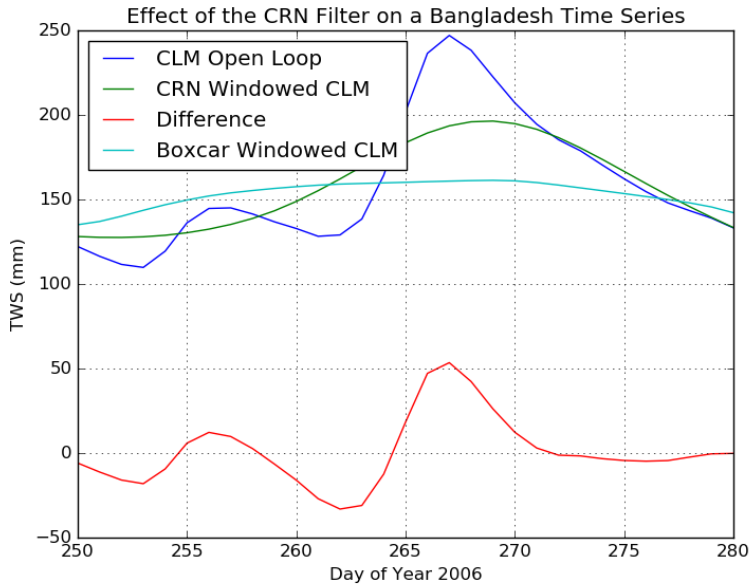

Figure 2.6: Close-up of TWS deviations in Bangladesh between the CLM and CRN/CLM time series

2.3.3 Time-Correlation of the RSWM Product

The daily sampling rate of the RSWM time series greatly increases the range and power of signal retrieval from the GRACE data. This section analyzes if this increased sampling rate causes unrealistic time-correlation in the RSWM product due to the overlapping data usage in adjacent daily solutions. For example, will a rainstorm two days from now be evident in today's solution and, if so, what is the time length and magnitude of the effect? Sections 4.1 and 4.2 addressed this issue to a certain extent. It was determined that a CR9-47C21 windowed time series will very rarely differ from a "truth" time series outside of the GRACE error bounds. The time-correlation effect of this processing scheme is now additionally analyzed via an autocorrelation com-

parison to a land surface model dataset. This analyzes whether the correlation in adjacent daily fields is similar to or above what is expected naturally from hydrological processes. For a discrete series x(t) with T time steps and a lag time of τ the autocorrelation can be calculated as:

$$R(\tau) = \frac{\frac{1}{T-\tau}\sum_{t=1}^{T-\tau} x(t)x(t+\tau)}{\frac{1}{T}\sum_{t=1}^{T} x(t)x(t)} \tag{2.15}$$

The autocorrelation, R, was calculated for the RSWM and NLDAS datasets at each grid point according to Equation 2.15, after the dominant periodic and secular signals have been removed. Removal of the annual, semi-annual and trends allows the analysis to focus on the sub-seasonal variability, the new high frequency information content from the RSWM product. NLDAS was chosen for this comparison because it has the best resolution in space and time of the modeled TWS datasets. The NLDAS forcing data assimilates a great amount of surface observations and other information to create a high fidelity regional dataset at 1/8 degree and a 6-hourly time step. For this analysis, the NLDAS fields have been averaged to daily means so the temporal resolution is consistent with that of the RSWM time series. The NLDAS time series is used to establish a baseline correlation length for hydrological processes by which the RSWM product characteristics can be tested.

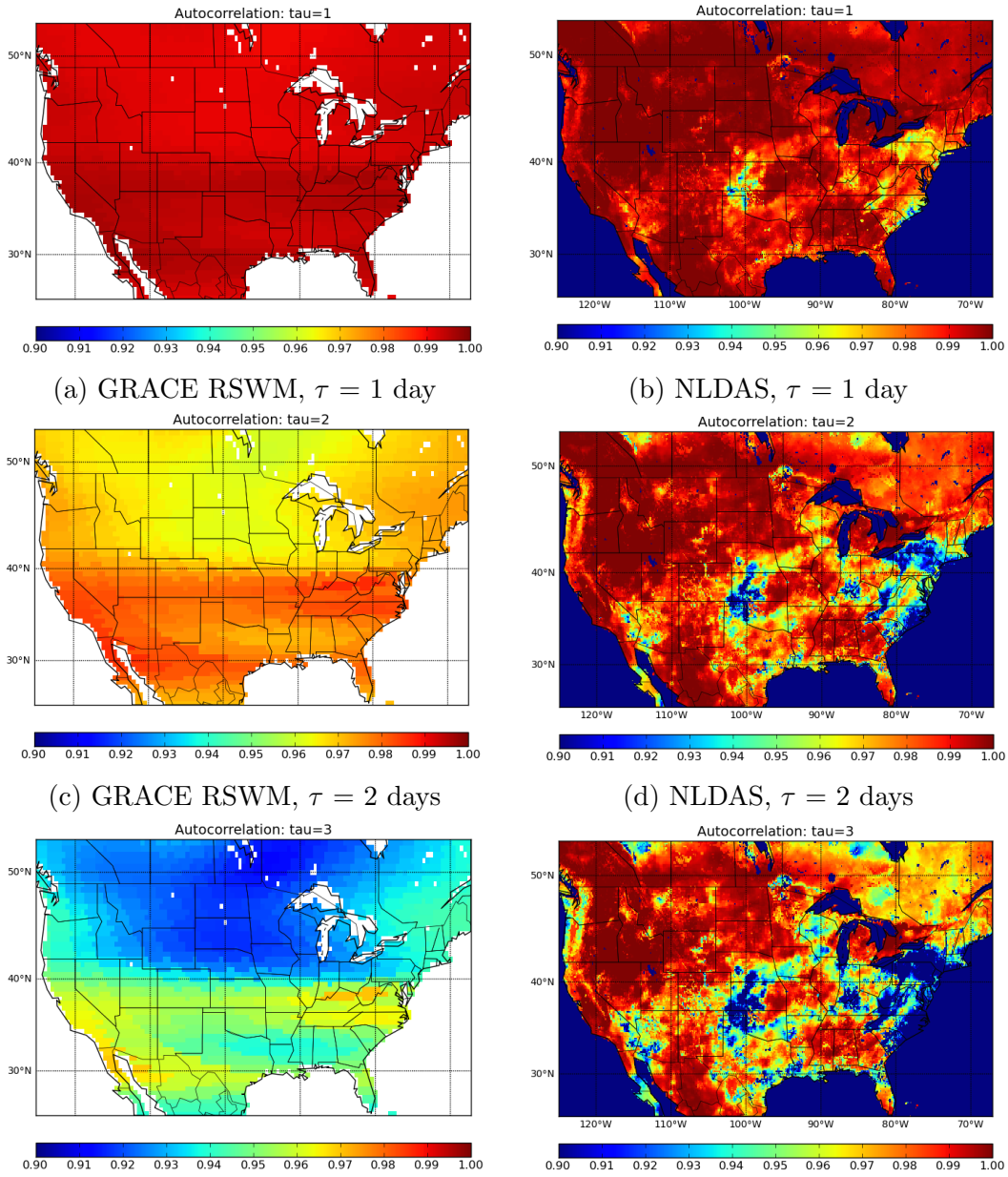

(a) GRACE RSWM, $\tau = 1$ day

(b) NLDAS, $\tau = 1$ day

(c) GRACE RSWM, $\tau = 2$ days

(d) NLDAS, $\tau = 2$ days

(e) GRACE RSWM, $\tau = 3$ days

(f) NLDAS, $\tau = 3$ days

Figure 2.7: Comparison of Autocorrelation between GRACE RSWM and NLDAS TWS Data

Figure 2.7 presents the autocorrelation over North America for the

RSWM and NLDAS datasets. With a time lag of one day as shown in (a) and (b) both fields exhibit very similar high levels of correlation. When $\tau = 2$ days the fields start to diverge as shown in (c) and (d). The higher resolution of the NLDAS dataset is clear and the autocorrelation drops over small regions in the Midwest and East Coast. In contrast, the RSWM time series shows a slight decrease in correlation (the color scale ranges only between 0.9 and 1.0) with broad regional variability - the middle latitudes show slightly higher correlation than the southeast and more northern latitudes. The depth of this pattern continues to increase as τ increases, as seen in (e) and (f) for τ=3, and beyond. The basis for the east-west correlation pattern in the RSWM product is not yet understood.

The mean autocorrelation over the NLDAS region is compared in Figure 2.8. For τ of one to three days the RSWM fields have a slightly higher time-correlation, however, for $\tau \geq 4$ the NLDAS fields have a higher time-correlation. Neighboring days are naturally expected to be highly correlated due to land-surface memory and the mean autocorrelation values are very similar between the two data sources. In addition, as TWS rarely exhibits variations above the GRACE resolution at these short time scales, the majority of the signal profile within the GRACE resolution will reflect a lower time correlation in the RSWM product than the best model estimates. It is impossible to determine if this discrepancy in temporal correlation is due to uncorrelated noise in the GRACE data or over-correlation in model physics. It is likely a combination of the two error sources. The RSWM field is therefore a reasonable approximation of a daily product, as daily sampling will allow cap-

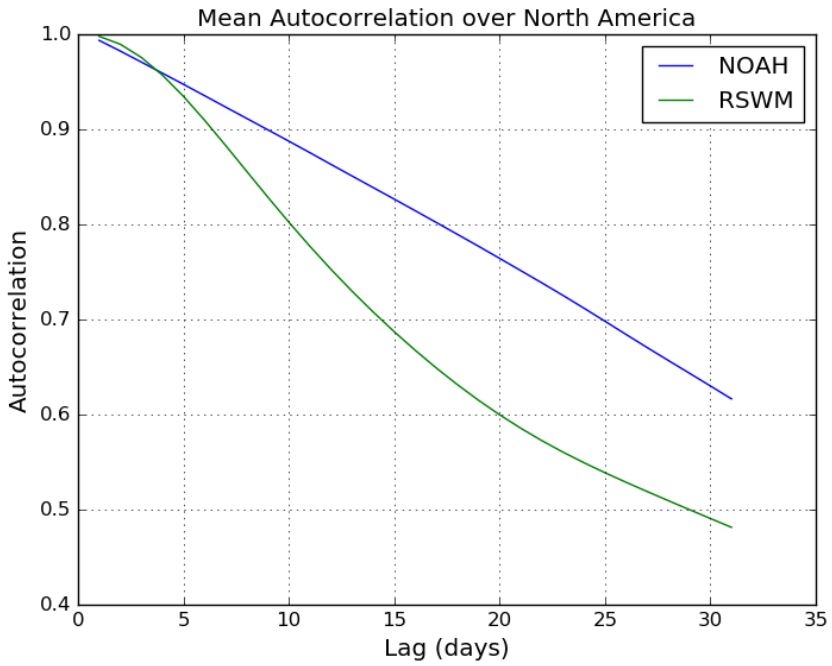

Figure 2.8: Mean Autocorrelation Values over NLDAS Domain for Time Lags of 1 to 31 Days

ture of greater signal power, shows similar levels of time-correlation to land surface model estimates, and captures most of the signal profile within the GRACE resolution.

2.4 Information Content of the RSWM Product

2.4.1 Spatial Resolution and Variance

The magnitude and spatial pattern of the hydrological signal is assessed with the spatial variance (SV) statistic, calculated as the standard deviation of the time series at each grid point. For all of the terrestrial water storage datasets, the spatial variance is calculated for each gridcell according to

Equation 2.16.

$$SV(\lambda,\phi) = \sqrt{\frac{1}{T}\left(\sum_{t=0}^{t_f} TWS(\lambda,\phi,t) - \overline{TWS}(\lambda,\phi)\right)^2} \tag{2.16}$$

Where T is the number of points in the time series, TWS is the 3-D matrix of a time series of geophysical grids of GRACE data, $\overline{TWS}$ is the mean of TWS in time, λ is longitude, and ϕ is latitude.

The spatial variance fields, particularly with the dominant periodic and trend signals removed, can be used as a preliminary estimate of the noise in the solution. The annual, semi-annual, and trend signals account for a great deal of the signal content and thus will be removed for certain analyses. Once these components are modeled and removed from a dataset, the resulting field will represent primarily residual signal (with frequencies greater than 2 cycles per year) as well as noise. In areas where little to no residual signal is expected the residual field is dominated by noise.

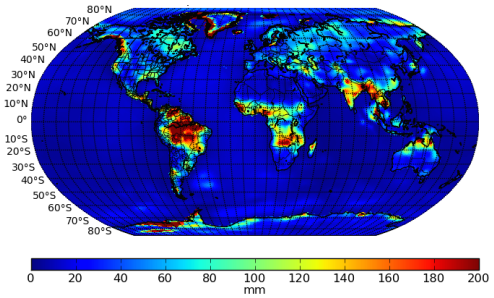

(a) Spatial Variance of the RSW GRACE Product

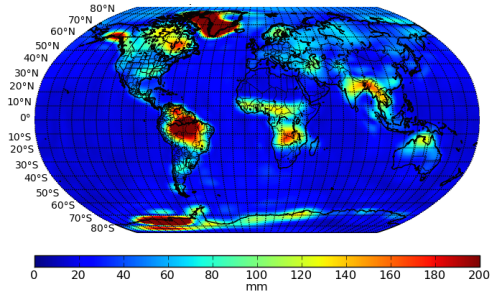

(b) Spatial Variance of the RL05 GRACE Product

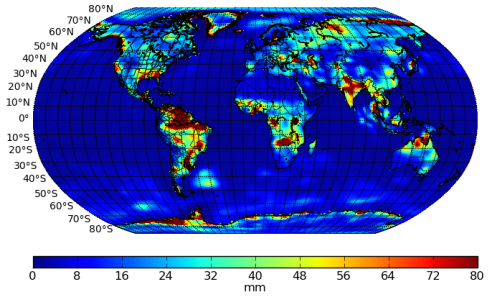

(c) Spatial Variance of the RSWM GRACE Product with Signal Removal

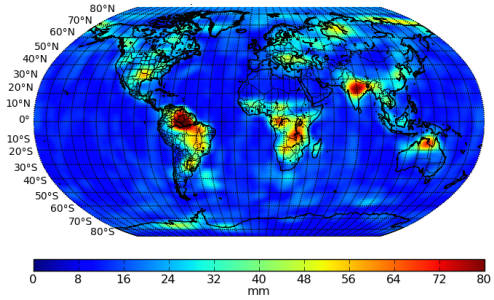

(d) Spatial Variance of the RL05 Grace Product with Signal Removal

Figure 2.9: Comparison of Spatial Variance between Sliding Window and Monthly RL05 Solutions

The spatial variance of the RSWM is first compared to the CSR RL05 series to assess any differences between two purely GRACE solutions, shown in Figure 2.9. Regions with large hydrological processes dominate the global map, particularly those with strong monsoon seasons such as the Amazon and Congo basins or with strong secular trends such as Antarctica and Greenland. The first map, Figure 2.9 (a) shows the spatial variance of the RSWM series and Figure 2.9 (b) shows the spatial variance of the CSR RL05 series. Overall, the size and geographic location of the TWS signal is quite similar between the two images. We generally observe that the signals are more clearly defined,

GRACE Field	Land Mean SV	Ocean Mean SV
RSW	63.5 mm	14.7 mm
CSR RL05	61.5 mm	23.5 mm
RSW w/ Signal Removal	27.8	7.05 mm
CSR RL05 w/ Signal Removal	20.9	14.0 mm

Table 2.3: Land and Ocean Mean Spatial Variance

particularly in polar regions, in the RSWM spatial variance map. The more clearly defined signal placement represents a reduction in leakage in comparison to the RL05 product due to the use of regularization and mascons.

As the regionally specific large signals in Figure 2.9 (a) and (b) tend to obscure smaller scale hydrological processes, the annual, semi-annual, and secular trend signals were fit and removed from each time-series in (c) and (d). While the RSWM in (c) and RL05 in (d) SV maps again show general similarity, greater differences can be seen. In regions such as the Orinoco Basin, central India, or the Gulf of Carpentaria where large off-annual variability is known to exist ([*Tiwari et. al.*, 2009], [*Tregoning et. al.* , 2008], [*Frappart et. al.*, 2015]) both maps capture the residual signal, however, the RL05 has a consistently lower magnitude and smoother appearance. The increased residual power in the RSWM series (particularly in these regions expected to have high levels of non-seasonal signal) highlights the increased capture of high frequency signals which the are aliased or smoothed in the RL05 product.

A clear indication that the increased SV of the RSWM series is not dominated by noise is the reduction of variance in deserts and ocean regions without strong currents, such as the Sahara and Gobi Deserts, the Australian

outback, and the central Pacific. These regions are not expected to have residual variation above the noise level of GRACE and as such, the SV in these regions is primarily noise. The mean SV over land and ocean for the maps in Figure 2.9 is quantified in Table 2.3. The SV of the RSWM over oceans is significantly less than the RL05 solutions. Because of the low mean variance expected over global oceans this is primarily due to the regularization reducing noise and systematic error in the solution. In contrast, the SV of the RSWM fields is greater than the RL05 over land both pre- and post-signal removal. This is again in part due to the use of regularized mascons for the RSWM series rather than the DDK-2 filtered RL05 solutions. However, this is also driven by the different frequency content of each time series.

The spatial variance of the RSWM is additionally compared to that of the NLDAS soil moisture and snow water equivalent, shown in Figure 2.10. There is a noted resolution discrepancy between the two fields; the NLDAS dataset is provided at 1/8 degree resolution and informed by topography, land surface type, and a high-resolution atmospheric forcing dataset [*Mitchell et. al.*, 2004] while GRACE is generally considered to have a spatial resolution of 300 km. Despite the spatio-temporal resolution discrepancy, the two fields exhibit a great amount of similarity. Figure 2.10 (a) and (b) show the spatial variance of the full signal. The larger annual signals along the western coast and south-east regions are especially evident, with similar levels of variation. The most obvious difference between the two is the large signal in British Columbia in the RSWM spatial variance map. Time series analysis show that the GRACE RSWM seasonal signal is consistently much stronger in this region

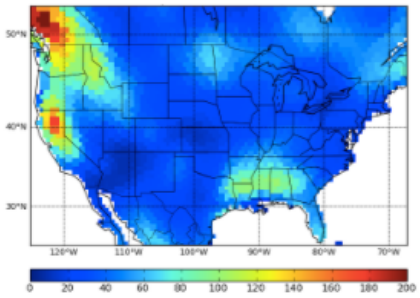

(a) Standard Deviation of the Sliding Window Mascon Fields

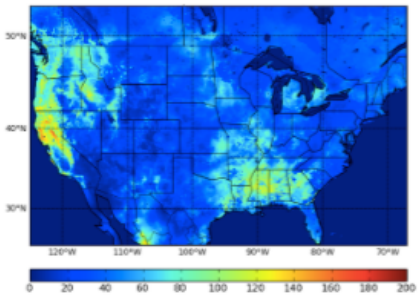

(b) Standard Deviation of the NOAH Soil Moisture Data

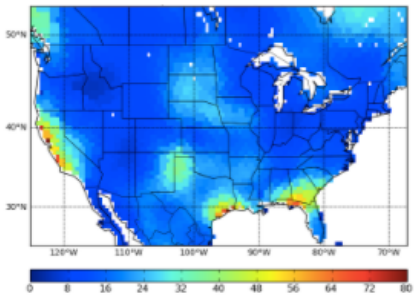

(c) Standard Deviation of the Sliding Window Mascon with Signal Removal

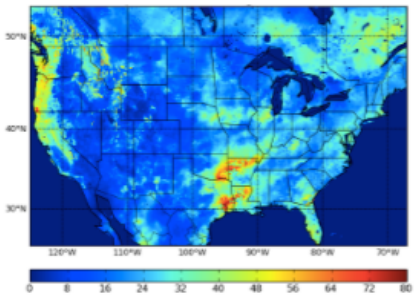

(d) Standard Deviation of the NOAH Soil Moisture Data with Signal Removal

Figure 2.10: Comparison of the spatial variance between RSW and NLDAS solutions

than NLDAS. Whether this difference is due to mismodeling in the NOAH model, error in the atmospheric forcing dataset, or leakage in the GRACE data bears further investigation. Comparison of the mean spatial variance over the NLDAS region in Table 2.4 shows that the RSWM series shows a slightly higher level of variance.

To isolate the higher frequency signal content, the trend, annual, and semi-annual signals were removed from each data source and the residual spa-

TWS Field	Mean Spatial Variance
RSW	44.7 mm
NLDAS	41.2 mm
RSW w/ Signal Removal	16.9 mm
NLDAS w/ Signal Removal	16.1 mm

Table 2.4: GRACE RSW and NLDAS Mean Spatial Variance

tial variance is plotted in Figure 2.10 (c) and (d). The two data sources are again similar, with residual signal along the Pacific and Gulf coastal regions. The RSWM fields visually exhibit a coarser spatial resolution in contrast to the NOAH data, however the mean spatial variance, in Table 2.4, is very similar evidencing that the two data sources contain a similar level of power at sub-seasonal frequencies. NLDAS has a higher level of variation (relative to GRACE RSWM) post signal removal, probably due to its higher (1/8 degree) spatial resolution as the higher resolution signals are attenuated the most in the GRACE processing and may not be observable by GRACE. Due to these structural differences and individual error characteristics of the two data sources they will naturally differ, however the overall agreement between the two confirms the accuracy and localization of the RSWM spatial signal content.

Precise definition of a spatial resolution for the RSWM product is complicated by the estimation process. Typically, the GRACE resolution can be defined by the smoothing radius applied to the unconstrained harmonic solution. The use of regularization and representation in mascon basis functions, however, removes the need for post-processing. A truncation to a maximum degree and order of 120 is inherent in the currently implemented estimation

process and imposes a maximum theoretical resolution of approximately 125 km. However, the constraint from regularization and signal attenuation at shorter wavelengths degrade this resolution.

To further inform this investigation the degree variance of the RSWM product is compared to global TWS estimates from the Global Land Data Assimilation (GLDAS) and WaterGAP Global Hydrological Model (WGHM). The RSWM fields exhibit more power at low degrees but at a certain point the higher resolution of the land surface models becomes dominant and these fields have a higher signal variance at this *degree crossover* and higher harmonic degrees. The degree crossover point of the RSWM fields and each hydrological model is noticeably higher than that of the filtered RL05 series. The degree crossover of the RSWM and WGHM fields is typically between 40 and 60, and between 65 and 90 for the RSWM and GLDAS fields (in comparison to typically at degrees less than 30 for RL05 and model estimates). Figure 2.11 shows two representative month comparisons. A gravity field with a maximum degree of 60 corresponds to an approximate spatial resolution of 300 km, with a maximum degree of 90 the resolution is approximately 166 km. The spatial resolution cannot be precisely determined but these statistics show that the resolution of the RSWM dataset can be reasonably bounded within 200 and 300 km.

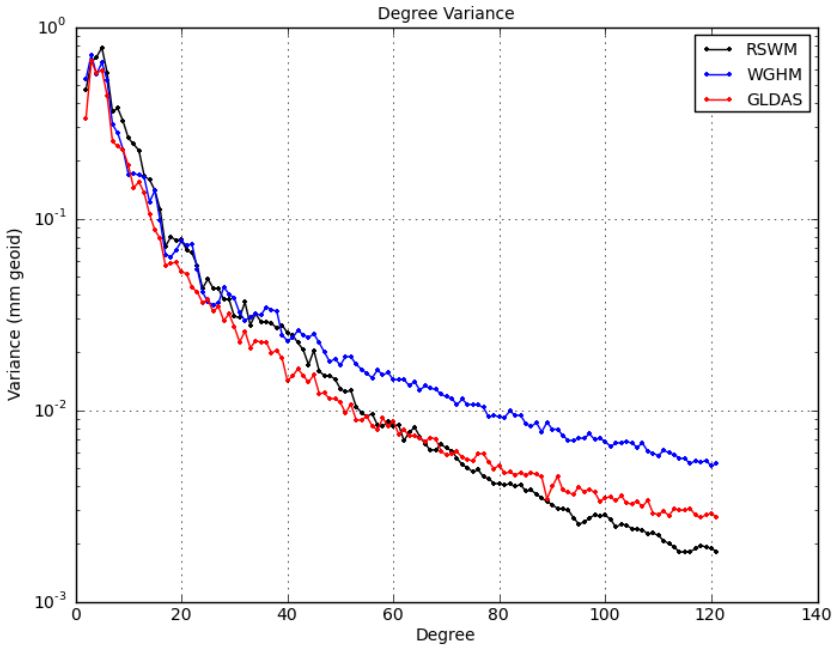

(a) 2008-03

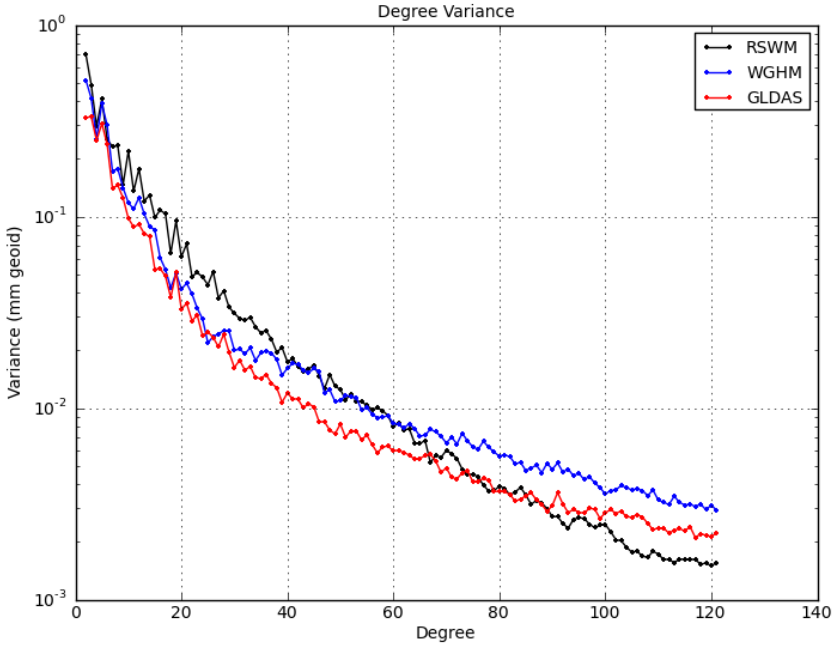

(b) 2008-07

Figure 2.11: Degree variance comparison of the RSWM product with output land surface models from GLDAS and WGHM. Oceans and ice sheet regions are masked out before comparison.

2.4.2 The Signal and Frequency Profile

A comparison of the total water storage of the state of Texas is shown in Figure 2.12 (a) for the RSWM, CSR RL05, CLM, and NLDAS datasets. The RSWM and two model time series show a very similar TWS evolution over time and, indeed, have a Pearson correlation of greater than 0.9. Even when there is an offset between the time series - as seen from July 2006 to January 2007 - the signal pattern is very similar. The amplitude spectrum of the time series reflects this in Figure 2.12 (b). The frequency range of the CSR RL05 time series is limited by the Nyquist frequency - half of the sampling rate of the time series - thus the RL05 can, at best, capture signals up to 6 cpy. The RSWM dataset is limited by the cutoff frequency of the CRN filter of 20 cpy, while the model datasets with daily resolution have a theoretical bandwidth at their Nyquist frequency of 182.625 cpy. The RSWM and model time series show very similar amplitude retrieval at frequencies up to between 20 and 30 cpy. The RSWM series is thus capturing similar amplitudes as the model data at all frequencies up to its cutoff frequency. As can be seen from Figure 2.12 (b), the amplitude of signals with frequencies higher than approximately 10 cycles per year is less than a millimeter and below the significance level of variation in GRACE or model data.

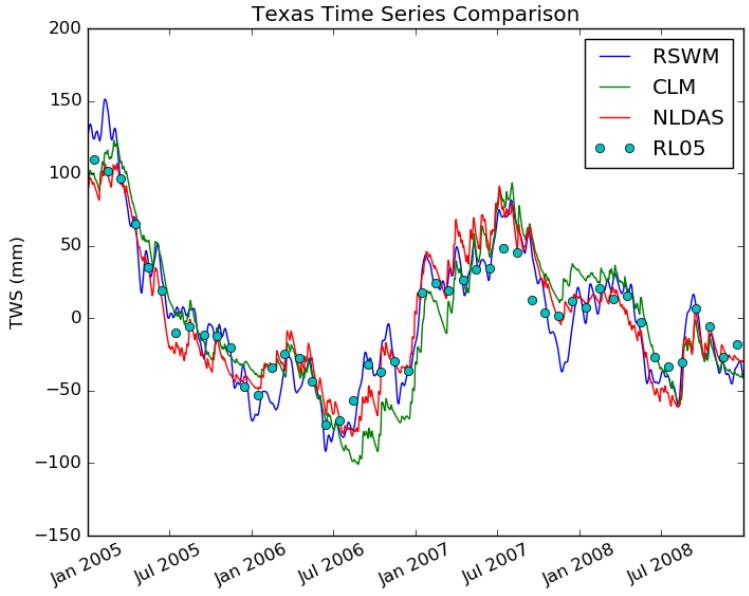

(a) Texas TWS 2005-2008

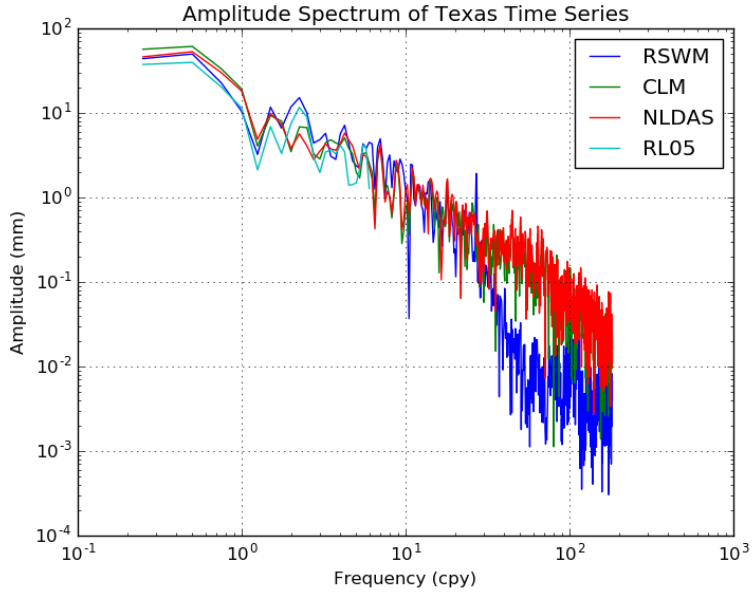

(b) Amplitude Spectrum

Figure 2.12: Signal and frequency profile of Texas terrestrial water storage

The coherence of the RSWM and each model time series is additionally computed to further examine the relationship between the frequency content of the datasets. The coherence between two signals x(t) and y(t) is defined as:

$$C_{xy}(f) = \frac{|G_{xy}(f)|^2}{G_{xx}(f)G_{yy}(f)} \tag{2.17}$$

Where G_{xy} is the cross-spectral density between x and y and G_{xx} and G_{yy} are the auto spectral density of x and y respectively. The significance of the coherence value can be calculated from Equation 2.18 derived from the F-distribution, number of observations, and bandwidth as described in [*Shumway*, 2000].

$$C(p) = \frac{F_{2,df-2}(p)}{df/2 - 1 + F_{2,df-d}(p)} \tag{2.18}$$

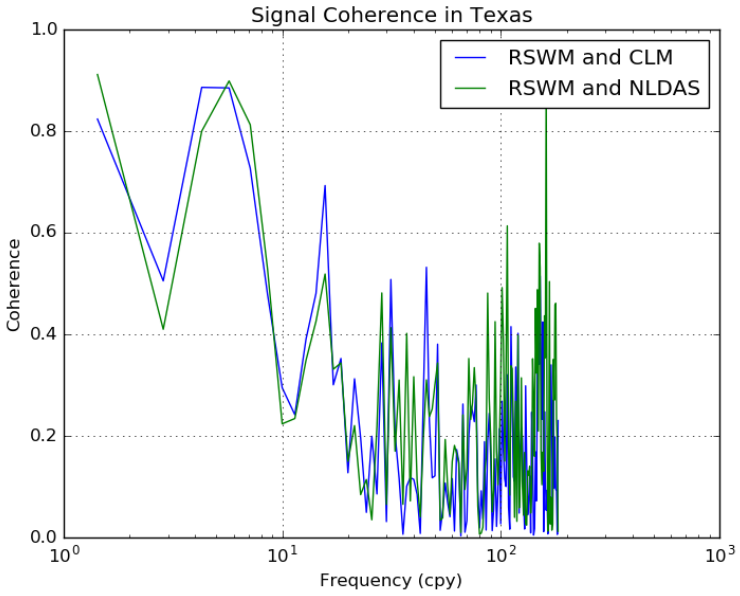

Figure 2.13: Coherence of GRACE RSW with CLM and NLDAS Texas Time Series

The coherence is calculated for the RSWM/CLM and RSWM/NLDAS pairs, shown in Figure 2.13. The significance level of the signal coherence is approximately 0.4. The RSWM and model data show a significant level of correlation until around 10 cycles per year, the same frequency to which the amplitude of the signal content remained above the error bounds of the GRACE data. At frequencies higher than 10 cpy the amplitude of the periodic signal content is sufficiently small to be indistinguishable from noise. As described previously, the CR9-47C21 window has a cutoff frequency of approximately 20 cpy, therefore in this region the temporal resolution of the GRACE product is limited not by the window design, but other error sources - instrument noise, sampling, geophysical model error, etc. - that limit the resolution of the GRACE data. The RSWM product is thus capturing all of the periodic signal within the resolution of GRACE.

The total water storage of Bangladesh is compared in Figure 2.14 (a) for the RSWM, RL05, CLM, and in-situ time series. While all series similarly capture the dominant seasonal signal, the CLM time series clearly damps the amplitude in comparison to the RSWM, RL05, and in situ series. The amplitude spectrum of the four time series in Figure 2.14 (b) shows clear peaks at 1 and 2 cycles per year - the annual and semi-annual seasonal cycles - and very good agreement to about twenty cycles per year. Careful examination of the peaks at 1 cpy shows that the in situ dataset has the most power at that frequency, followed by the RSWM, RL05, then CLM series. The RSWM dataset therefore - in Texas as well as Bangladesh - appears to better retrieve the signal amplitude in addition to accurately capturing the signal content at

higher frequencies than the RL05 solutions. At frequencies greater than 20 cpy the RSWM signal amplitude clearly drops below that of CLM. This is in part due to the sliding window acting as a low pass filter on the time series, however is also expected from Figure 2.14 (a) as CLM exhibits larger higher frequency variations than the GRACE (and in situ) data.

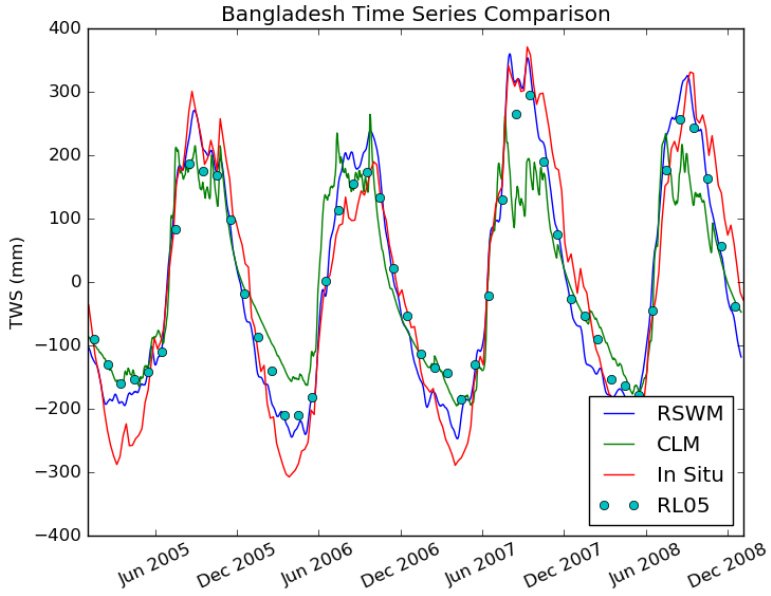

(a) Bangladesh TWS 2005-2008

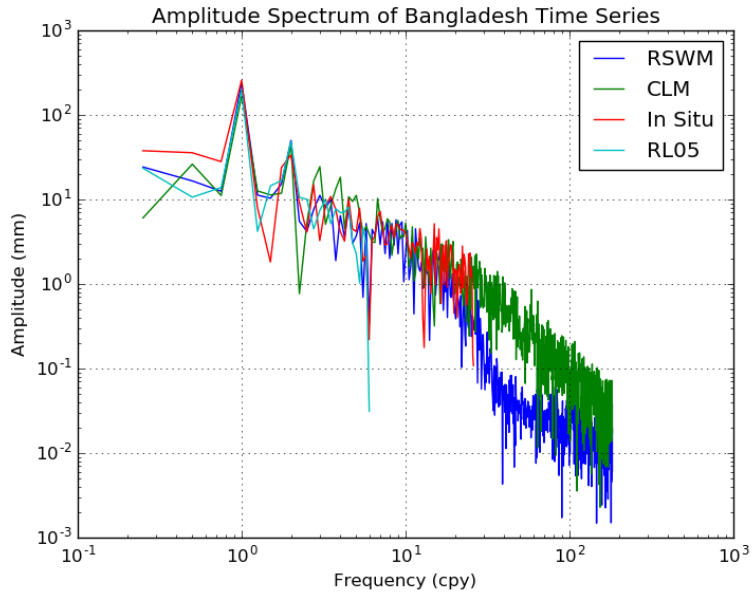

(b) Amplitude Spectrum

Figure 2.14: Signal and frequency profile of Bangladesh terrestrial water storage

Bangladesh experience extreme flooding in the summer of 2004. While this transient extreme event is outside the signal range of the RL05 GRACE data, it is observable in the RSWM product and the in situ time series (Figure 2.15). The onset, peak, and abatement of the the flood found in the RSWM signal aligns with the timeline described in official reports of the flooding event [20]. The 2004 flooding event in Bangladesh is representative of the greatest benefit of the RSWM product - with its increased sampling rate, improved window design, and estimation strategy flooding events such as these can be measured and studied for prediction and environmental studies for disaster planning.

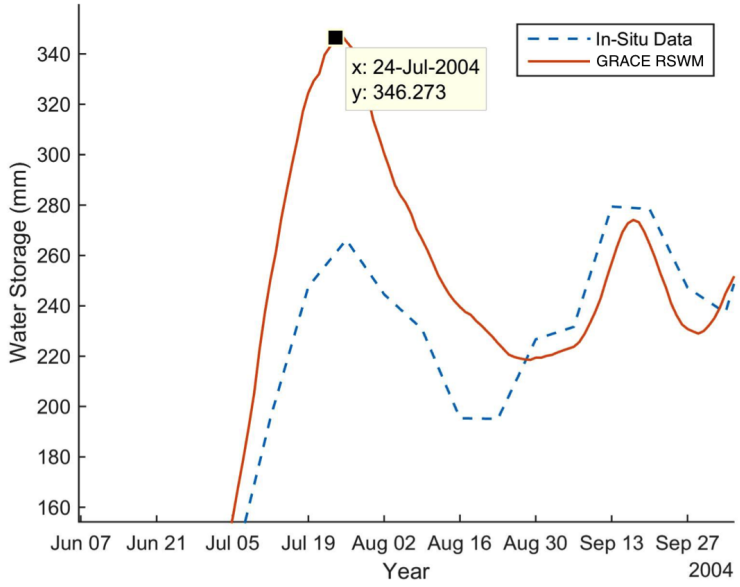

Figure 2.15: The 2004 flooding event in Bangladesh as captured by the GRACE RSWM and in situ datasets

It is clear from the frequency analysis of Texas and Bangladesh time series that the RSWM mascon product effectively captures high-frequency sig-

nal content within the resolution of GRACE. Periodic signals with significant amplitudes (greater than 2 cm) generally reside at frequencies up to 10 cycles per year. The GRACE RSWM time series shows a high level of similarity to hydrological model and in situ time series at these frequencies, and captures as much or more power as the comparison datasets in this range.

2.5 RSWM Product Discussion

Improvements to the current GRACE product and improved accuracy from future missions will increase the range and application to which this knowledge can be applied. This chapter has presented a method for improved high frequency signal capture and decreased aliasing via a regularized sliding window mascon product for the GRACE mission. The RSWM product is characterized by an improved filter design which reduces aliasing by decreasing gain ripple, increases the sampling rate, and greatly increases the effective bandwidth. Implementation of the regularization methods and representation in mascon basis functions according to *Save et. al.* (2015) better conditions the solution and therefore reduces noise and increases the spatial resolution of the product. The use of these techniques results in a product that is able to better capture the range and power of hydrological signals and eliminates the need for post-processing (filtering or smoothing) to reduce the correlated errors present in the unconstrained spherical harmonic solutions.

Analysis of the CR9-47C21 window found that it increased the filter bandwidth from 7 to 20 cycles per year and better captures the amplitude and total power of hydrological signals in comparison to the 30 day boxcar window

currently implemented in the monthly mean RL05 fields. The RSWM product shows very similar time-correlation levels over short time scales to high fidelity model data. Therefore for most regions of the world the majority of the TWS signal within the resolution of GRACE is present in the RSWM product. For certain regional areas or extreme events, the low-pass filtering effect of the window can attenuate the signal and analysis of these events and regions may require specialized processing and careful use.

The RSWM product is additionally characterized by an improved spatial resolution in comparison to the operational RL05 GRACE solutions. Comparison of the spatial variance and degree variance of the GRACE and model TWS estimates showed the RSWM to have greater signal power overall and particularly at higher spatial and temporal scales in comparison to both model and the CSR RL05 product. The regional comparison in Texas and Bangladesh found the RSWM and model datasets clearly captured periodic signals very similarly for frequencies up to 20 cpy. This represents a significant gain from the monthly mean products, as sub-seasonal and transient events can now be quantified in the GRACE time series. The RSWM product showed a very similar signal profile to the land surface model time series and best matched the in-situ Bangladesh validation dataset. The RSWM time series captured the same power as model and in situ data for geophysical signals up to 20 cpy. As nearly all of the hydrological signal power within the resolution of GRACE resides at frequencies below 10 cpy, the RSWM time series captures nearly all of the signal within the resolution of GRACE. Above 20 cpy, the CR9-47C21 window acts as a low pass filter and attenuates this noise dominated high

frequency band.

The new GRACE RSWM product is the first independent daily GRACE solution. Previous investigations with high-frequency GRACE products have typically relied on model data with a Kalman smoother in increase the temporal resolution [42] The daily time series greatly expands the range of signals that can be analyzed from GRACE. The product is particularly useful for data assimilation as less smoothing in time and space is required. The daily time step is much closer to land surface model time resolution thus reducing computational requirements and simplifying assimilation algorithms.

Chapter 3

Error Analysis of the RSWM GRACE Product

This chapter analyzes the full error profile of the GRACE regularized sliding window mascon product. In order to fully explore and define this field, a simulation analysis was designed to quantify the error size, structure, and sources in the GRACE observations and processing methods. Quantification of the error present in the GRACE product is complicated by the lack of validation datasets, the complexity of the estimation process, aliasing of signals, and the numerous interactions between potential error sources. The simulation analysis provides quantifiable error fields and a covariance for the new GRACE sliding window mascons that is particularly useful for assimilation into land surface models. With a reliable, comprehensive error characterization of GRACE the assimilation algorithms more optimally calculate the model state update.

First, the error sources in the GRACE mission and the effect these sources have on gravity field retrieval are identified and discussed. The simulation experimental design is then presented including the background models, noise models, and processing methods to simulate a truth and recovered gravitational field. The simulation is designed to analyze not only the total error

in the GRACE mission, but the contributions of each class of error source. By separating the total error into its primary contributors, the effect of future improvements in processing methods, models, or instrumentation improvements on the overall error budget can be analyzed and limiting error sources identified. The total estimated error for the RSWM GRACE product is calculated for use in assimilation as a spatially varying covariance field. The specific application of these fields and methods to data assimilation will be expanded in Chapter 4.

Note: The simulation study design, implementation, and analysis described in this chapter was a joint effort between the author (C. Sakumura), Christopher McCullough, Furun Wang, and Srinivas Bettadpur all at the Center for Space Research at The University of Texas at Austin.

3.1 An Overview of GRACE Errors

There are a number of different components that contribute to error in data products from the GRACE mission such as instrumentation noise, data processing and representation, and error in the geophysical models. The quality of each solution is affected by the ground track pattern, spatial coverage, downward continuation, etc. Spatial and temporal aliasing, while diminished with the formulation as regularized sliding window mascons, will still be present. The total error in the GRACE product - how much the recovered gravity field differs from the truth - can be generally classified as errors of omission and errors of commission. Errors of omission include high spatial and temporal resolution gravity field variability. These error sources are

not observed by the current GRACE mission as they are below the attainable spatial and temporal resolution. We estimate the magnitude and distribution of spatio-temporal omission errors in Section 3.3. Errors of commission include noise in the observations themselves and the effect of processing and modeling the observational data. Commission errors can be caused by incorrect parameter values, incorrect models, instrument noise, etc. The simulation study in this chapter was designed to comprehensively quantify the errors of commission.

GRACE commission errors have typically been subdivided into two categories: (i) errors in the GRACE observations and solution processes themselves and (ii) errors due to mismodeled or unmodeled gravitational variations incorrectly attributed to terrestrial water storage [90]. Category (i) errors include measurement errors, processing errors (i.e. estimation, filtering), and leakage errors; it is this type of error we are seeking to fully characterize. Category (ii) errors are introduced by the background models used to remove gravitational variations not caused by terrestrial water storage changes such as the atmospheric and oceanic dealiasing fields or solid earth and tide models. Category (ii) errors are continually reduced as atmospheric, oceanic, and tidal (solid earth, pole, luni-solar) models advance. The two categories are interconnected and both contribute to aliasing and leakage error characteristics of the GRACE data.

Category (i) errors can be further subdivided into observational error and representation error. Observational errors are those caused by error in the measurement of the intersatellite range rate, accelerometer error, etc. [45].

These instrument errors are an unavoidable component of satellite data analysis. Models for bias and drift in the instruments are implemented to reduce the effect upon the final gravity field in data processing. Instrumentation improvements will reduce some of this baseline error level in future missions. Representation errors are those caused by data processing methods and the expression of the gravity field solution - whether in the physical or spectral domain. Post-processing and regularization methods, while reducing the total amount of error in the gravity field, can attenuate or distort the signal and contribute to this error category.

3.2 Simulation Experiment Design for Error Characterization

In this section, we formulate a comprehensive simulation study to quantify the magnitude, distribution, and attribution of errors in the RSWM GRACE product. This end to end simulation of the mission implements improved GRACE error models, simulates error in the geophysical models, and follows the operational process for gravity field recovery from observations. Prior GRACE error studies have focused on calibration of the formal error estimates from the estimation process [47], analysis of the effect of leakage and signal attenuation [45], as well as a mix of the two methods [90]. However, the formal error estimates capture primarily the uncertainty in the estimation process and previous studies of the filtering effects have used hydrological model data rather than true GRACE data which could lead to under- or over-estimating the error due to model characteristics. The end to end simulation

therefore is more representative of the complete error profile in the GRACE gravity field products.

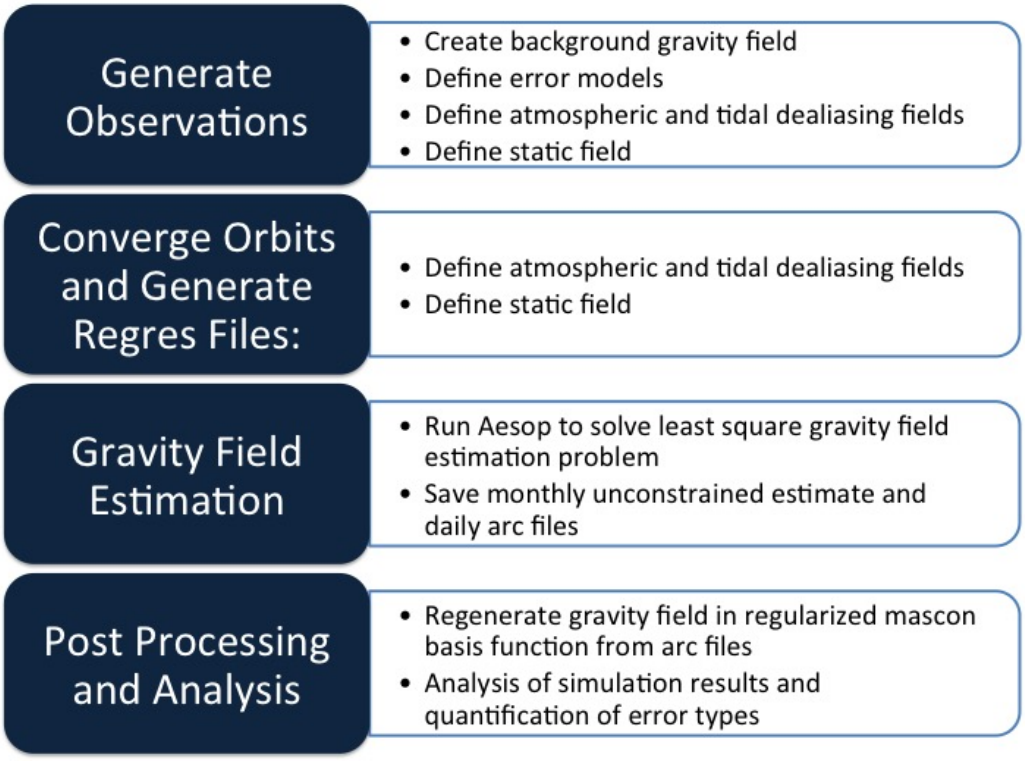

Figure 3.1: Diagram of the simulation of the GRACE mission observations and error characteristics

The basic setup of the simulation experiment is illustrated in Figure 3.1. The first simulation run - referred to as a Mode 5 run for the MSODP software simulation - uses a defined background gravity field to propagate the satellite orbits starting from the real GRACE satellite initial conditions to generate simulated observations. The background gravity field used to propagate the satellite orbit in this Mode 5 run is considered the "truth" field in the simulation space. The process of creating a truth background

field that best represents the size and resolution of real geophysical time-variable gravity is not trivial, and required blending of multiple datasets. The background time variable gravity field used in this work is referred to as XBL, and will be described in the next section. Noise in the GRACE observations due to instrument error is simulated with models for the GPS double difference, accelerometer, star camera, and K-band measurements [*Furun Wang, personal communication*].

After the Mode 5 run has generated the simulated satellite observations the second run, referred to as a Mode 4 run, calculates the "best fit" satellite orbit. This run generates what are referred to as regres files which contain the system parametrization and observations - the H and $\mathbf{y}$ from Equation 2.1. To simulate errors in the ocean tide models and atmospheric and oceanic dealiasing fields, different models for these fields were used to converge the orbits than those used to generate the observations in the Mode 5 run. A full description of the dealiasing and noise models is given in section 3.2.2.

The regres files generated from the Mode 4 run were then used to solve the least squares solution to estimate the gravity field using the Advanced Estimation Solver for Parallel Systems (AESoP). In this analysis we calculate 21 day sliding window mascons to estimate the error in the RSWM product, however the same process can be used to estimate error in the boxcar unconstrained harmonics, or other solution types. The simulated satellite observations undergo the exact same process as the actual satellite observations to form an estimate of the gravitational field. The difference between the gravitational field calculated from the simulated observations and the defined

truth field represents the error in the simulated solution.

3.2.1 Background Gravity Field Creation

In order to get realistic estimates of error in the GRACE products the truth field needs to represent the amplitude and frequency of variations in the terrestrial water cycle as accurately as possible. The truth field over land was therefore constructed by blending the best characteristics of GRACE and land surface model data into a designed field, hereafter referred to as XBL. The broad scale and long period (annual, semi-annual, and trend) signals are generally considered to be more accurate from GRACE while the GLDAS-1 model [63] was used to augment the spatial resolution and high-frequency temporal resolution of the XBL field.

Figure 3.2 illustrates the process to blend the two data sources (RSWM and GLDAS-1) to create the XBL fields. The two input datasets are both reformatted into quarter degree, daily grids. Therefore the half degree daily RSWM fields are interpolated to a 0.25 degree grid and the 4-hourly quarter degree GLDAS-1 are time-averaged into daily grids. Next, masks are applied to each dataset. A GLDAS-1 land mask is applied to the RSWM fields so that only the land surface signals are blended together. The ocean truth field is purely the RSWM mascon time series. A Greenland mask is applied to the GLDAS-1 fields so only RSWM signal is used in Greenland.

Each data source is then separated into "Signal Only" and "Signal Removed" grids. The Signal Only grids are composed of a modeled bias, slope, quadratic, annual, and semi-annual signal from each input data source.

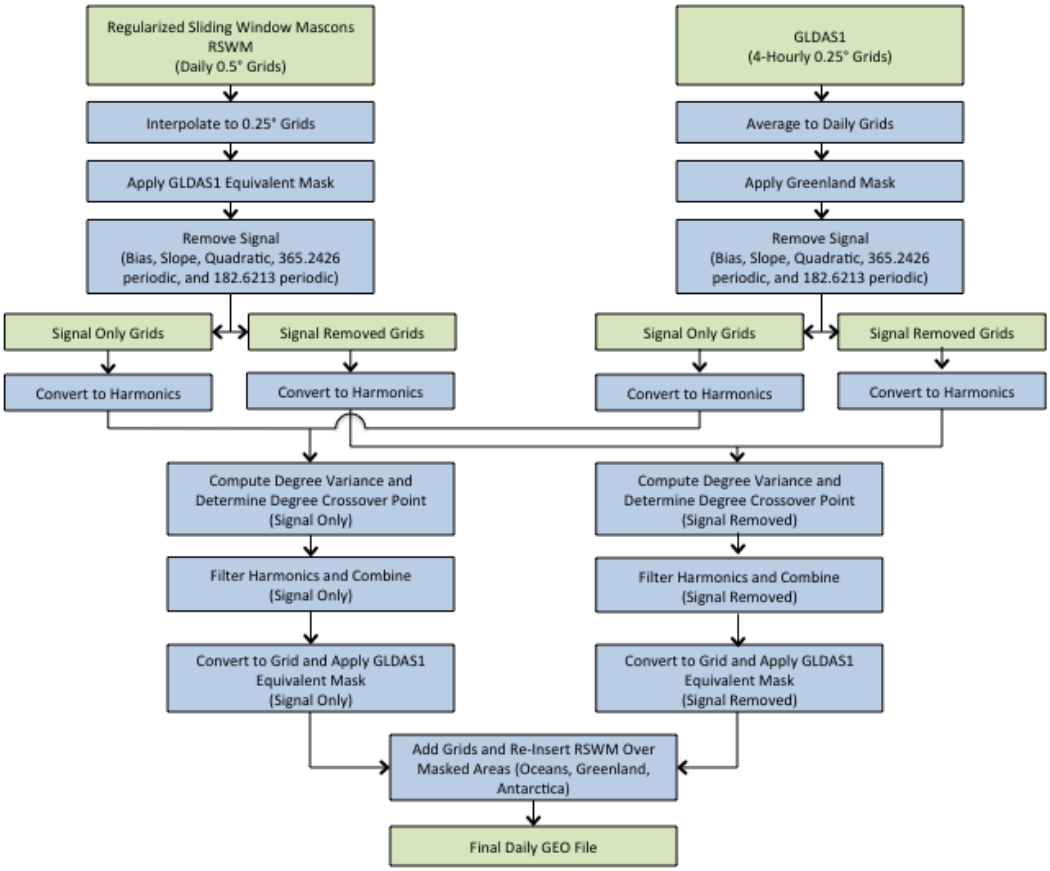

Figure 3.2: Design process of the background gravity field [*Christopher McCullough, personal communication*]

The Signal Removed grids are the residual information once the "Signal Only" fields have been removed. All four of these grids (RSWM Signal Only, RSWM Signal Removed, GLDAS-1 Signal Only, GLDAS-1 Signal Removed) are then converted into spherical harmonic coefficients out to degree and order 720. Figure 3.3 illustrates these steps in the blending process. (a) and (b) show the original input fields, (c) and (d) show the Signal Only components of the grids, and (e) and (f) show the Signal Removed residuals of the original grids.

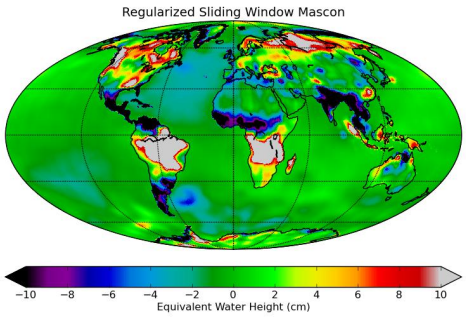

(a) GRACE RSWM Original Grid

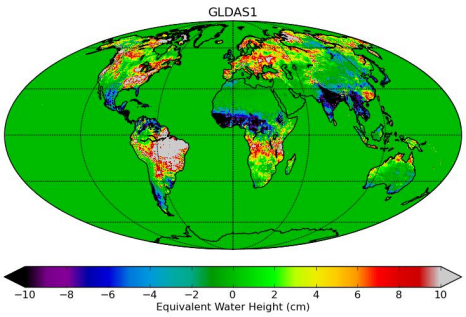

(b) GLDAS-1 Original Field

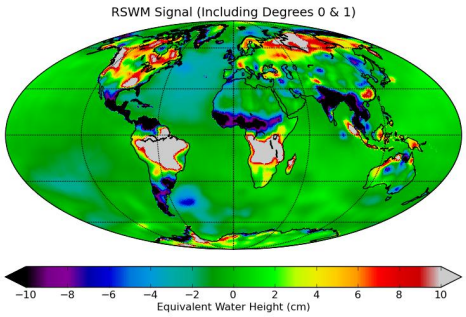

(c) GRACE RSWM, Signal Only

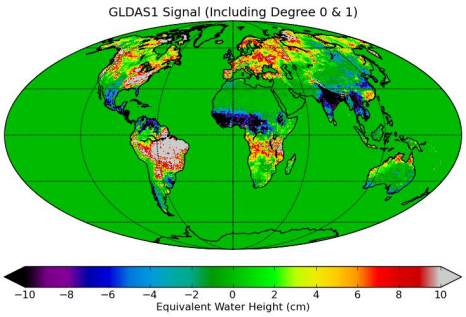

(d) GLDAS-1, Signal Only

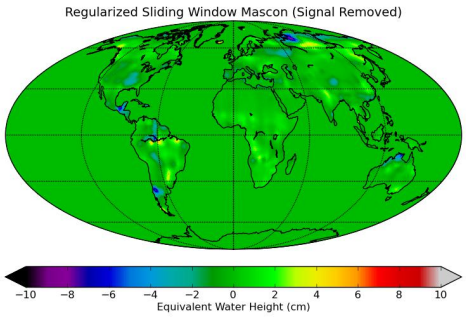

(e) GRACE RSWM, Signal Removed

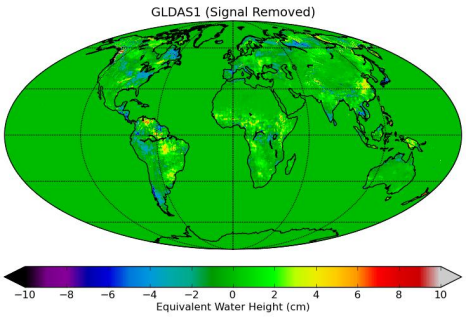

(f) GLDAS, Signal Removed

Figure 3.3: GLDAS and RSWM Blending Process

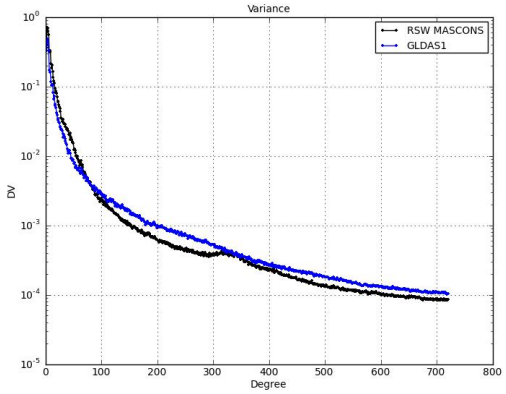

(a) Signal Only Grids Degree Variance: First 100 Degrees

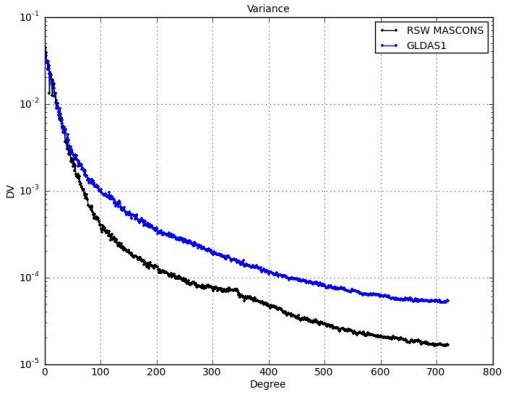

(b) Signal Removed Grids Degree Variance: First 100 Degrees

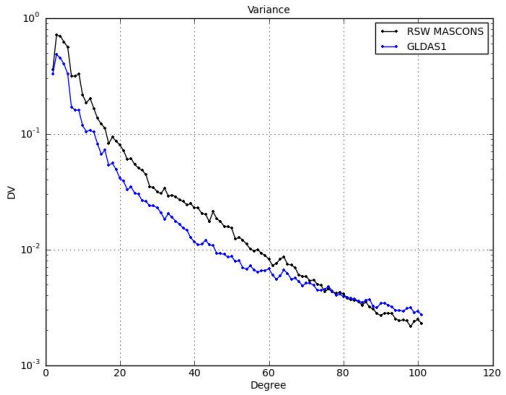

(c) Signal Only Grids Degree Variance: First 100 Degrees

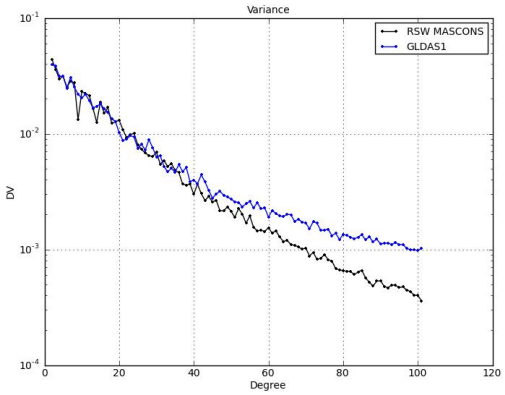

(d) Signal Removed Grids Degree Variance: First 100 Degrees

Figure 3.4: Degree Variance Analysis: Figures (a) and (b) show the degree variance of the full spectrum, while (c) and (d) zoom in on the first 100 degrees to better view the crossover point where GLDAS has more power at shorter wavelengths

To maximize the amount of signal and spatial resolution, it is desired to use each field where it retains the highest level of power. It is possible to quantify this point in the spherical harmonic domain by degree through analysis of the degree variance. At long wavelengths (lower harmonic degree), the RSWM GRACE product has more power, however, at some point the higher spatial resolution of GLDAS will become evident and that dataset will therefore have more power at shorter wavelengths (higher harmonic degree). This crossover point is illustrated for the Signal Only and Signal Removed grids in Figure 3.4. Figure 3.4 (a) and (b) show the full degree variances. Particularly in (a) the RSWM power at low degrees is evident, and then the GLDAS higher power at higher degrees. This crossover point is highlighted in Figure 3.4 (c) and (d). In (c), the Signal Only grids degree variance, this crossover happens at about degree 80 while in (d) for the Signal Removed grids this point occurs at a much lower degree. GLDAS-1 was expected to dominate the Signal Removed grids as is shown because these represent the higher spatio-temporal resolution information.

This degree crossover point is used to inform a Gaussian averaging of the spherical harmonic coefficients by degree. The two fields are each weighted with a Gaussian normal function with the half width max at the crossover point and peak at the respective end at which each series has more power. This weighted averaging is done separately for the Signal Only and Signal Removed grids. The combined Signal Only and Signal Removed grids are then added back together along with the RSWM signals over the ocean, Greenland, and Antarctica. An example of a combined daily, quarter degree background field

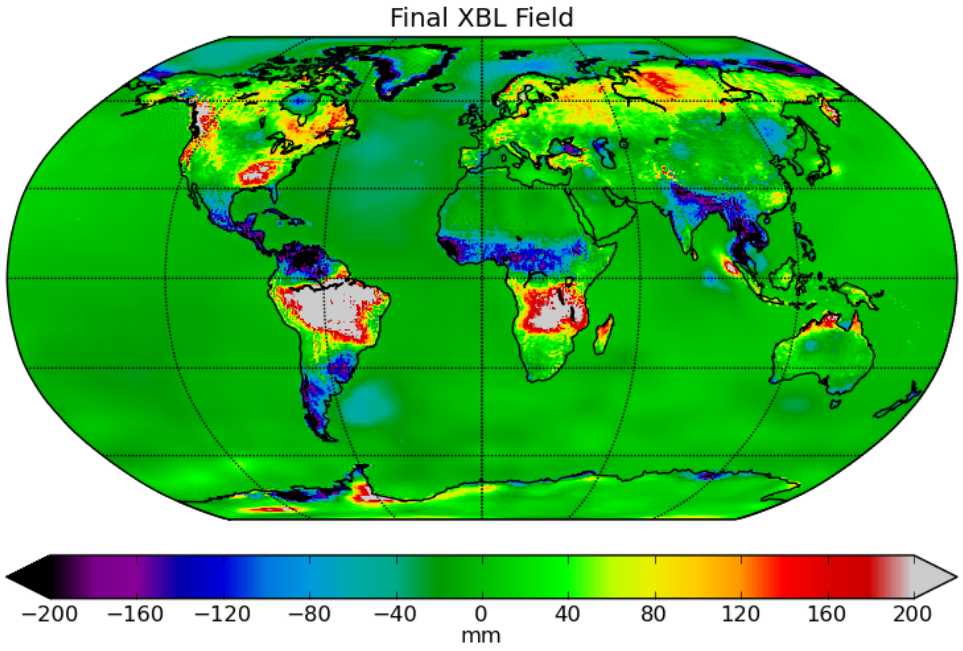

Figure 3.5: Background Gravity Field from Blended RSWM and GLDAS-1 Fields

grid is shown in Figure 3.5. Examination of this field shows that it retains the higher broad scale signal power of the GRACE RSWM fields - seen in the extent and magnitude of large signal patterns. The higher spatial resolution of the GLDAS-1 data is evident in the XBL fields as smaller scale variations and finer signal localization.

3.2.2 Representation of Noise and Error Sources

Two types of commission error are represented in the simulation study, instrument errors and errors in the geophysical models used in the estimation

process. Instrument errors are defined by simulation noise models for the GPS, ACC, SCA, and KBR data. The instrument noise models were designed by [*Wang*, 2013], and a full description of the methods and error spectra can be found in that document.

Errors in the geophysical models are represented in the simulation by implementing different models for the ocean tides and atmospheric and oceanic dealiasing (AOD) in the Mode 5 and Mode 4 runs. The models used in the Mode 5 run to generate the observations define the "true" gravitational variations due to mass movement in the atmosphere, oceans, and over land in our simulated Earth system. The differences between these models and those used to converge the satellite orbits in the Mode 4 run represent the error in the models used in real GRACE processing. The geophysical models used in this analysis are presented in Table 3.1. The background gravity field, representing gravitational variations due to changes in terrestrial water storage, is defined with the XBL field in the Mode 5 run. This is the scientific product currently delivered by the GRACE mission and therefore no model for the TWS variations is used in the Mode 4 run.

Component	Mode 5	Mode 4
Background Gravity Field	XBL (N_{max}=360)	–
AOD	RL05 (N_{max}=100) [26]	NCEP IB (N_{max}=100) [38]
Ocean Tides	GOT4.8 (N_{max}=100) [61]	FES-2004 (N_{max}=100) [48]

Table 3.1: Geophysical models for the simulation analysis

The operational RL05 AOD fields from the European Centre for Medium-Range Weather Forecasts (ECMWF) [26] are used in the Mode 5 run and a

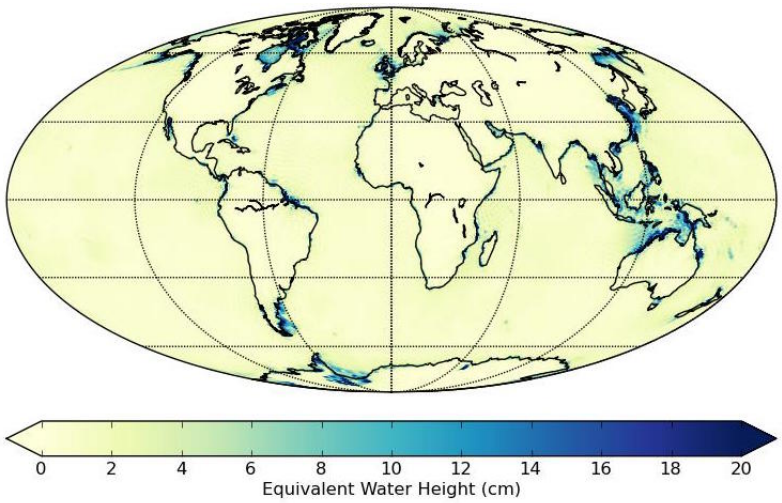

Figure 3.6: Standard Deviation of the difference between the GOT 4.8 and FES-2004 ocean tide models

reanalysis dataset from the National Center for Environmental Prediction corrected with inverted barometer measurements (NCEP IB) [38] is used in the Mode 4 run. There is a mean bias between these two models which will be removed from the simulated RSWM fields and both are defined to a maximum degree and order of 100. The GOT 4.8 ocean tide model [61] along with additional modeled long period variations are used in the Mode 5 run, and the FES-2004 [48] ocean tide model implemented in the Mode 4 run, both with self-consistent equilibrium (SCEQ) and defined to a maximum degree and order of 180. The ocean tide models primarily differ near coastlines as shown in Figure 3.6, with essentially zero mean bias. Both the Mode 5 and Mode 4 run will use the Desai Ocean Pole Tide model with a maximum degree and order of 360.

3.3 Error Analysis

The total error field from the simulation study is the difference in the RSWM mascon field calculated from the simulation data and the defined truth field. This full error field represents the error due to the sum of errors of omission and commission in the final product. By additionally breaking the error estimates down into their component sources we can understand the relative impact of each error source. Figure 3.7 illustrates the method by which the error components are defined in this analysis. The full error is first subdivided into errors of omission and commission. The errors of omission represent the features of the background gravity field which can't be recovered due to truncation at spherical harmonic degree and order 120 and from the low-pass filtering effect of the CRN window. These are quantified in section 3.3.1.

The errors of commission are those features of the XBL field that are lost due to instrument error, aliasing, high frequency attenuation, and errors in the geophysical models. The error fields generated from the simulation include errors of omission as well as the errors of commission defined by the noise models and methods described in the previous section. Four simulation runs were performed to isolate the effect of different commission error sources on gravity field retrieval in space and time, as is described in section 3.3.2. This section then maps and quantifies the full error field and an error covariance for the RSWM product.

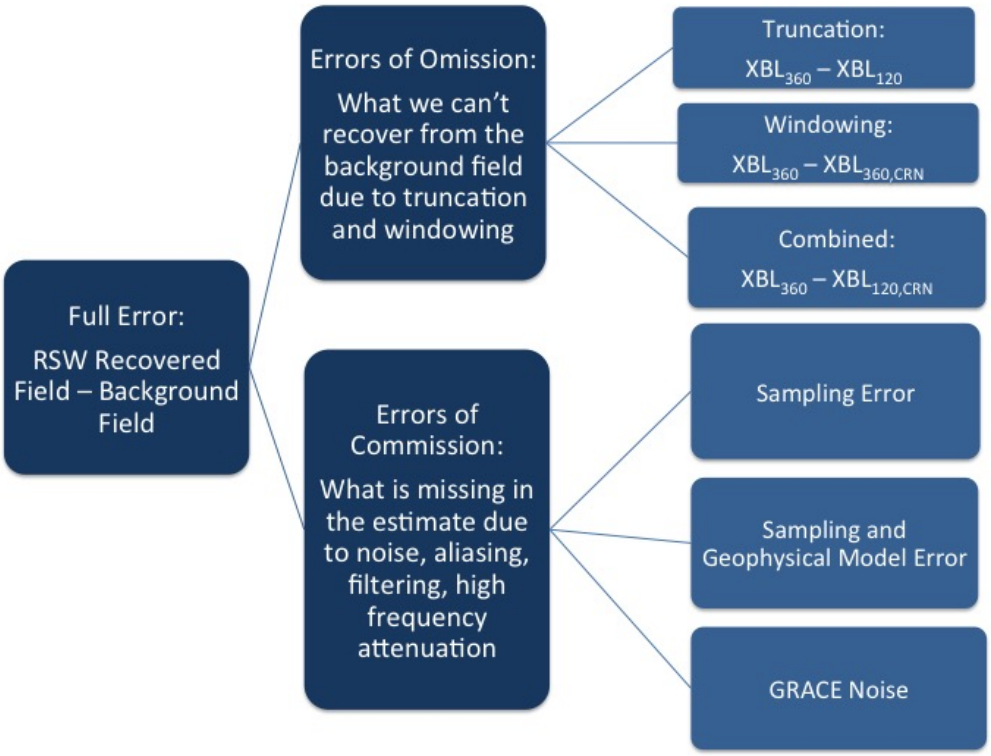

Figure 3.7: Components of the error in the GRACE RSWM Product

3.3.1 Errors of Omission

The omission errors analyzed here are those due to truncation of the gravity field and windowing. Representation of the gravitational field in spherical harmonics - as discussed in Appendix A - while theoretically an infinite series, must practically be cut at a maximum degree and order,N_{max}. The maximum degree determines the spatial resolution of the gravity field as $\frac{\pi R}{N_{max}}$ [60]. Therefore, a higher N_{max} results in a finer resolution of the gravity field and reduces truncation error. However, harmonic coefficients are increasingly dominated by noise at higher degrees. N_{max} is chosen to balance the reduc-

tion in high-frequency noise in the gravity field while retaining the maximum amount of signal. This truncation of the spherical harmonic series will reduce the spatial resolution that is theoretically recoverable from the data and is therefore a source of omission error.

The RSWM product assumes a maximum degree and order of 120 in the estimation process. The XBL fields, in contrast, have a maximum degree and order of 360. Truncation of these fields to 120 will result in loss of some high-frequency spatial information. This effect is calculated from the difference between the XBL field and a Gaussian smoothed XBL field with an effective radius of 125 km. This smoothing radius simulates truncation of the gravity field to degree and order 120 while avoiding artifacts such as ringing which could occur from a simple truncation. The smoothing radius (SR) is calculated for an N_{max} of 120 according to:

$$SR = \frac{\sqrt{8 * log(2)}}{N_{max} * N_{max}} a_e \tag{3.1}$$

The truncation error is then determined by calculating the standard deviation at each gridcell over the test year (2008), mapped in Figure 3.8. It can be seen from Figure 3.8 that mostly high resolution spatial information is lost due to this truncation. This error effect is only valid over land as only the RSWM fields were used over oceans to calculate the XBL truth field, and thus the oceans have already been truncated to N_{max} 120. The mean global truncation error is found to have a very low bias of 2.9 mm with a global mean standard deviation of 22.3 mm and a mean standard deviation of 27.3 mm

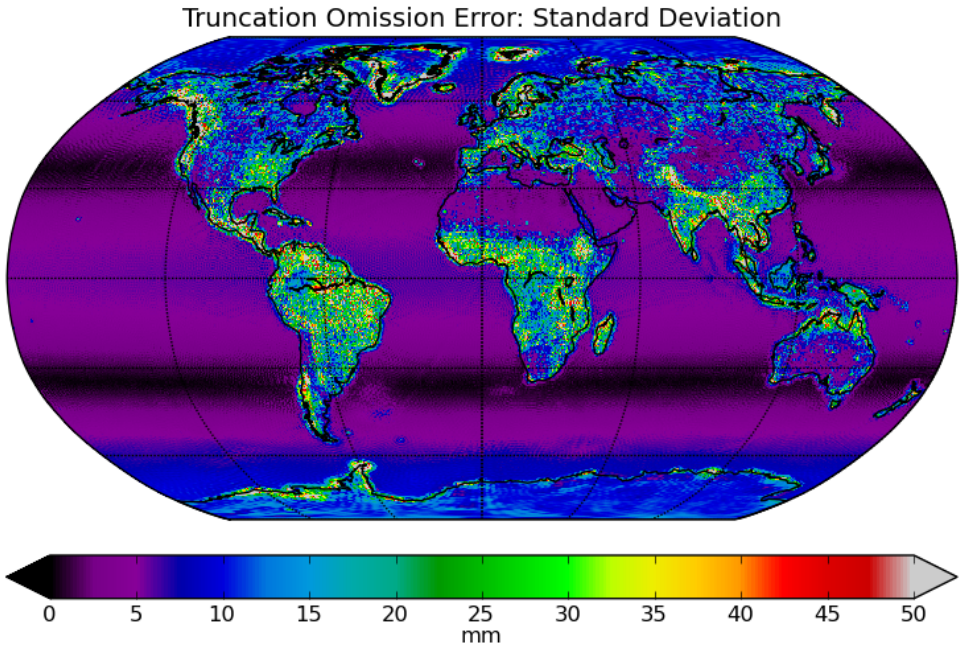

Figure 3.8: Omission Error due to truncation of the gravity field (mm)

over land, as tabulated in Table 3.2.

Similarly to the windowing analysis in Chapter 2, the XBL field is windowed with the CR09-47C21 window to quantify the signal lost due to the window's low pass filtering effect. The windowing error is then also calculated as the standard deviation of the residual at each grid point, and mapped in Figure 3.9. The windowing error is much smaller than the truncation error, causing essentially no bias and a global mean error of 4.2 mm and 5.3 mm over land - both well under the attainable resolution of GRACE.

Finally, the XBL field is both smoothed and windowed to estimate the

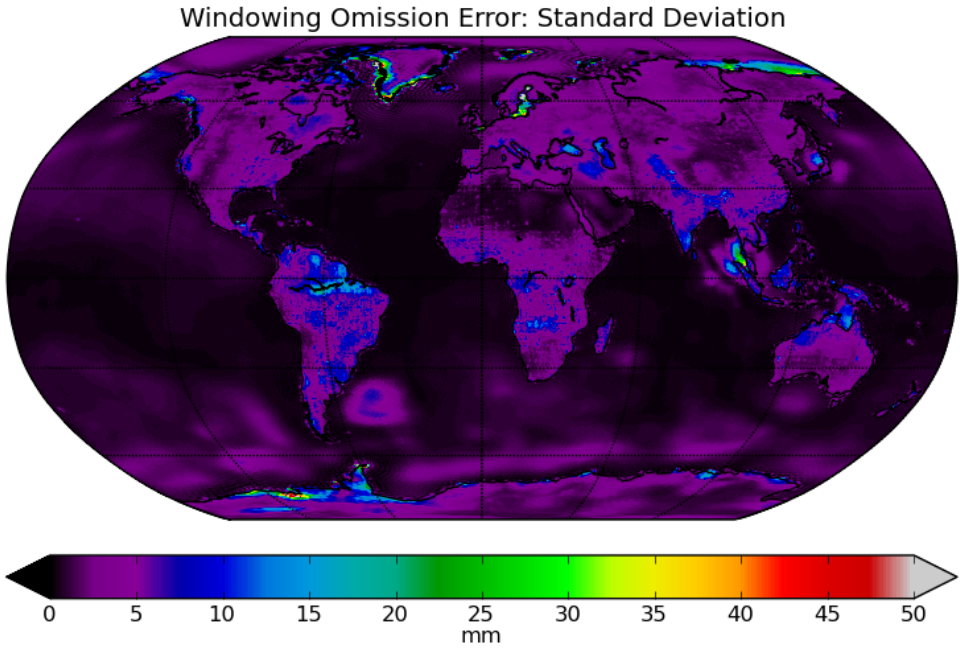

Figure 3.9: Omission Error due to temporal windowing of the gravity field

combined, or total, omission error as defined in this analysis. It is noted that this is the omission error from our simulation "truth" field. For real-world applications additional signal exists at short wavelengths above 360 degrees. Shown in Figure 3.10, it is dominated by the truncation error, however, the windowing error clearly adds some features in the oceans and coastal areas - the Falkland current is particularly evident - and amplifies some regions over land. The total omission errors are included in Table 3.2 and are only slightly higher than the truncation errors.

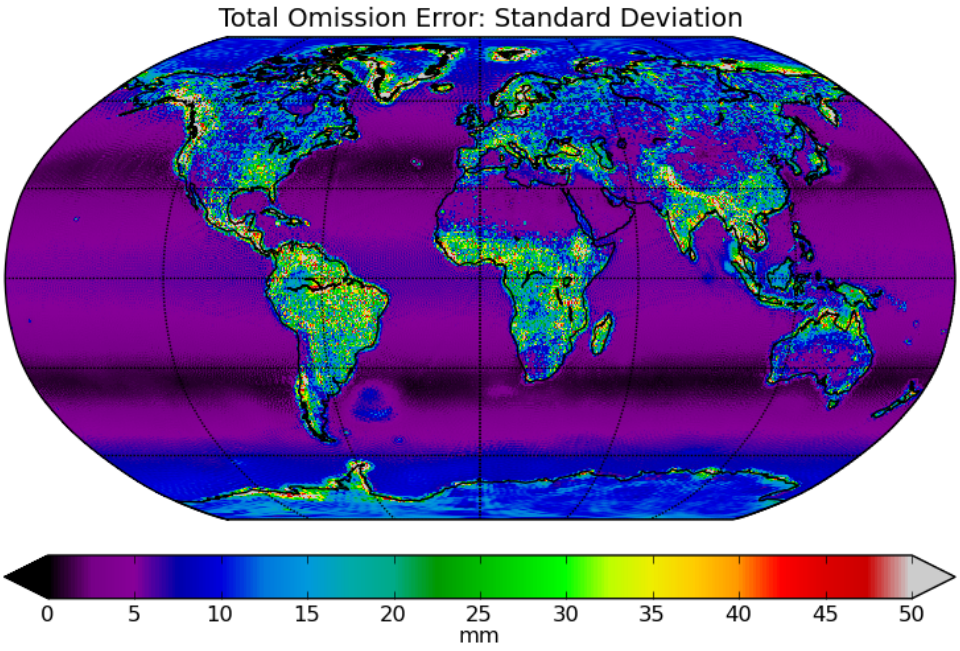

Figure 3.10: Omission Error due to truncation and temporal windowing of the gravity field

Omission Type	Bias	Global Std. Dev.	Land Std. Dev.
Truncation	2.9 mm	22.3 mm	27.3 mm
Windowing	0.002 mm	4.2 mm	5.3 mm
Total	2.9 mm	22.6 mm	27.8 mm

Table 3.2: Mean errors of omission due to truncation and windowing of the gravity field

3.3.2 Simulation Error Results

Four versions of the error simulation were defined to estimate the effect of each noise component on retrieval of the gravity field. These four simulations

are outlined in Table 3.3 which shows which error sources (as defined in Table 3.1) are included in each simulation run. The instrument noise case is meant to determine the baseline error caused by imperfect measurements, and the background gravity field is not used. The sampling error and geophysical model error cases assume perfect observations and show primarily the effect of aliasing and omission error in retrieval of the background field. The sampling error case represents the error in the RSWM product with perfect AOD and Ocean Tide models and no instrument noise while the geophysical model error case adds on the error in the AOD and Ocean Tide models. Finally, the total error case estimates the total amount of error in each RSWM field.

Case	TVG	AOD Error	Ocean Tide Error	GRACE Noise
Instrument Noise	no	no	no	yes
Sampling Error	yes	no	no	no
Geophysical Model Error	yes	yes	yes	no
Total error	yes	yes	yes	yes

Table 3.3: Error and Noise models included in each simulation run

The Instrument noise case will be handled slightly differently from the other error cases as no geophysical signals are included. Therefore perfect instruments would return a zero field, and any variation represents error added by the instruments. Figure 3.11 maps the monthly unconstrained estimate of the gaussian smoothed GRACE measurement error with an effective radius of 500 km. The overall error is small and clearly shows the typical GRACE North-South striping, with a mean global standard deviation of 29 mm. It is used to show the pattern and form of the gravity field errors due to instrument error.

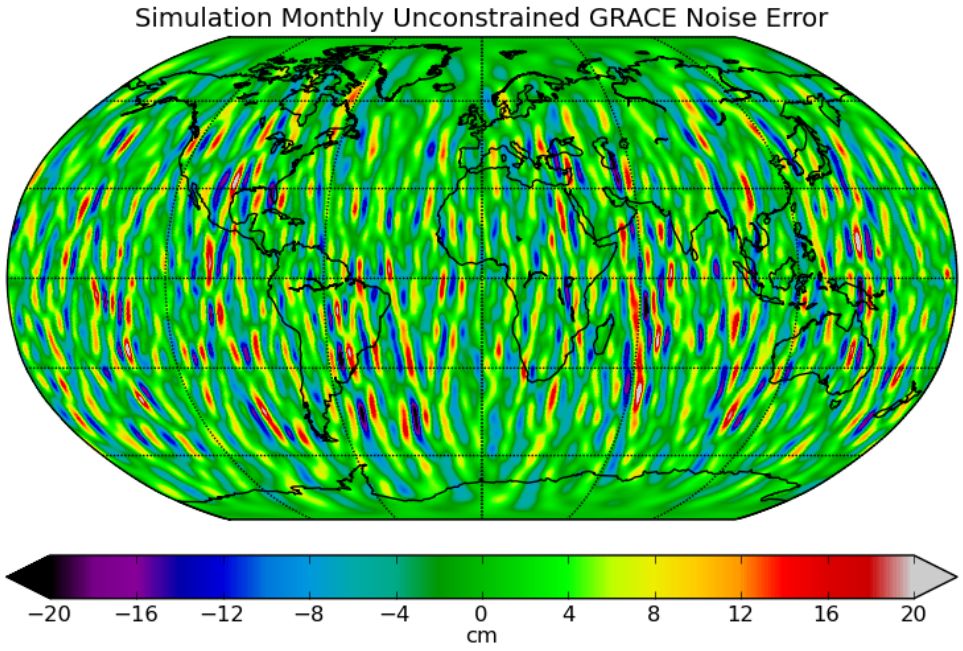

Figure 3.11: Instrument Noise

The remaining three cases are all estimated as regularized mascons with the same methodology as the RSWM product for use in the following analysis. The sampling error case is representative of the best attainable gravity field with the GRACE mission configuration - assuming the instruments, AOD, and Ocean Tide models are perfect. The errors in the recovered gravity field due to aliasing, groundtrack coverage, errors of omission, etc. are presented in Figure 3.12. The error maps are calculated as the root mean square (rms) of the residual field between the XBL background gravity field and the recovered mascon field and are slightly higher than the instrument noise case - note the

larger color scale axis. The oceans are masked out for the following images as the simulations were designed to primarily assess the accuracy of the RSWM product for land hydrology and as the AOD fields are not restored for ocean assessment. The correlated north-south striping pattern is not evident, and signal attenuation of particularly high resolution signals is most evident in tropical regions with large TWS signals. The global mean bias and standard deviation of this and the following two error cases is found in Table 3.4.

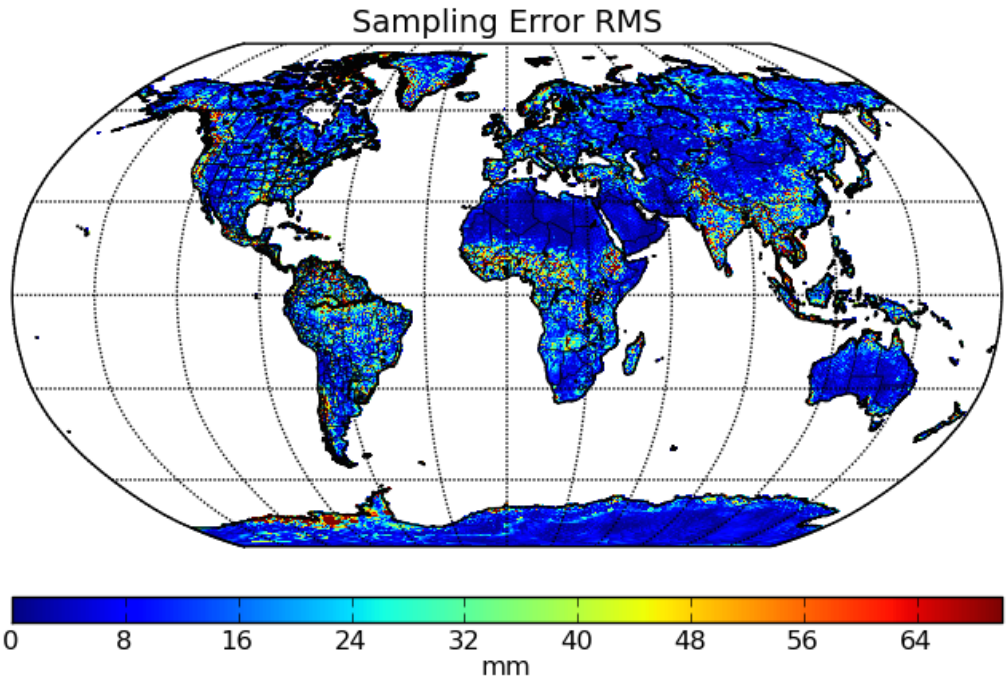

Figure 3.12: Sampling Error in the RSWM Product

The geophysical model case is representative of the sampling error as well as the error due to imperfect AOD and ocean tide models, shown in Figure 3.13. It shows a clear increase in the overall error level, more evident

striping, as well as regionally specific error patterns in areas with stronger and higher frequency signal patterns. The omission error due to truncation and windowing the gravity field is also evident here as high resolution "speckling" in many land regions.

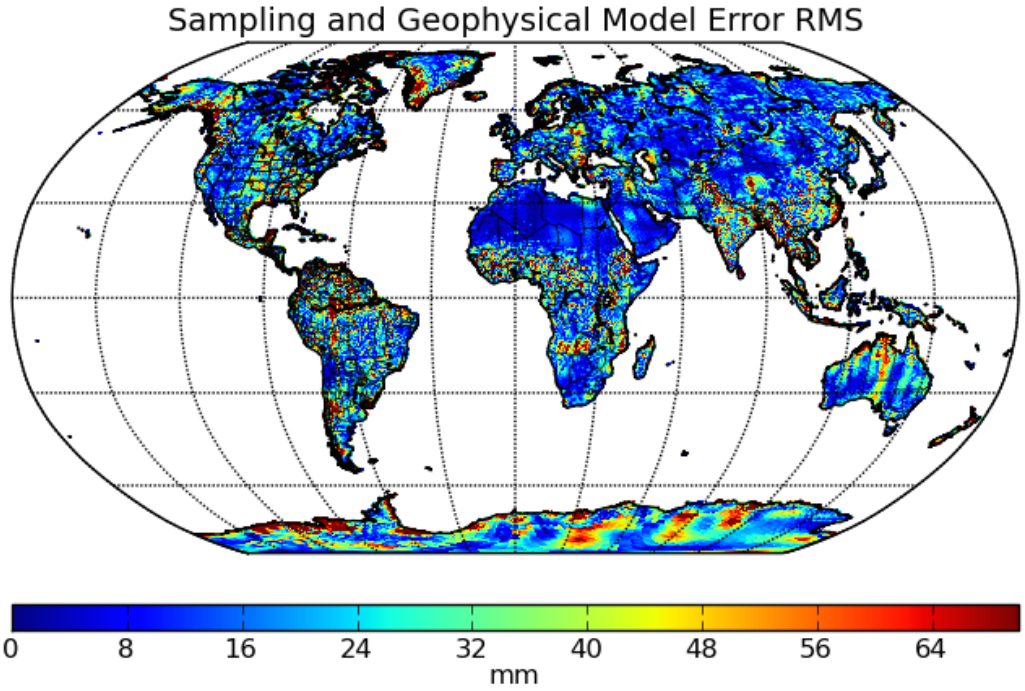

Figure 3.13: Sampling Error and Geophysical Model Error in the RSWM Product

The Total Error case is our final, complete error estimate for the RSWM mascon product, mapped in Figure 3.14. The total error case shows regionally specific patterns with a global land mean error of 3 cm. This error RMS plot while broadly representative of the error in the RSWM product does not reflect some of the known error patterns in GRACE. The characteristic striping patterns, for example, are not evident in Figure 3.14 however do still

exist in the error residuals. Additionally, the anisotropic and correlated nature of GRACE error cannot be represented in a single map.

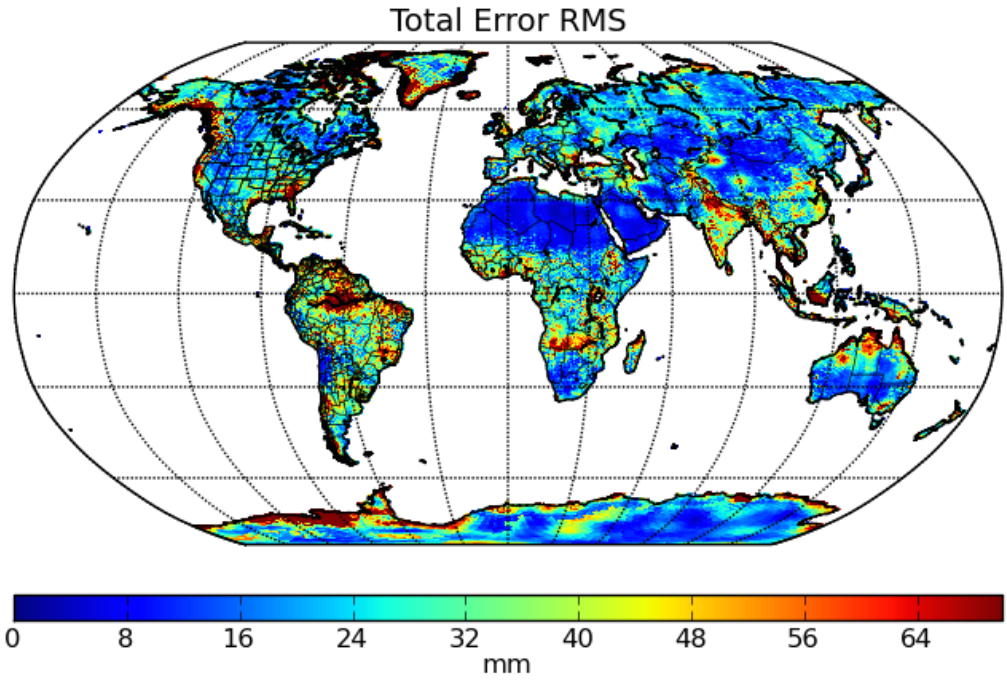

Figure 3.14: The complete GRACE Error Field

Case	Bias	RMS	RMS over Land
Sampling	-0.03 mm	7.7 mm	5.1 mm
Geophysical	-0.02 mm	15.9 mm	7.7 mm
Total Error	-0.86 mm	30.4 mm	30.6 mm

Table 3.4: Mean and Standard Deviation of Error Residuals

To provide a more complete representation of error in the RSWM product we use the daily error residual fields to construct an error covariance. This is calculated by accumulating the error residuals (the difference of the RSWM simulated daily field and the XBL field for that day) into a matrix R. The

covariance is calculated from R according to:

$$C_{RSWM} = \frac{RR^T}{N-1} \tag{3.2}$$

where N is the number of residual grids. If this calculation were done in the mascon grid domain the dimension of C_{RSWM} would be 259,200 x 259,200, far too large to estimate with a year of error residuals. In order to reduce the number of variables but still provide a global estimation of the covariance, the error residual grids undergo a spherical harmonic decomposition and the covariance is calculated for these harmonic coefficients. The error variance of each harmonic coefficient resides along the diagonal and the correlation information is contained in the off-diagonal elements. This covariance along with the mean error field are used to define a multivariate normal distribution to generate error samples which will be used to perturb the observations in the assimilation algorithms.

The multivariate normal distribution returns samples of the covariance, or, "error clones". Implementation of multiple of these error clones in the data assimilation process is discussed in Chapter 4. An ensemble of error clones provides more information about the full error profile of the RSWM product than the error variance alone. The clones, as shown in Figure 3.15, capture regionally specific error patterns, the north-south striping error patterns, error caused by the atmospheric and oceanic dealiasing product, etc.

The analysis in this chapter conducted an end to end simulation of the GRACE mission to quantify the error characteristics from the GRACE mission

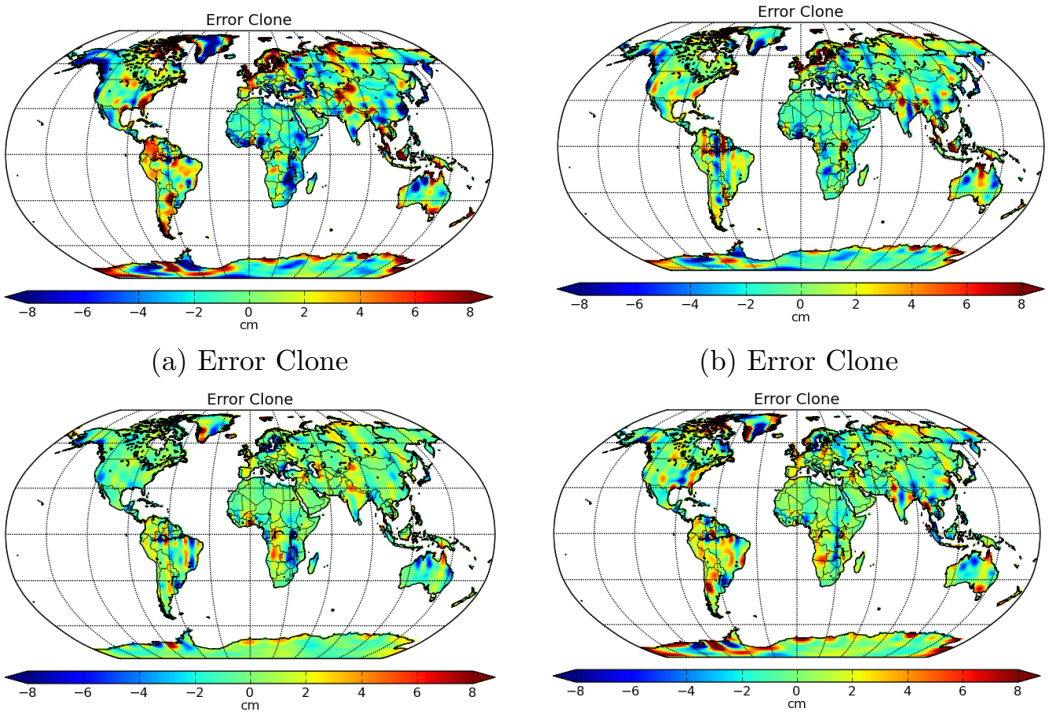

(a) Error Clone (b) Error Clone

(c) Error Clone (d) Error Clone

Figure 3.15: Samples of the GRACE Error Covariance

and, specifically, in the RSWM product over land. The RSWM product was found to have a global land mean error rms of 3 cm with regionally specific and "stripe" patterns. The error residuals were then used to construct a more representative error covariance for GRACE. Sampling of this covariance with a multivariate normal function was used to create error clones, or multiple realizations of the GRACE error fields, to more completely represent the size, pattern, and correlated nature of error in the GRACE RSWM product. The simulation methodology developed in this chapter is extensible to GRACE Follow-On and future satellite gravity missions. The implications of this improved error model for data assimilation of GRACE into land surface models

is explored in Chapters 4 and 5.

Chapter 4

The Data Assimilation Framework

The RSWM data product and associated error estimates formulated in the previous two chapters offer great advances for land data assimilation of the GRACE data. The higher temporal resolution of the RSWM fields eliminates the need for temporal smoothing in the DA process. This reduces computational requirements and brings the GRACE data more in line with the land surface model resolution. The newly formulated error covariance is more representative of the magnitude and structure of error in GRACE. Incorporating this information in the form of error clones better informs the assimilation algorithms without greatly increasing computational requirements. This chapter builds on these two advances to construct a flexible, extensible framework for land data assimilation of GRACE type satellite data products.

4.1 Framework Overview

Data assimilation with GRACE diverges from traditional methods due to the nature of the GRACE product. Because GRACE accumulates many satellite observations into a global estimate (as described in Chapter 2) the data product has a unique error profile and coarser spatial and temporal resolution than many other in situ or remote sensing measurements. In addition,

because it measures the total water column, the assimilation state update must be disaggregated vertically as well as horizontally in the assimilation process. The assimilation algorithms and methods must therefore be tuned to maximize the information gained while properly modeling the structure of satellite gravity products. The key elements of the data assimilation process for land data assimilation of satellite gravity products are as follows:

- *Realization of Observations*: The RSWM GRACE product represents the first daily time series from GRACE without model or outside information. This daily product along with the error clones created from the simulation-derived error covariance are better tuned to the data assimilation process needs and land surface model temporal scales.

- *Modified Assimilation Algorithms*: Traditional Ensemble Kalman Filter (EnKF) routines use the observation error variance to perturb the observation in calculation of the state update. This method, however can introduce noise into the assimilation leading to the development of methods such as the Ensemble Adjustment Kalman Filter (EAKF) [3]. To better represent GRACE error patterns, the assimilation equations are modified to use the full covariance information to perturb the observations and calculate the assimilation update.

- *Gaspari-Cohn Localization Radius*: Due to its relatively coarse (200-300 km) spatial resolution it is necessary to spatially smooth the assimilation state update for the RSWM and other satellite gravity products. Gaspari-Cohn localization is a commonly implemented methodology for

this in data assimilation. The key parameter definition for Gaspari-Cohn localization is the smoothing radius to determine the spatial extent of the influence of each gridcell observation.

- *GRACE Assimilation Update Rate*: Analysis of the model and GRACE temporal profiles showed similarly high levels of correlation over short time scales. To reduce the computational burden it is possible to assimilate the observational data less frequently than daily while still maintaining the benefits of GRACE data assimilation.

- *Latency and Open-Loop Error Growth*: The intensive post-processing methods and large number of observations required to estimate each RSWM field necessitate a certain amount of latency between the time tag of the RSWM product and its operational delivery. However, data assimilation has been shown to calibrate the model, essentially, to improve the initial conditions and thus produce more accurate open loop runs [22]. The time scales over which these improved initial conditions have a significant impact help to determine the latency requirements for operational assimilation of the GRACE data.

The data assimilation framework, and the tools used to implement it, will be further expanded throughout this chapter and Chapter 5. The framework developed here is used to assimilate the RSWM product into the Community Land Model 4.0 [57] with modified assimilation routines of the Data Assimilation Research Testbed [55]. Section 2 will present an overview of CLM and DART and their components and methods that are particularly relevant

to GRACE TWS assimilation. The assimilation algorithms and specialization to incorporate the GRACE error clones are discussed in Section 3. Finally, Section 4 will detail the additional assimilation features and methods - horizontal smoothing of the assimilation updates, the assimilation update rate, and open loop error growth.

4.2 The Assimilation Setup

This study uses the Data Assimilation Research Testbed (DART) [55] software developed at NCAR to assimilate the daily RSWM TWS measurements into the Community Land Model 4.0 (CLM4) [57]. Of critical importance to GRACE data assimilation, CLM4 includes an aquifer in its water column structure, a feature not present in many other global hydrological models, and has a strong heritage of competitive performance. We were able to build upon previous work coupling the two systems [96] and modify the open source platform for daily, covariance-informed data assimilation of terrestrial water storage. Figure 4.1 gives a top level view of how these components of the assimilation setup fit together. DART reads in the ensemble of land surface model states and the GRACE observation and error sequences at the defined epoch. The data assimilation algorithms then calculate the model state update, update the CLM states and feed the new initial conditions back to CLM. The model then propagates these updated states forward in time and the process repeats.

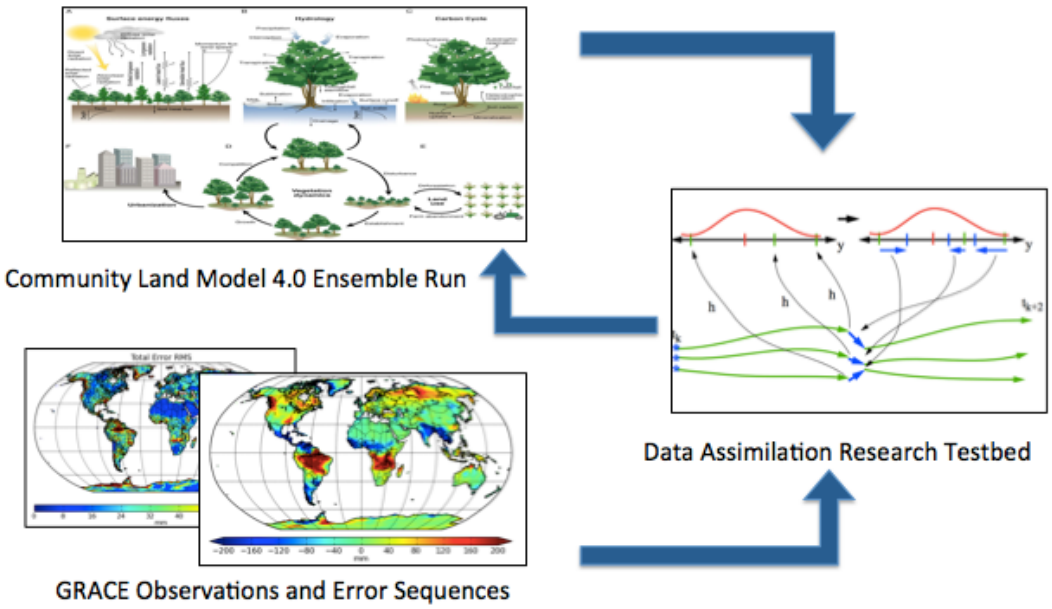

Figure 4.1: The CLM/DART GRACE Data Assimilation System

4.2.1 The Community Land Model 4.0

CLM, the dynamic land model component of the Community Earth System Model (CESM), is developed by a collaboration of scientists and overseen by several working groups at NCAR [57]. The primary goal of the model is to simulate the cycle of energy, water, chemical elements, and trace gases throughout the land surface. CLM was initially developed as a lower boundary condition for the Community Atmosphere Model (CAM), and thus the focus was on the top-level water and energy states. It has now considerably evolved to fully model the full spectrum of land-surface processes within the Earth system. A forty member CLM 4.0 ensemble run within CESM version 1.1.1 was used for this analysis [57]. Forty ensemble members were used to ensure a

sufficiently large ensemble spread and reduction in sampling error while minimizing the computational burden [3]. The program was run in *offline* mode, meaning the land model was the only active component of the system. A bias corrected atmospheric forcing dataset composed of an ensemble of CAM reanalysis fields provided precipitation, solar, wind, and land surface temperature information [96] [59]. The current, scientifically validated model surface datasets and parameterizations were used.

CLM 4.0 shows greatly increased complexity and accuracy than previous releases [54]. As noted in *The Community Land Model Philosophy: model development and science applications* document: "One major challenge facing CLM is an appropriate balance across the processes represented: the overall model will suffer if excessive attention is paid to one set of processes at the expense of others". Thus, a balance must be reached between complexity and accurate modeling of each of the key processes in the model. Figure 4.2 illustrates these processes as they are modeled in CLM.

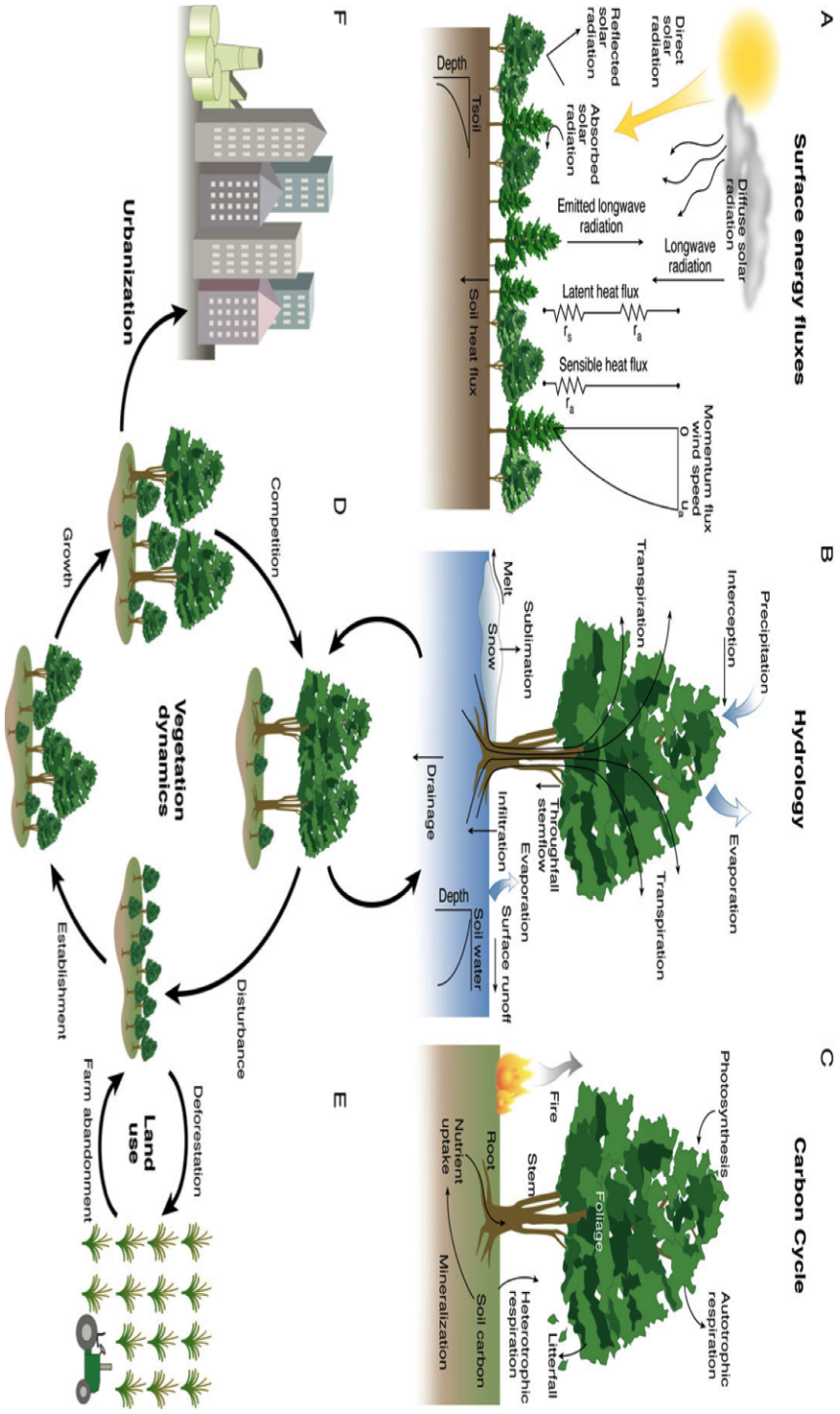

Figure 4.2: The Community Land Model 4.0 Structure [54]

CLM first subdivides the global land surface into latitude-longitude gridcells; in this analysis the default 0.9 x 1.25 degree resolution was implemented. Each gridcell is represented by a nested sub grid hierarchy as a function of landunits, snow/soil columns, and plant functional types (PFTs). The structure is as follows: first a gridcell is subdivided into one or more land units: glacier, wetland, vegetated, lake, and urban. Each landunit can again be subdivided into columns and the columns subdivided into PFTs [57]. Figure 4.3 demonstrates this structure for a vegetated landunit.

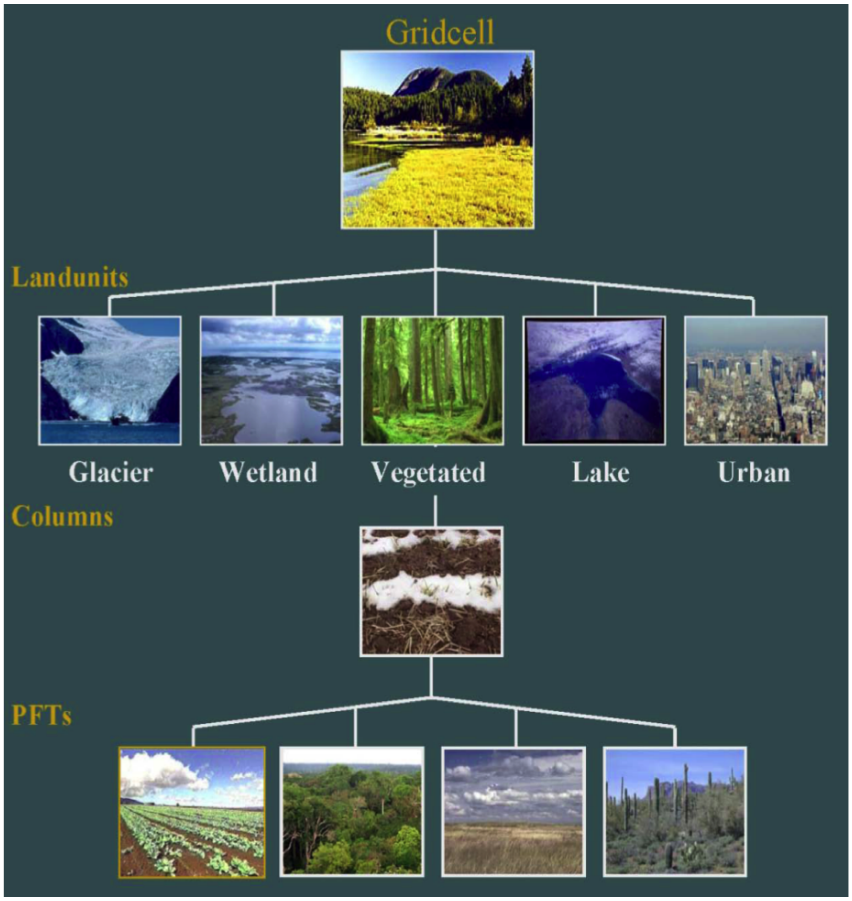

Figure 4.3: The CLM Cell Structure [57]

The landunit, the first subgrid level, aims to capture the broadest patterns of spatial heterogeneity within the subgrid. From there, the column aims to capture variability within soil or snow levels within that landunit. The soil column contains 15 layers covering the first 40m of the land surface, and the snow column can contain up to 5 layers. The third level, the PFT, is used to model the biogeophysical and biogeochemical differences between broad plant categories. Each column can be composed of up to 16 PFTs. While the boundary fluxes and hydrological state variables are defined at the column level, the surface fluxes and vegetation state variables are defined at the PFT level [57].

A more detailed program flow for an offline model run is shown in Figure 4.4. The model is first spun-up for a sufficient amount of time for the hydrology and energy balances to reach equilibrium. The initial condition dataset of [*Zhang*, 2014], defined on January 1, 2003 with a 500 year spin-up time, was used in this analysis. These initial states define the temperature, energy fluxes, water storage, and hydrology fluxes for the model. The parameters of the model such as root distribution, aerodynamic resistance, photosynthetic parameters, albedos, etc. are defined using the best available data for each gridcell or column. Surface datasets are used to define the gridcell landunit and PFT types as well as leaf area indices, canopy height, and soil characteristics. This definition of the model and surface information is critical for the model physics to accurately simulate the system while maintaining balance in complexity of all model components.

The land-atmosphere boundary conditions are defined either by coupling the land surface model with an atmospheric model or using reanalysis

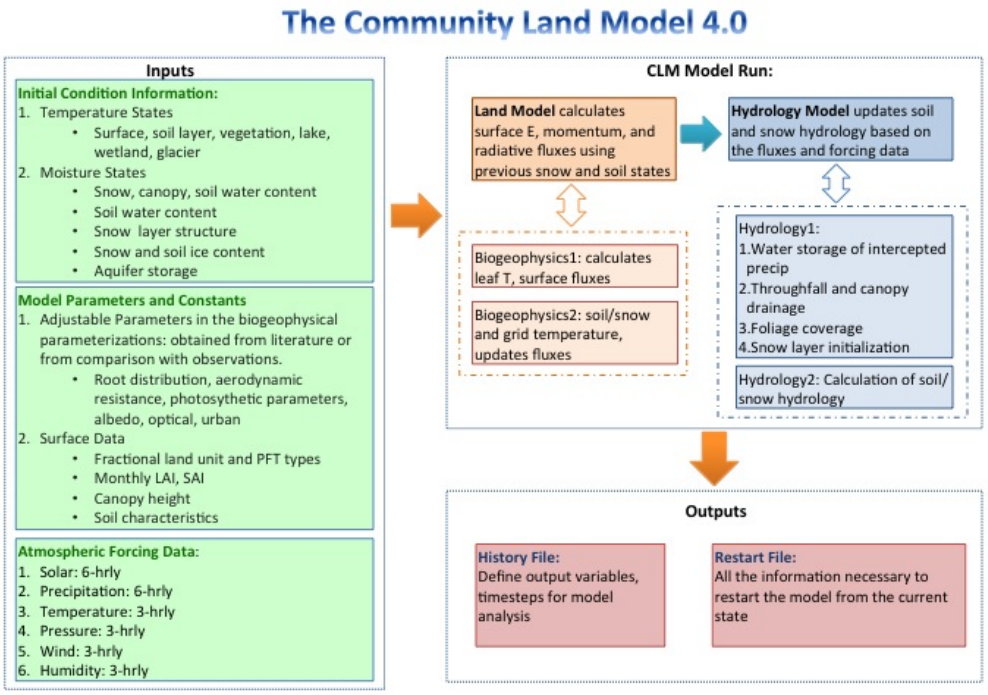

Figure 4.4: The CLM Model Run

data of precipitation, solar fluxes, atmospheric winds, etc. as was done here. Precipitation, the primary contributor of water to the land surface, must be accurately partitioned into runoff and infiltration by the land surface characteristics, current state, and physics built into the LSM. As there will be inaccuracies in the model parameterization and physics, these forcing fields will similarly contain inaccuracies which must be accounted for. As previously stated, this analysis employs an ensemble of forcing fields from the Community Atmosphere Model. The ensemble spread of the atmospheric forcing fields is structured to represent the estimated error bounds of the atmospheric forcing information [73]. Therefore, propagation of this ensemble of forcing information through CLM will result in an ensemble of land surface states that are

representative of the statistical error arising from the land surface model, as well as in the atmospheric forcing information.

Each model run consists of two main components, a land model and hydrology model. The land model calculates the surface energy, momentum and radiative fluxes from the initial snow and soil states. These calculations are done in two biogeophysics modules run consecutively. Next, the hydrology model updates the soil and snow hydrology based on the fluxes and forcing data. Within these two models, CLM simulates the following land surface processes: Ecosystem Composition and Structure, Surface Albedos, Radiative Fluxes, Momentum, Sensible, and Latent, Stomatal Resistance and Photosynthesis, a Lake Model, a Dust Model, a River Transport Model, an Urban Model, and a Carbon-Nitrogen Model.

The GRACE TWS product represents the variability of the entire water column - from surface water storage to deep aquifers. In CLM, terrestrial water storage is vertically disaggregated into an unconfined acquifer, 15 soil layers, up to 5 snow layers, and canopy water, as shown in Figure 4.5. The water balance is calculated according to Equation 4.1 both at the gridcell level and globally. The sum of the variation in canopy (ΔW_{can}) , snow (ΔW_{son}) , soil moisture ($\Delta w_{liq,i}$ and $\Delta w_{ice,i}$ for each soil layer, i) , and aquifer storage (ΔW_a) must balance the flux of water entering and exiting each gridcell through precipitation (q_{rain} and q_{sno}), evaporation (E_v and E_g), runoff (q_over), drainage (q_{drai}), and glacier melt (r_{rgwl} and $q_{snowcp,ice}$).

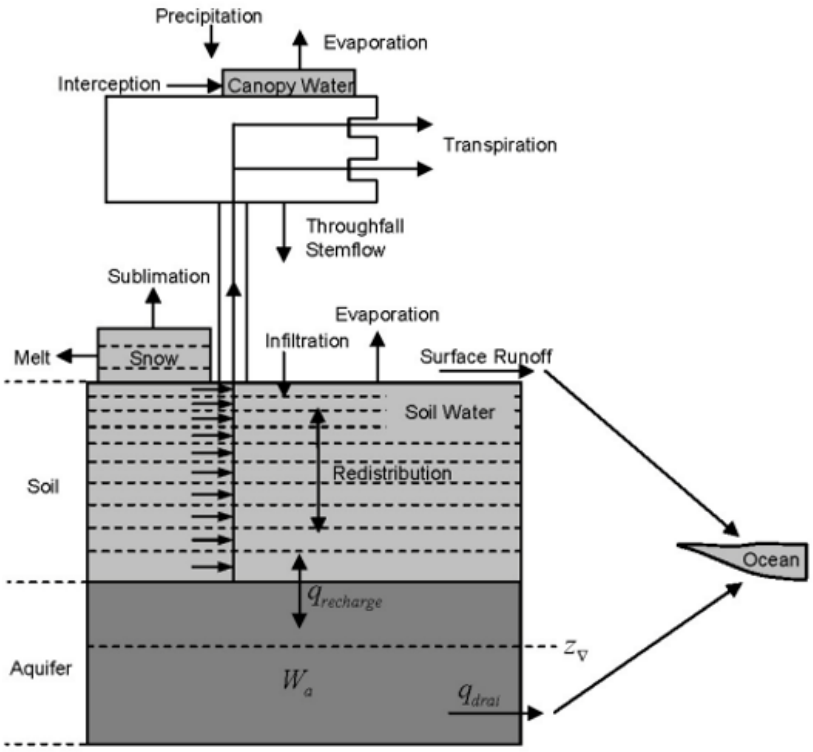

Figure 4.5: Hydrological states and processes in CLM 4.0 [57]

$$\Delta W_{can} + \Delta W_{sno} + \sum(\Delta w_{liq,i} + \Delta w_{ice,i}) + \Delta W_a = \\ q_{rain} + q_{sno} - E_v - E_g - q_{over} - q_{drai} - r_{rgwl} - q_{snwcp,ice} \tag{4.1}$$

Each layer of the CLM water column is parametrized and constrained separately. The model dynamics simulate interception, throughfall, canopy drip, snow accumulation and melt, water transfer between snow layers, infiltration, evaporation, surface runoff, sub-surface drainage, redistribution within the soil column, and groundwater discharge and recharge to calculate the fluxes of energy and water through boundary layers [57]. For the rest of this analysis, the contribution of canopy storage is neglected in this analysis as it makes up

a minuscule component of TWS and large relative variations in this parameter could easily lead to large, unnatural updates to this parameter and degrade performance of the DA system.

The GRACE TWS fields are defined to be the equivalent of the left side of Equation 4.1, the sum of variation in the total water column. The EnKF assimilation methods, discussed in the next section, read in the CLM snow, soil moisture, and groundwater water storage state variables along with the GRACE observation and error sequences and calculate an update to these CLM state variables. Only the TWS associated model state variables are updated as *1.* the ensemble data assimilation methods do not contain an adjoint model for the land surface model dynamics so false correlations could cause uncorrelated state variables to be incorrectly adjusted and *2.* the modular nature of the CLM model will allow the model physics to properly calculate the associated changes in other model state variables. The mechanics of this data assimilation process will be discussed further in the following sections.

4.2.2 The Data Assimilation Research Testbed

The Data Assimilation Research Section (DAReS) at NCAR develops and maintains the Data Assimilation Research Testbed (DART) as a community facility for ensemble data assimilation. DART is developed in a modular programming environment so that it can easily be customized and implemented in many computational models and assimilate a wide variety of observational datasets. Therefore modelers, observational scientists, and others can explore the assimilation of measurements using different techniques and

algorithms specific to their field of expertise. Furthermore, the community approach of DART allows each advance to be incorporated into the model and distributed to the community for further scientific advancement [55]. Figure 4.6 shows an overview of the process. The DART run is defined by a Fortran namelist defining the observations, algorithms and methods to use, and model states and locations. The filter executable reads in the name list, initial ensemble state, observations, and calculates the state update. The initial model states are updated, the model is advanced, and the process is repeated.

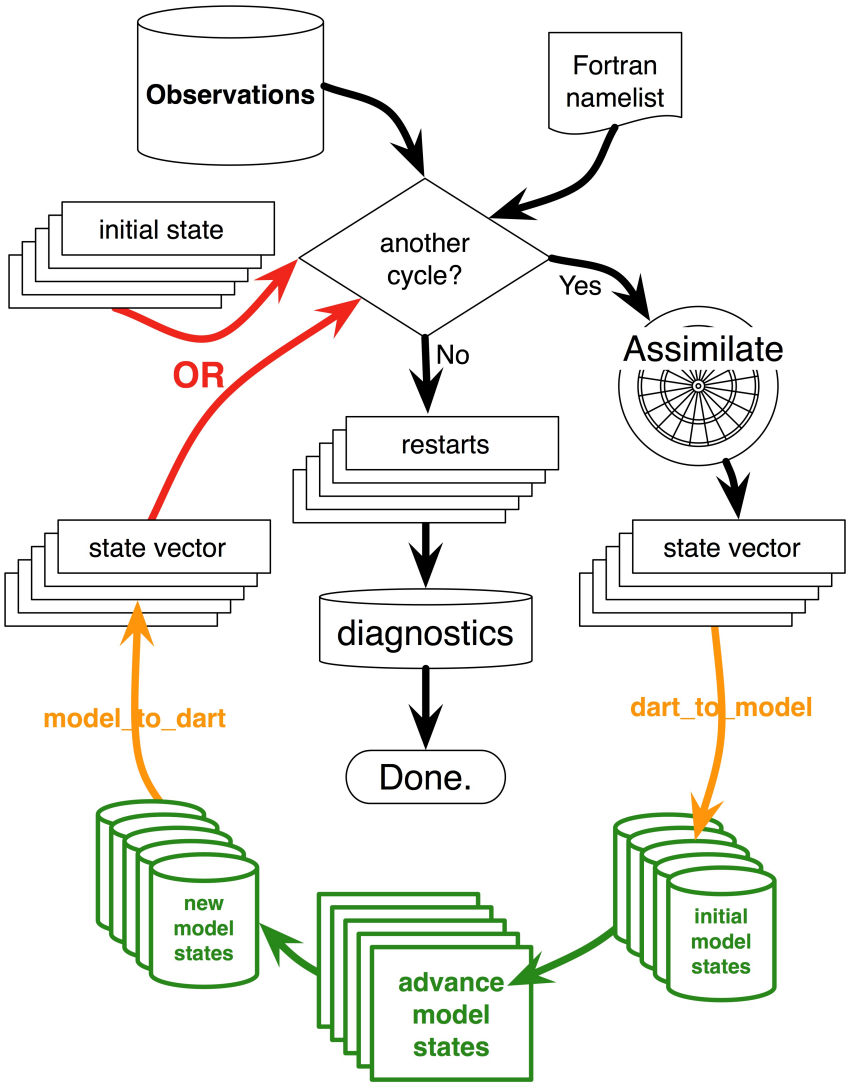

Figure 4.6: Schematic of Ensemble Data Assimilation with DART

DART provides a number of tools to ensure efficient, optimal assimilation and to help scale the ensemble DA methods to large systems. Two such tools implemented in this study are sampling error correction and ensemble inflation. Sampling error refers to the error caused by observing a

finite number of ensemble members to represent the spread rather than the entire population. Thus, false or inaccurate correlations can appear between states and incorrect updates calculated based on these false correlations [55]. Sampling error is reduced as the number of ensemble members increases and samples more of the distribution. [59] developed a sampling error correction algorithm based on experimental results that is implemented in this analysis. In addition, it was shown that 40 ensemble members is a sufficient sample size. Increasing the ensemble size beyond this will have minimal performance gains while greatly increasing the computational load.

Ensemble inflation is implemented to combat *filter divergence* (where the filter becomes too confident of the model estimate as the ensemble spread decreases and ignores new information) by continually adjusting the ensemble spread of the CLM state variables. There are several "flavors" of ensemble inflation that may be implemented in DART. We use observation space, spatially varying ensemble inflation which calculates the inflation coefficients based on the previous model state. As will be discussed in Chapter 5, the ensemble inflation parameters must be carefully adjusted to ensure the ensemble spread is well-distributed throughout the global land surface.

The assimilation process we implemented via DART is shown in Figure 4.7. First, the GRACE and CLM inputs must be correctly formatted. The GRACE dataset estimates the variation in TWS relative to an epoch or background gravity field. The baseline static field is defined here as the 2005-2008 mean signal. The RSWM 2005-2008 mean signal is thus removed from the daily fields. Then, to make the GRACE estimate compatible with the CLM

model states the 2005-2008 mean TWS equivalent (sum of aquifer, soil moisture, and snow) from an open loop (without assimilation) CLM ensemble run is added to the daily RSWM grids. These fields and the associated error estimates are then converted into the DART observation sequence format. The CLM model states are transformed into observation sequences after summing the components of the water column in each gridcell and interpolating the 0.9x1.25 degree CLM grid cells to a 1x1 degree grid to match the GRACE resolution.

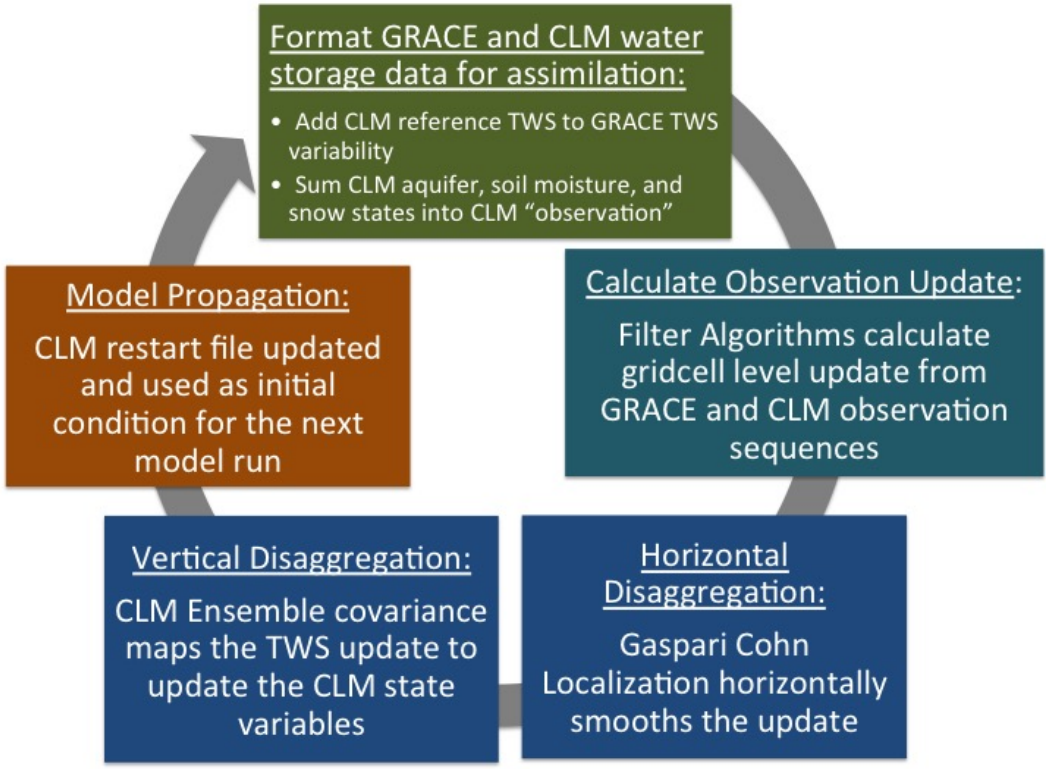

Figure 4.7: GRACE data assimilation into CLM4 via DART

DART uses the observation and error sequences in the assimilation al-

gorithms to calculate an update in "observation space", a gridcell level update for the total water column. The equations and theoretical basis behind this update are detailed in the next section. To account for the spatial influence of the GRACE data, this update is horizontally smoothed - in 2D latitude/longitude space - according to a user-defined localization radius (discussed in Section 4.4.1). The ensemble spread is used to define a mapping function to disaggregate the TWS update back to column-level updates of the CLM aquifer storage, soil moisture, and snow-water equivalent. These state updates are then applied to the CLM restart file which is used to initialize the next model run.

4.3 Algorithms and Methods

The data assimilation system is designed to optimally fuse the land surface model and observational data sources, accounting for their unique error patterns and spatial and temporal resolution discrepancies. CLM4, as implemented in this study, has a 0.9 x 1.25 degree spatial resolution and simulates land surface processes at a 30 minute temporal resolution. The land surface states contain uncertainties due to incorrect or incomplete model parameterization, physics, surface datasets, and atmospheric forcing information. In contrast, the typical GRACE RL05 product has a 300+ km spatial resolution and monthly temporal resolution. The daily, 200-300 km resolution RSWM product was developed to reduce this resolution discrepancy and thus capture shorter term hydrometeorological signals important to the land surface model. As discussed in Chapter 3, the GRACE dataset contains uncertainties due to

instrument noise, aliasing, windowing, etc. The DA algorithms are designed to appropriately incorporate the independent, accurate observational data into the land surface model which provides global and temporal continuity.

To illustrate the calculation of a model state update, Figure 4.8 shows a sample assimilation of a single variable (univariate) with five model ensemble members. The initial ensemble of model states (the green stars) define a prior probability distribution function (pdf) in green. The observation (the red circle) is defined along with a likelihood function in red. The assimilation algorithms - the Ensemble Adjustment Kalman Filter for this example - determine a posterior probability distribution function. The initial ensemble of states are then updated to reflect this posterior pdf. The data assimilation algorithms define how this update is calculated for each gridcell and then distributed in space.

Data assimilation theory is based upon the mathematical framework of estimation theory. Several methods have been employed for geophysical data assimilation; the most common are Variational (VAR), Particle Filter (PF), and Ensemble Kalman Filter (EnKF) Methods. EnKF and PF are Bayesian-based approaches while VAR minimizes a cost function. Each has advantages and drawbacks based on the type of geophysical model, observational data, and computational load of the DA problem. This section will give a brief background of variational and particle filter methods and then a more detailed explanation of the Ensemble Kalman Filter routines use in this analysis. Finally, we will discuss localization, the method by which the model update is spatially distributed.

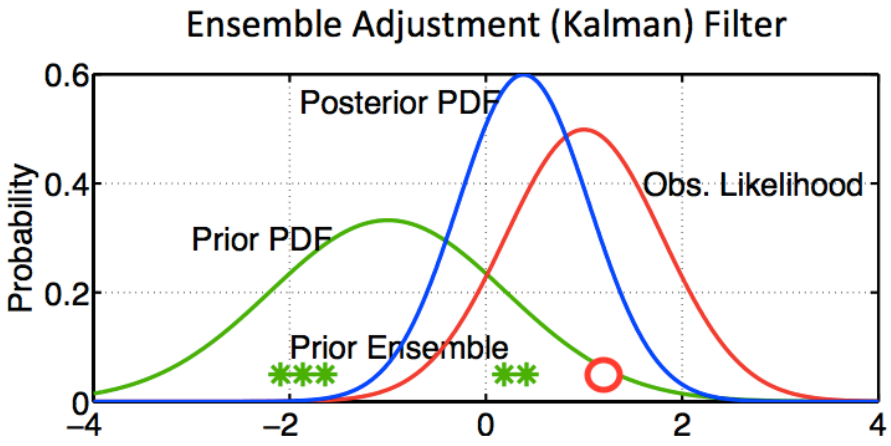

(a) The DA algorithms read in the ensemble of model states, the observation data and likelihood information, and calculate the posterior pdf. [55]

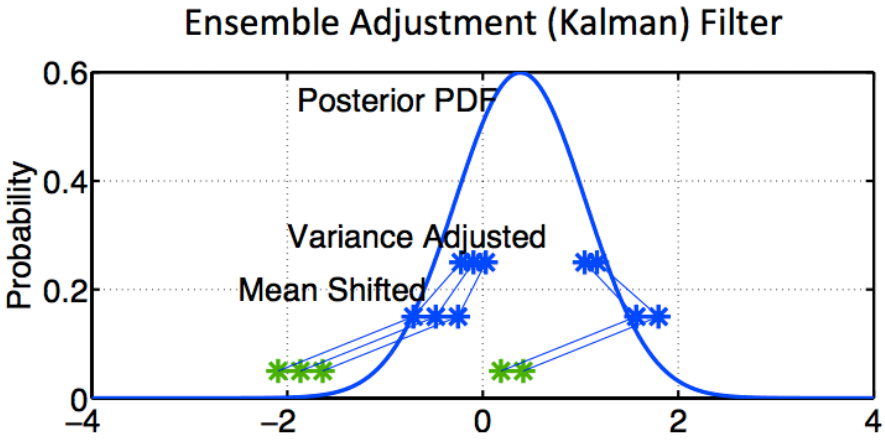

(b) The initial model states are then adjusted according to this posterior pdf. [55]

Figure 4.8

4.3.1 Variational and Particle Filter Methods

Variational DA defines an assimilation window from time k-n though k, over which a cost function is minimized for the state vector, $\mathbf{x}_{k-n}$ [53]. The

process is as follows: for a nonlinear system,

$$\mathbf{x}_{k+1} = g_{k+1,k}(\mathbf{x}_k) \tag{4.2}$$

with a model observation estimate $\mathbf{y}$:

$$\mathbf{y}_k = h_k(\mathbf{x}_k) + \mathbf{v}_k \tag{4.3}$$

where g_{k+1} is a nonlinear function relating the state at time k to k+1, h_k is a nonlinear function relating the state and observation at time k, P^-_{k-n} is the background error covariance, and R_i is the uncertainty in the observations. The cost function, J, for the window k-n to k is:

$$\begin{aligned} J(x_k) =& \frac{1}{2}(\mathbf{x}_{k-n} - \hat{\mathbf{x}}^-_{k-n})^T (P^-_{k-n})^{-1} (\mathbf{x}_{k-n} - \hat{\mathbf{x}}^-_{k-n}) \\ &+ \frac{1}{2} \sum_{i=k-n}^{k} [\mathbf{y}_i - h_k(\mathbf{x}_i)]^T R_i^{-1} [\mathbf{y}_i - h_i(\mathbf{x}_i)] \end{aligned} \tag{4.4}$$

The cost function is designed to balance the apriori information with the new observational information [53]. These methods typically require an adjoint model of the system - very difficult for the large land-surface system and modular model structure - and do not propagate forward covariances, both of which restrict their use and contributed to the decision to not use them in this study.

Particle Filters, in contrast, employ a sequential estimation process; effectively the sequential analogue of Markov Chain Monte Carlo (MCMC)

batch methods. The EnKF, discussed in the next section, can be considered a special case of the PF with the Bayesian update step approximated with a linear update step. Thus, the two methods begin with the same system definition:

$$\mathbf{x}_k = f(\mathbf{x}_{k-1}, \mathbf{w}_{k-1}) \tag{4.5}$$

$$\mathbf{y} = h(\mathbf{x}_k) + \mathbf{e} \tag{4.6}$$

Where $\mathbf{x}_k$ is the current model state calculated by nonlinear function f from the previous state $\mathbf{x}_{k-1}$ and any model error w. The observation $\mathbf{y}$ is a nonlinear function h of the current model state $\mathbf{x}_k$ with associated error, $\mathbf{e}$. PF methods approximate the posterior probability density function (pdf) as a group of random samples from the transition pdf and prior pdf at time step k-1. The extent to which the particles accurately represent the posterior pdf determine filter performance. Determination of this posterior field to sample is complicated, and the lack of model error information can further degrade the system performance. Resampling methods, typically the Sequential and Residual Resampling Methods [53], must be used to properly characterize the posterior pdf. Particle filter methods can become incredibly computationally burdensome due to this resampling step, particularly for larger models with many state variables.

4.3.2 Ensemble Kalman Filter Routines

Ensemble Kalman Filter methods evolved from the sequential Kalman Filter which uses the model and observation covariances and a Jacobian of the model to optimally update the model state. However, an adjoint model for a large geophysical system is incredibly complicated, and due to inaccuracies in the model physics, often ineffective. The EnKF uses an ensemble of model runs, with an ensemble spread representative of uncertainty in the model, to form a sample covariance [22]. The model sample covariance along with the observation error information is used to calculate the Kalman Gain and determine the update to the model states. Because of the sample covariance construction, the EnKF can assimilate observations with a nonlinear relation to the model state without an adjoint model [3].

EnKF methods assume that all probability density functions are Gaussian, and the update scheme is based on the recursive application of Bayes rule. Several variants are available, the ones specific to this research will be discussed in the following sections. Other variants can adjust the update to be calculated in batch form or incorporate observations at different time scales than the model such as the Ensemble Kalman Smoother (EnKS). The EnKS includes covariances between states at different time steps so that observations that span longer periods than the model time step can be accounted for. Data assimilation with the monthly GRACE fields required ENKS methods to smooth the monthly mean update to daily time scales - a step now avoided with the RSWM product. The EnKF can also be extended to estimate model parameters, in addition to the state variables, to further calibrate the model

for forecasts. The EnKF has been shown to outperform variational methods for lower order systems, and scale easily to much larger applications for use in parallel computation [3]. For these reasons, EnKF assimilation methods are implemented in this study for assimilation of the GRACE RSWM product into CLM4.

The traditional EnKF algorithm is as follows for a system defined by Equations 4.5 and 4.6. The model covariance, C_e, is defined from the spread in the ensemble states as:

$$C_e = \frac{1}{N_e - 1}(\mathbf{R}\mathbf{R}^T) \tag{4.7}$$

where N_e is the number of ensemble members used in the analysis, $\mathbf{R}$ represents a matrix of the residuals of each ensemble states from the ensemble mean. The update to the model states can then be calculated from:

$$\mathbf{X}^+ = \mathbf{X} + K(Y - H\mathbf{X}) \tag{4.8}$$

where K represents the Kalman gain calculated from C_e, the observation covariance, R, and the matrix H which maps the model state variables to the observation.

$$K = C_e H^T (H C_e H^T + R)^{-1} \tag{4.9}$$

The data assimilation algorithms are implemented in a modular form in DART, as alluded to in Figure 4.7. The model "observation" update is

calculated at the gridcell level for each of the N CLM ensemble members, represented by x_i where i = 1...N in Equation 4.10. To model the GRACE error variance a defined error variance for each observation is used to perturb the observation, y, to form y_i. For each of the N CLM ensemble members, x_i, there is thus a corresponding GRACE observation, y_i. The EnKF update, $\hat{x_i}$, for each ensemble member is calculated from:

$$\hat{x}_i = \frac{1}{\frac{1}{\sigma_p^2} + \frac{1}{\sigma_o^2}}(\frac{x_i}{\sigma_p^2} + \frac{y_i}{\sigma_o^2}) - x_i \tag{4.10}$$

where σ_p^2 is the variance of the model estimate and σ_o^2 is the variance of the observation. The gridcell level updates are then horizontally smoothed with Gaspari-Cohn localization (described in the next section) and vertically disaggregated into state level updates with the Kalman Gain.

4.3.2.1 The Ensemble Adjustment Kalman Filter

The Ensemble Adjustment Kalman Filter (EAKF), typically recommended for use with DART, offers improvements in calculation of the gridcell level update over the traditional EnKF by ensuring that the mean and covariance of the updated state agree with that expected by filtering theory. The EAKF has been shown to improve upon the EnKF by reducing noise introduced by perturbing the observations with a random gaussian, y_i in Equation 4.10 [3]. In contrast, the EAKF does not randomly perturb the observation. Instead, it calculates the expected mean and variance of the updated ensemble and adjusts the update to this calculated distribution. The new mean is

calculated with:

$$\bar{x}_{new} = \frac{\sigma_o^2}{\sigma_p^2 + \sigma_o^2}(\bar{x} + \frac{\sigma_p^2 y}{\sigma_o^2}) \tag{4.11}$$

and the update from:

$$\hat{x} = \sqrt{\frac{\sigma_o^2}{\sigma_p^2 + \sigma_o^2}}(x - \bar{x}) + \bar{x}_{new} - x \tag{4.12}$$

The EAKF has been shown to reduce noise in the update step and produce more accurate assimilation results [3]. However, both the EnKF and EAKF only take the error variance of the observation into account. This is acceptable for many measurement sources, however, due to the anisotropic and correlated nature of the GRACE data assimilation of the full covariance information adds a great deal of value. We therefore explore updating the assimilation algorithms to include the GRACE covariance information.

4.3.2.2 The Covariance Ensemble Kalman Filter

The filter developed for this analysis is an upgraded version of the Ensemble Kalman Filter as it incorporates the observation covariance information into the assimilation process, and is referred to in this study as a Covariance Ensemble Kalman Filter (CEnKF). The CEnKF filter is designed to incorporate the observational error covariance by using an ensemble of observation "clones" to calculate the updates to the ensemble of model states. The implementation is nearly identical to that of the traditional Ensemble Kalman Filter. The gridcell level update is calculated according to Equation 4.13,

however the method of perturbing the observation y_i is different. Rather than perturbing the observation with a gaussian normal distribution defined by zero mean and the error variance, the full observation covariance matrix is used to define a multivariate normal distribution that generates error clones to perturb the observation, as discussed in Chapter 3.

$$\hat{x}_i = \frac{1}{\frac{1}{\sigma_p^2} + \frac{1}{\sigma_o^2}}(\frac{x_i}{\sigma_p^2} + \frac{y_i}{\sigma_o^2}) - x_i \tag{4.13}$$

This method is designed to reduce the random error in traditional EnKF methods and incorporate the GRACE error covariance information in the data assimilation methods. The traditional Ensemble Kalman Filter has been shown to introduce noise into the update because of the random gaussian perturbation to the observation. The CEnKF more intelligently forms this perturbation through the use of the covariance. The forty observation clones will reflect the spatial correlation in the GRACE data from the multivariate normal distribution used to generate them. Along with additional data assimilation tools such as Gaspari-Cohn localization, sampling error, and ensemble inflation, the CEnKF algorithm aids in properly representing the nature of the GRACE data source for optimal state update calculation.

4.3.3 Gaspari-Cohn Localization

The GRACE RSWM product is characterized by a coarser spatial resolution than the CLM model. Therefore, after the assimilation update is calculated at the one degree gridcell level it must be spatially distributed over

the GRACE resolution. The spatial, or "horizontal", smoothing of the update is performed over an averaging kernel representative of the observation resolution and typically referred to as localization for data assimilation applications. *Gaspari and Cohn* (1999) developed the methodology for construction of flexible, simply parametrized covariance functions in two and three dimensions commonly implemented in data assimilation systems. Gaspari-Cohn localization, as implemented in this study via DART, is defined by a localization radius [30]. The localization radius determines the half-width of a Gaussian spatial correlation function. The weight applied to an update will therefore have a value of 1 at 0 distance, 0.5 at the defined radius, and 0 at 2*cutoff. The choice of localization radius is important to ensure the RSWM product is correctly represented in the data assimilation space.

The foundation for Gaspari-Cohn localization is theoretically very similar to spatial smoothing of the unconstrained GRACE harmonic solutions. Both define an averaging kernel representative of spatial correlation characteristics - the GRACE error patterns for smoothing the unconstrained products and the GRACE product covariance for assimilation into land surface models. The GRACE covariance information could be used to define a more representative spatial distribution function, however, construction of this function would increase the DA computational requirements and is outside the scope of this thesis.

The localization radius as implemented in this analysis is therefore a measure of the influence in latitude-longitude space of an RSWM gridcell TWS value. Theoretically, truncation of the spherical harmonic expansion at

N_{max} 120 would give the RSW fields a spatial resolution of 125 km. However, the other error sources and processing methods degrade this spatial resolution and, as determined in Chapter 2, the RSWM product has a 200-300 km spatial resolution. Another method of measuring the spatial influence of each GRACE observation is shown in Figure 4.9 which plots the influence of the GRACE measurement as a function of distance from the satellite ground track. It shows a Gaussian-like distribution with an approximate half width of 400km. These bounds (200-400 km) are used to establish an appropriate localization radius for RSWM GRACE assimilation into CLM4, however, this parameter is easily tuned to other observational datasets and land surface models. The localization radius and its effect upon the spatial resolution of the assimilated time series will be further explored in Chapter 5.

4.3.4 Effect of Windowing on Assimilation

The current RL05 GRACE product requires temporal smoothing of the assimilation update, calculated as a monthly mean, to the higher resolution model states. The RSWM product was designed to reduce or eliminate this step by increasing the signal bandwidth through an improved filter design and increased sampling of the gravitational field. As was shown in Chapter 2, it is able to capture nearly all of the high frequency signal within the GRACE resolution and has similar temporal correlation properties as high fidelity LSM data over short time scales. The following experiment is designed to test the effect of different assimilation strategies with the RSWM product. Specifically, the differences in the assimilated results from assimilation of an RSWM day

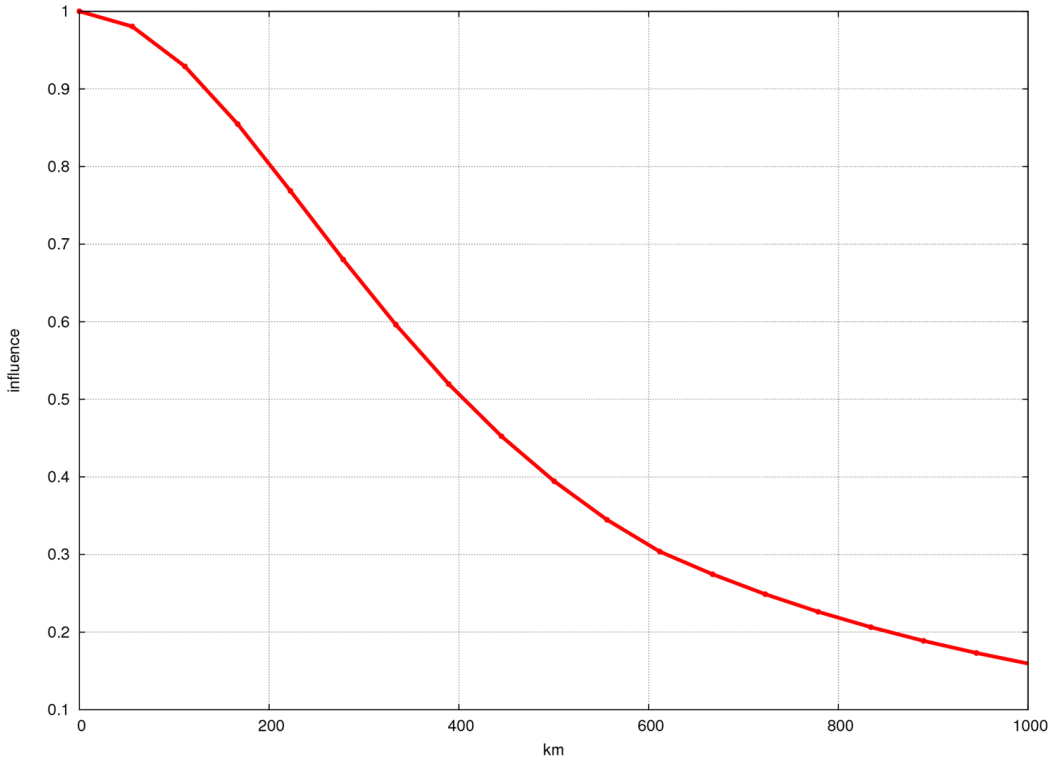

Figure 4.9: The Spatial influence of a GRACE observation [*Himanshu Save, personal communication*]

with a model day, a windowed model product, and smoothing of the assimilation update.

This experiment is performed on a simplified assimilation system: at one gridcell for one year. The input data, shown in Figure 4.10, is the GRACE RSWM time series and a 40-member ensemble of CLM total water storage states for a single gridcell in Bangladesh. First, assimilation is performed with the filter calculating an update each day comparing each ensemble model state to the GRACE observation. The ensemble spread of the CLM ensemble members defines the CLM error variance and a simple 2 cm error estimate

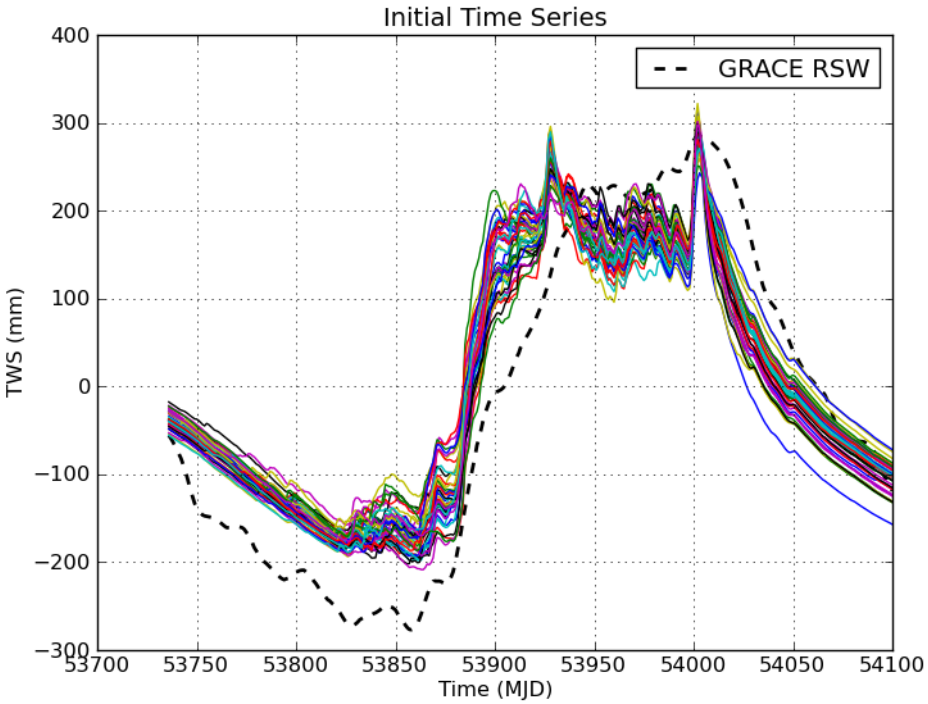

Figure 4.10: Open Loop CLM Ensemble States and GRACE Observations

is assigned to the GRACE data. The CLM ensemble states are propagated forward in time using the open-loop day to day variations. This simplification has little effect on the results as CLM is run in offline mode in the full assimilation system rather than coupled to an atmospheric model. The ensemble of assimilated model states (thin colored lines) along with the initial CLM open loop mean (dotted blue line) and GRACE observation values (dashed black line) are shown in Figure 5.11. Assimilation of the GRACE data moves the ensemble states closer to RSWM product while still sensitive to land surface model variations.

The second simulation case assimilates the RSWM product with a

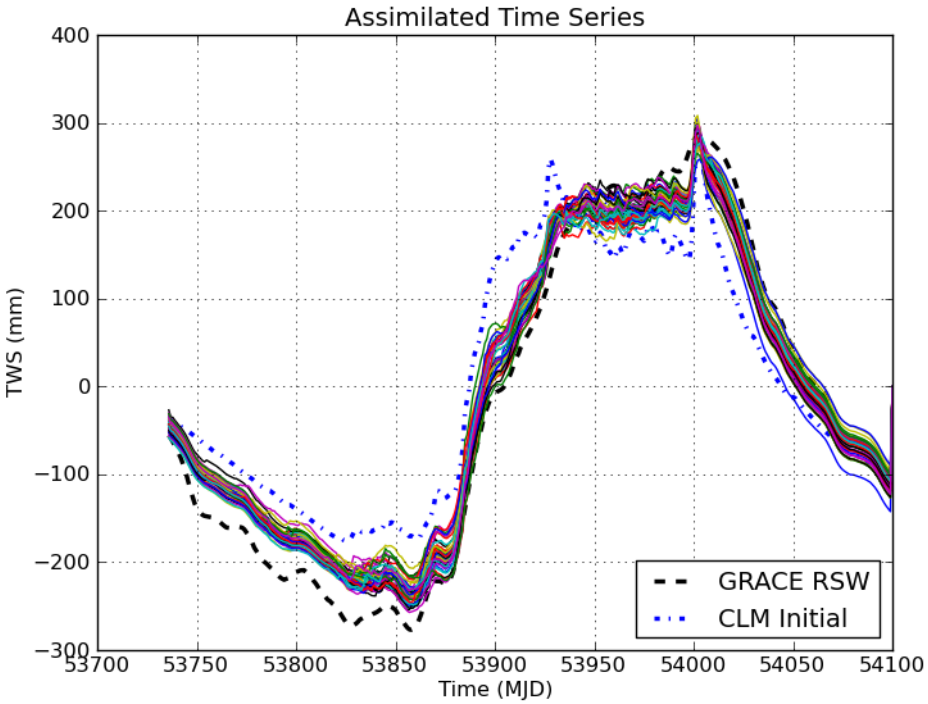

Figure 4.11: Gridcell Assimilation of GRACE into CLM

CRN-windowed CLM "observation" to calculate the model update and smooths the update in time. Thus, for each day the EnKF takes in an RSWM field, 40 CLM ensemble members each calculated over the CR9-47C21 window, and the error estimates for each. Each ensemble update will then be applied to each of the 21 input days to the CLM "observation". The CLM states are similarly propagated forward in time using the original model open loop day to day variations. This process is clearly more computationally intensive than the first case, especially if it were employed in the full land surface model assimilation system. Many more model runs would be required for the setup and application of each days assimilation.

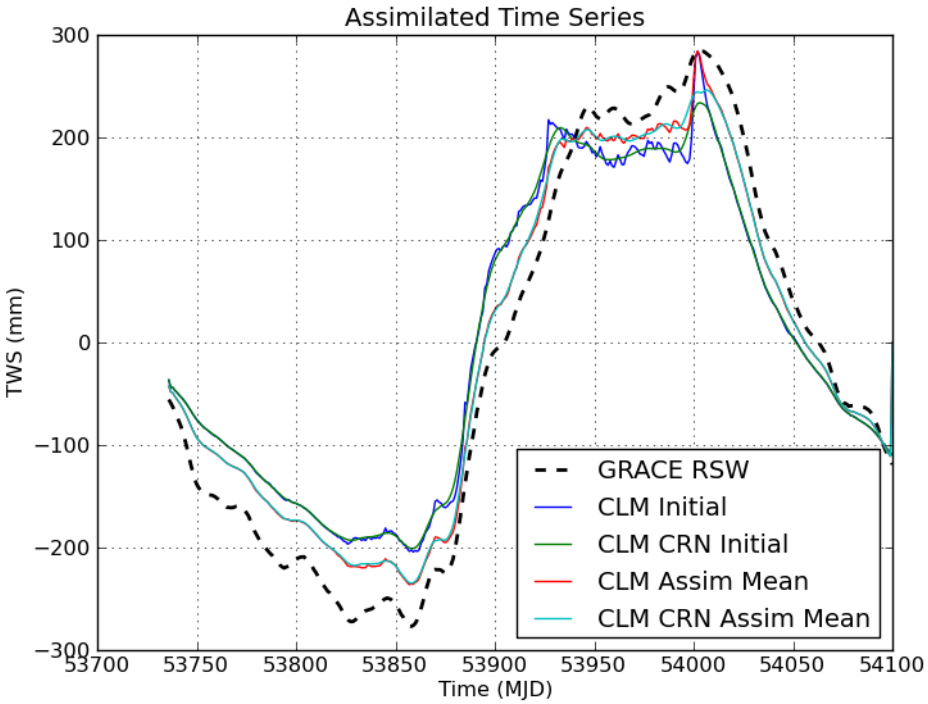

Figure 4.12: Assimilation Method Comparison

The resulting assimilated time series is very similar to the first case. The two are compared in Figure 4.12. The black dashed line represents the GRACE RSWM observations for the gridcell over the year. The blue line represents the ensemble mean of the open-loop CLM model run and the CRN-windowed CLM time series is shown in the green line for comparison. The red line is the ensemble mean of the first assimilation case and the cyan line shows the ensemble mean of the second assimilation case, where the model "observation" was windowed and smoothed in time. The two assimilated cases have a very similar overall structure. However, the second assimilation case clearly damps some of the high temporal frequency variations in the CLM assimilated

time series. The temporal smoothing of the assimilation update appears to overly constrain the model to the RSWM GRACE data and degrades some of the high resolution model information. The overall structure of the RSWM data is thus able to be conveyed with the simpler daily assimilation update and additionally better preserves the high temporal resolution information in CLM.

Chapter 5

Framework Analysis and Validation

The fundamental aim of data assimilation is to merge independent observational datasets with model predictions to improve the current model state so the model can then make more accurate predictions going forward. The observations provide independent and accurate information about one or more model states at a defined spatial and temporal resolution. The models provide continuity in time and space as well as dynamic coupling of the observations to adjacent and future states of the system [78]. A well designed framework for GRACE DA therefore correctly adapts and expands existing data assimilation techniques to the particularities of GRACE TWS assimilation. The assimilation system will continually improve the model accuracy while effectively downscaling the GRACE assimilation update to the higher resolution land surface model states. This thesis develops an assimilation framework that is effective, robust, and well-defined for assimilation of satellite gravity data into land surface models. The framework is constructed to be easily extensible for assimilation of the GRACE product into any land surface model and adaptable to GRACE Follow-On and future satellite gravity mission data.

5.1 The Experiment Design

To develop the GRACE data assimilation framework this study reconsidered the typical GRACE DA process. We combined a deep understanding of the GRACE mission with analysis of land surface models and data assimilation techniques to identify the elements of the GRACE product, assimilation algorithms, and methods which required adaptation to best fuse the two datasets. The foundation for current data assimilation systems was developed well before the GRACE mission for applications in atmospheric science, oceanography, etc. in addition to hydrology. Naturally, assimilation of a new data type will require the assimilation system to adapt and extend to optimally include the new data source. The new data source, in turn, can adapt to the needs of the assimilation system. This evolving system better updates and identifies deficiencies and strengths in the current hydrological model and assimilation techniques.

Assimilation of GRACE data presents a unique set of challenges as GRACE data products are calculated from a global inversion of the observations rather than by directly measuring a component of the system. The GRACE fields have anisotropic and correlated signal and error patterns at different temporal and spatial scales than LSM data. Previous studies performed basin scale [*(Zaitchik, 2008), (Houburg, 2012), (Forman, 2012)*] or regional [*Zhang, 2014*] assimilation of the monthly mean GRACE RL05 product with more simplistic error schemes. The assimilation framework improves the information available for and applicability of land data assimilation of GRACE TWS by:

- Innovative observational product formation to create a higher frequency GRACE RSWM product more representative of the hydrometeorological signal profile.

- Complete and accurate modeling of the signal and error content of the RSWM product for use in the assimilation.

- Adaptation and sensitivity analysis of existing data assimilation techniques to assimilate the GRACE RSWM information globally at the model one degree grid-space.

The larger signal profile available from the RSWM product and global, gridded assimilation reduces spatial and temporal smoothing requirements. More information from the GRACE data is thus input into the system with less spatial and temporal aliasing of the TWS signal. The framework elements (italicized) each address an aspect of the total assimilation system (the land surface model, the filter algorithms, and the observational data) that is developed, tuned, or adapted in this analysis to accomplish these items.

The RSWM product and associated error sequences developed in Chapters 2 and 3 (*realization of observations*) increase the hydrometeorological signal content, reduce signal aliasing, and better represent the magnitude and pattern of error in the observational data. The higher frequency GRACE RSWM product can be assimilated either daily into the land surface model or at different *assimilation update rates*. The experimental design determines the best assimilation rate for the new product over the focus regions. A constant

2 cm error estimate has typically been applied to the GRACE data in previous assimilation studies. We test the effect of updating the GRACE error in the assimilation system with the new error estimates and error clones via the *modified assimilation algorithms*. The assimilation update calculated from the comparatively coarser resolution GRACE data is spatially smoothed over the CLM grid. The extent of the spatial smoothing is tested in the assimilation system through variation of the *Gaspari-Cohn localization radius* to account for the resolution discrepancy between GRACE and CLM. Finally, we test the ability of assimilation to condition the model and thus improve forecast runs. Quantification and analysis of the *open-loop error growth* informs latency requirements for operational data assimilation systems.

Analysis of the GRACE land data assimilation framework is split into (i) The Spatial Dimension, (ii) The Temporal Dimension, and (iii) Effectiveness of the Assimilation Framework. The Spatial Dimension analyzes the signal placement, magnitude, and any artifacts of the assimilation update. The Gaspari-Cohn localization radius and GRACE error estimates are used to tune the magnitude and spatial distribution of the assimilation update. These parameters are tested in the assimilation system and define a baseline assimilation case for the rest of the chapter. The basic setup for the assimilation system, and the three primary cases defined in the spatial dimension analysis are outlined in Table 5.1. Case 1 performs daily assimilation of the RSWM product via the Ensemble Adjustment Kalman Filter (EAKF) with a globally constant error estimate of 2 cm as has been used in previous work ([74], [95]). Next, assimilation is performed again with the EAKF but with the

spatially varying error variance field developed in Chapter 3. The Ensemble Adjustment Kalman Filter is used in Cases 1 and 2 rather than the traditional Ensemble Kalman Filter as it was shown to reduce random noise introduced by the EnKF. Both the EAKF and EnKF methods use the same Bayesian foundation and have the same expected value for the assimilation update [3]. Finally, the error clones created from the full RSWM error covariance are implemented in the Ensemble Kalman Filter routines. Because the focus of this study is land hydrology, the GRACE RSWM estimates over Antarctica are not included in the assimilation.

Feature	Case 1	Case 2	Case 3
Land Surface Model	CLM	CLM	CLM
Atmospheric Forcing	CAM	CAM Ensemble	CAM Ensemble
Number of Ensembles	40	40	40
Observation	GRACE RSWM	GRACE RSWM	GRACE RSWM
Observation Error	2cm	Spatially Varying	Error Clones
Filter Type	EAKF	EAKF	CEnKF
Ensemble Inflation	Restart	Restart	Restart

Table 5.1: Assimilation Tools and Methods Specification

The Temporal Dimension entails analysis of the frequency profile of the baseline assimilated time series and the necessary rate of assimilation of the RSWM product. A correctly assimilated time series will reflect the high resolution land surface dynamics of the LSM while likely increasing power at low frequencies due to the (typically) larger overall signal of the GRACE data. As much of the power of land surface processes can be captured at sampling rates greater than one day we test the effect of reduced assimilation update rates. The assimilation update rate is a balance between computational limitations,

the necessary sampling rate of the time series, and the response of the DA system. Less frequent assimilation will reduce computational requirements, but at what cost to the assimilation system?

Finally, the performance and time evolution of the assimilation system is tested in the Effectiveness of the Assimilation Framework. We evaluate the evolution and accuracy of the data assimilation system, the ability of the assimilation framework to condition the model, and open loop error growth in forecast runs. Assimilation systems are prone to filter divergence, where the system becomes insensitive to new observational information. This is combated with ensemble inflation to ensure a reasonable variance between the model ensemble runs, a method which must be judiciously implemented to not upset the global water balance. Next, we quantify the assimilation spin-up time (the time for the model and observational data to be within their error bounds) and open loop error growth (the departure of conditioned model forecasts from the observational data without assimilation). These metrics are important for the implementation of operational data assimilation systems and advise latency requirements for observational data products.

5.2 The Spatial Dimension

As discussed in Chapter 4, the DART/CLM assimilation process follows: (1) calculation of an observation-space update (one degree, TWS), (2) spatial smoothing of the observation-space update as defined by the Gaspari-Cohn localization radius, and (3) vertical disaggregation to the CLM state variables. The updated CLM states are sensitive to the tunable parameters

(Gaspari-Cohn localization radius, GRACE error profile, assimilation update rate) in this process. The assimilation system was designed to improve the accuracy of the CLM water storage state variables while appropriately downscaling the coarser resolution GRACE data to the higher spatial and temporal resolution of CLM.

The assimilation update is controlled by filter parameters, the CLM ensemble spread, and the GRACE error profile. The filter rejects "outliers", observations greater than a defined distance from the CLM ensemble mean (3σ in this analysis). This ensures that outliers in the observational data, which could corrupt the model, will not be assimilated. Additionally, it prevents large overall increases or decreases in the LSM global water storage from a single assimilation update - which could upset the global water balance outside of the tolerance level. Particularly at the beginning of the assimilation process when there are larger discrepancies between CLM and GRACE TWS values, valid GRACE estimates may be excluded from assimilation. There is thus a necessary spin up, or calibration, time for the GRACE and CLM water storage values to converge and increasingly more observations are included in the assimilation (further examined in Section 5.3).

To introduce the discussion, the first assimilation update for Case 1 on January 2, 2005 is shown in Figure 5.1 (a). For comparison, the difference between the model estimated state on that day and the GRACE RSWM solution is shown in Figure 5.1 (b). Figure 5.1 (a) follows the general pattern of the GRACE and CLM difference in (b), particularly in mid-latitudes, but is lower in magnitude overall. This magnitude discrepancy is expected so the

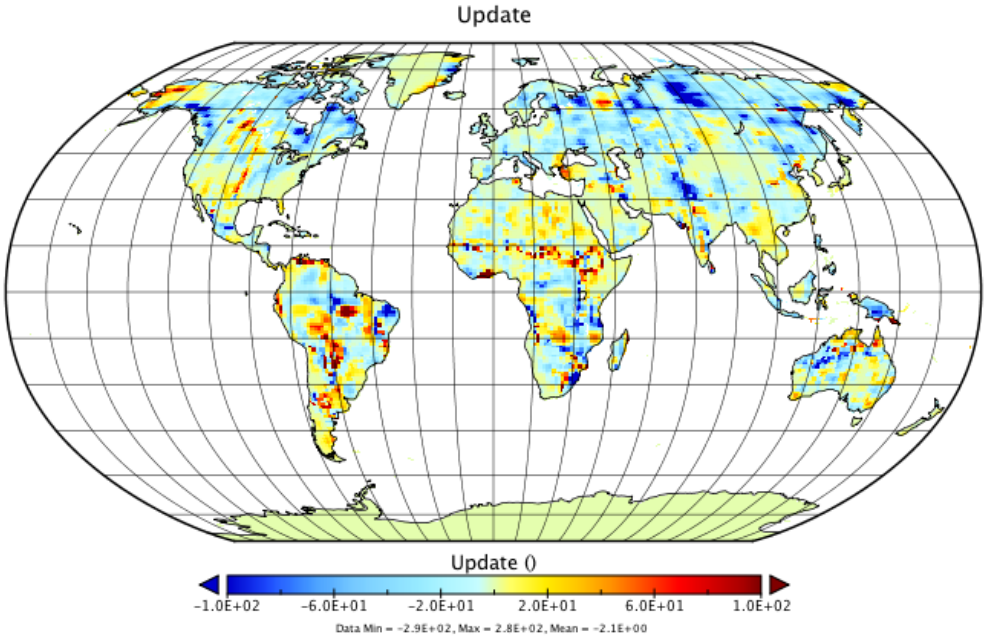

(a) Case 1 first assimilation update to CLM with the RSWM GRACE data

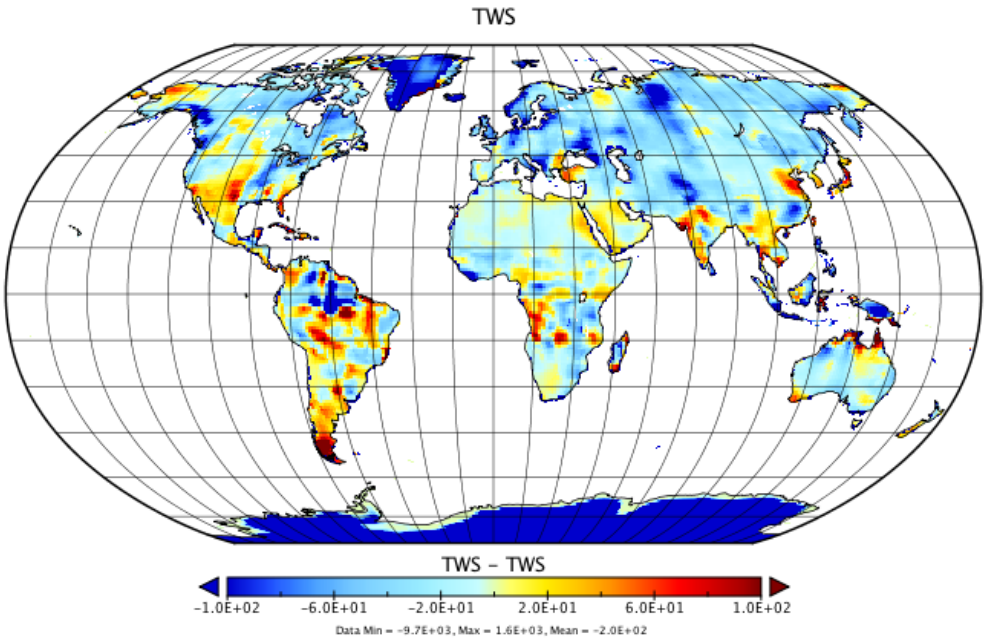

(b) TWS difference between the CLM Open Loop Run data and the RSWM GRACE information

Figure 5.1: Comparison of the assimilation update and CLM/GRACE differences for 2005-01-02 at the start of the data assimilation process.

assimilation system does not force the model to follow GRACE, but balances the signal and error profiles of the model and observational data. Additionally, large net increases or decreases in land TWS from the assimilation update could upset the global water balance of the land surface model. Global and regional assimilation characteristics will be discussed in more detail throughout this chapter.

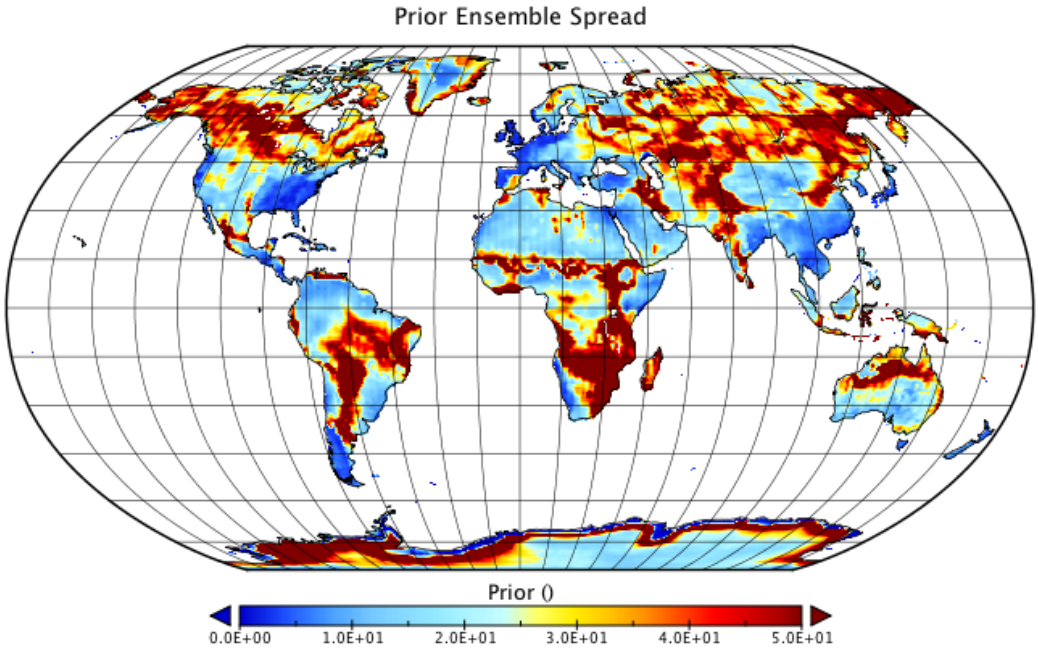

Figure 5.2: Standard deviation of the CLM ensemble TWS "observation", 2005-01-02, prior to assimilation

The threshold for outlier rejection, the weight given to the LSM data in the filter, and the ensemble covariance used to downscale the observation space assimilation update are computed from the spread of the CLM ensemble states. The ensemble states, as discussed in Chapter 4, are spun up for several hundred

years with the ensemble atmospheric forcing dataset to represent uncertainty in CLM and the input atmospheric forcing data. Figure 5.2 shows the standard deviation of the CLM ensemble states at the first date of assimilation, January 2, 2005. GRACE observations in regions of higher CLM ensemble variance are less likely to be rejected as outliers and more favorably weighted by the filter algorithms.

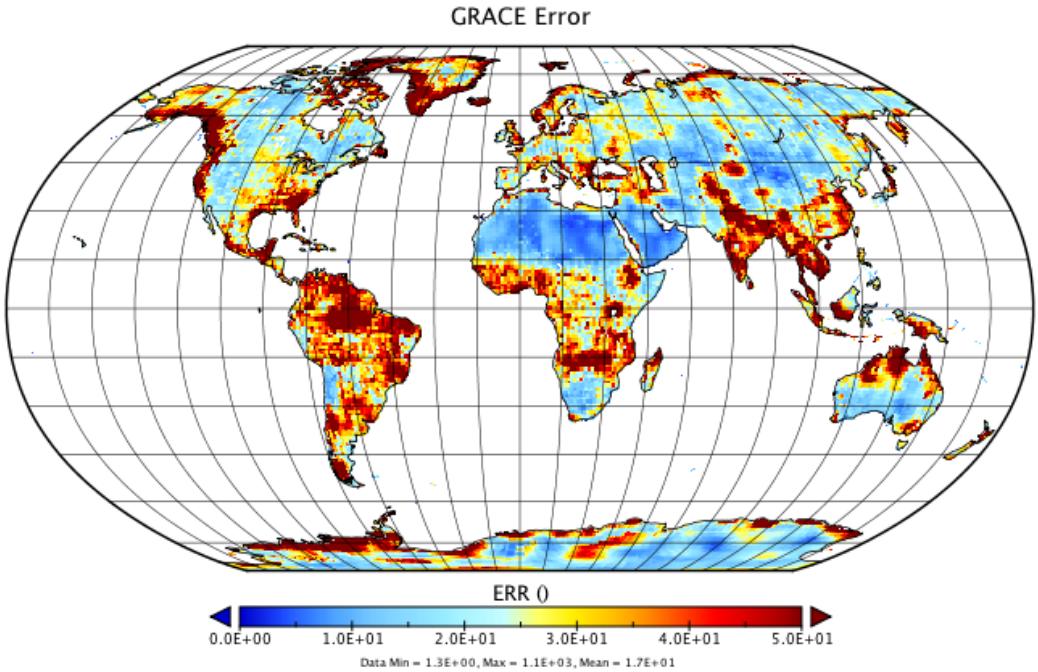

Figure 5.3: The GRACE spatially-varying error estimate

Similarly, the weight assigned to the GRACE observational data in the filter is advised by the GRACE error profile. Figure 5.3 shows an approximation of the error in the RSWM product - the RMS of the error estimates developed in Chapter 3. This section will test the effect of the GRACE error estimate on the assimilated results with respect to the CLM ensemble spread.

As this study is focused on the elements of the assimilation framework specific to assimilation of satellite gravity data, characterization of the land surface model error profile and determination of the ensemble perturbation methods is outside of the scope.

The tunable parameters relevant to the spatial dimension of the GRACE assimilation framework are the Gaspari-Cohn localization radius and GRACE error estimate. Analysis and assessment of these parameters further specializes the data assimilation framework for the unique error profile and formulation of the GRACE product. Horizontal smoothing via the Gaspari-Cohn localization radius reflects the coarser resolution and spatial correlation of the GRACE data. The improved error estimates from the simulation analysis in Chapter 3 better represent the various components and sources of error and their representation in science data products. In addition to error inherent in observational data from the GRACE mission, the new error estimates are specialized to represent the unique signal and error properties of the RSWM dataset.

5.2.1 Tuning the Gaspari-Cohn Localization Radius

The Gaspari-Cohn localization radius, as described in Section 4.3.3, determines the spatial smoothing of the assimilation update. Specifically, localization defines the weight and extent of the spatial distribution of the observation space (one degree gridded, TWS) update to the CLM state variables. The GRACE RSWM data has a spatial resolution of 200-300 km, coarser than the 1 degree grid it is represented and assimilated at. Spatial smoothing

appropriately distributes the assimilation update in space. The localization radius is defined by a halfwidth angular distance, in radians. The Case 1 assimilation setup is used to test the differences between localization radii of 0.03, 0.04, and 0.05 radians corresponding to approximately 150, 200, and 250 km (halfwidth) spatial resolutions. The assimilation updates calculated with the three localization radii are compared in Figures 5.4 and 5.5.

	0.03 rad	0.04 rad	0.05 rad
Global Update Power	31.3 mm	36.8 mm	41.5 mm
RMSE of Difference from RSWM	70.0 mm	69.9 mm	70.0 mm

Table 5.2: Assimilation update specification

Figure 5.4 shows the three observation space assimilation updates for January 2, 2005. All show very similar placement of the assimilation update at a global scale. As the localization radius increases, the magnitude and spatial extent of the signal updates can be seen to slightly increase. The overall power in each global assimilation update, calculated as the global RMS of the update, increases with increasing localization radius from approximately 3 cm with a 150 km localization radius to 4 cm with 250km (documented in Table 5.2). The RMSE between CLM and GRACE, calculated as the root mean square error of the difference between the updated CLM state and the GRACE RSWM product stays relatively static with increasing localization radius. This suggests that overall power in the GRACE/CLM difference is relatively insensitive to the localization radius. At the global scale it is difficult to assess the differences and relative strengths of each assimilation case. Thus, we next take a regional view of the assimilation updates for a more focused

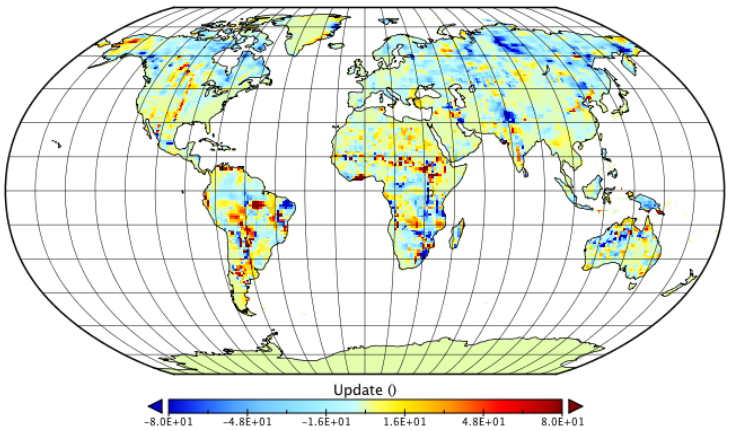

(a) 150 km (0.02 rad) localization radius

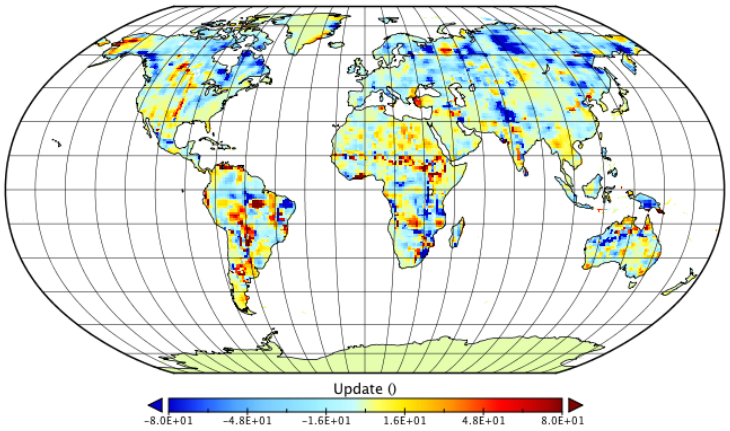

(b) 200 km (0.03 rad) localization radius

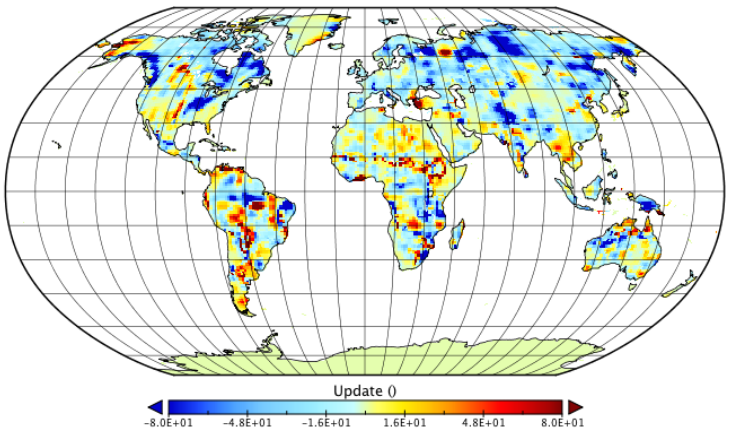

(c) 250 km (0.04 rad) localization radius

Figure 5.4: Case 1 assimilation update tested with different localization radii

analysis.

The initial difference between the GRACE RSWM dataset and the CLM modeled TWS is compared with the three assimilation updates over the United States in Figure 5.5. The assimilation updates (b), (c), and (d) correspond to increasing localization radii of 150km, 200km, and 250km. Again, the magnitude and (spatial) size of the update increases with increasing localization radius. However, with this closer view we can see that the Figure 5.5 (d) overestimates the assimilation update in the Ohio River Valley and in Quebec. The large localization radius is compounding the assimilation update in these regions. Essentially, adjacent gridcells are spatially smoothing each TWS update on top of each other. This clearly shows that the localization radius is too large. Rather than ensure the magnitude and extent of the slightly coarser resolution GRACE data is accounted for, the large Gaspari-Cohn localization radius is amplifying the signal content of the assimilation update.

In contrast, the assimilation update using the smallest localization radius in (b) is quite small, essentially zero in the eastern and western United States. The tighter localization radius limits the range over which the observation-space TWS update is distributed to the CLM state variables. The assimilation update in Figure 5.5 (c), with a 200km localization radius half-width, balances the characteristics of (b) and (d). The magnitude and extent of the assimilation update in (c) most closely matches that of the GRACE/CLM difference, without over-amplifying the signal or losing information. Analysis of other regions shows similar results, as seen in Figure 5.6 for the second focus region, Bangladesh. Again, the 200 km localization radius half-width is able to best

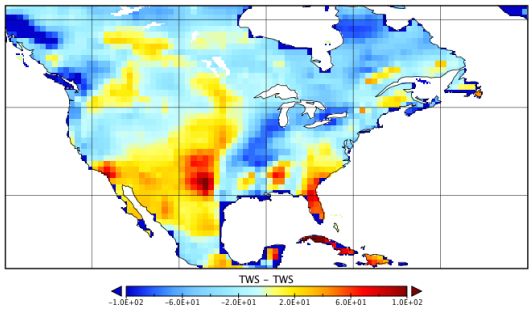

(a) GRACE-CLM Difference

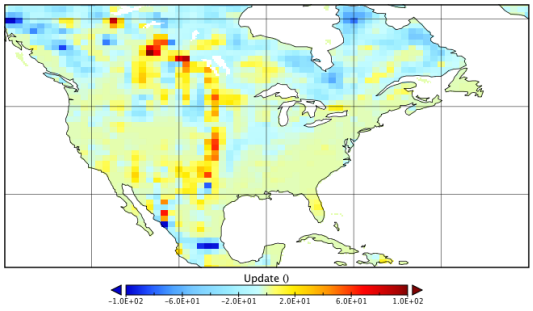

(b) Assimilation update: 150 km

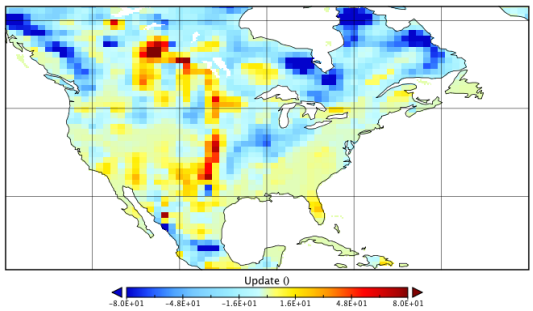

(c) Assimilation update: 200 km

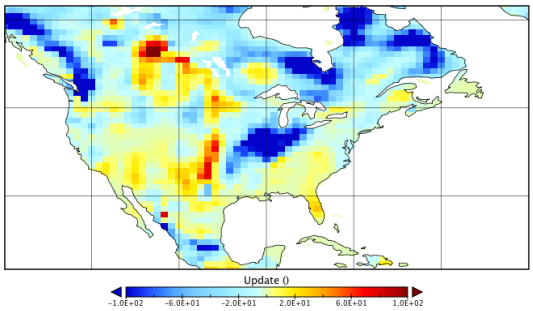

(d) Assimilation update: 250 km

Figure 5.5: Spatial pattern of the assimilation update differences in the United States

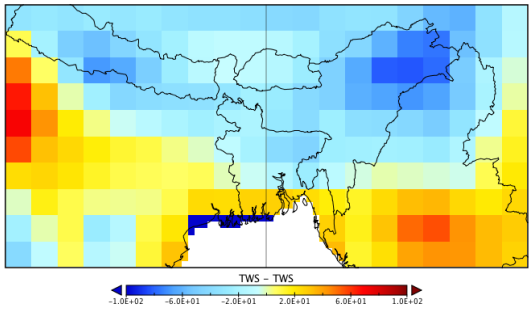

(a) GRACE-CLM Difference

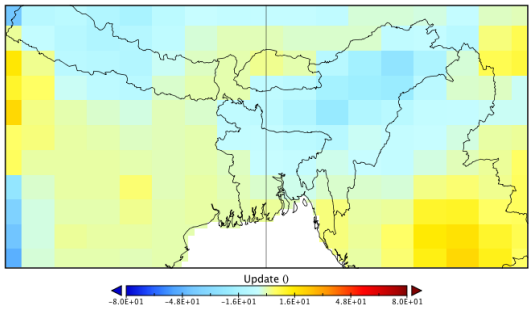

(b) Assimilation update: 150 km

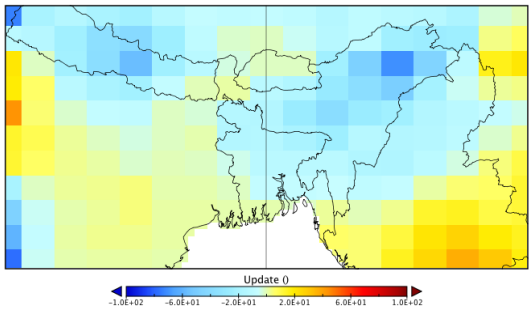

(c) Assimilation update: 200 km

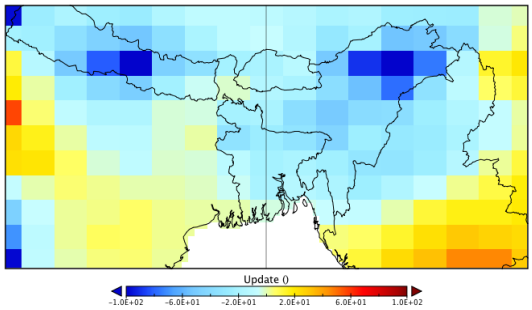

(d) Assimilation update: 250 km

Figure 5.6: Spatial pattern of the assimilation update differences in Bangladesh

capture the magnitude and spatial pattern of the GRACE-CLM difference. This analysis was performed at the first assimilation epoch so that the effects of the localization parameter in amplified in the larger necessary assimilation update. As will be seen in Figures 5.9 and 5.10 later in this section and in Section 5.4, the assimilation system correctly moves the assimilated data to an equilibrium between the CLM and GRACE signal and error estimates. The Gaspari-Cohn localization radius helps to maintain this steady state over time.

It is also noted that assimilation artifacts arise in some regions, such along the southern border of the Sahara, in Figure 5.4. As these artifacts can be disguised in a global view of the assimilated states, Figure 5.7 gives a closer view of this region. Figure 5.7 (a) shows the CLM estimated TWS without assimilation. After assimilation with localization radii of 200 km (b) the assimilation update clearly introduces artifacts into the CLM estimated TWS. These artifacts persist regardless of localization radius or GRACE error estimate assimilation scheme. The root cause is traced to a large amplitude small scale features in the ensemble spread, shown in Figure 5.7 (c). The assimilation artifacts are thus a limitation of the ensemble perturbation methods used in this analysis. They are, however, limited to regions such as the Sahara with little to no true TWS signal patterns to drive the ensemble spread. Therefore, neither focus region was prone to these artifacts (as would have been noted in Figures 5.5 or 5.6). The assimilation artifacts do highlight the necessity of regional tuning of the observation and model error estimates so that small scale errors do not upset the assimilated results.

Lastly, we test if the Gaspari-Cohn localization radius impacts the spa-

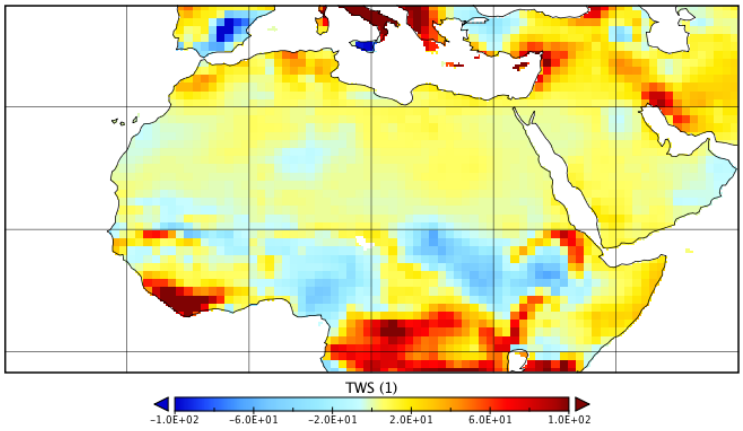

(a) Open-loop CLM TWS

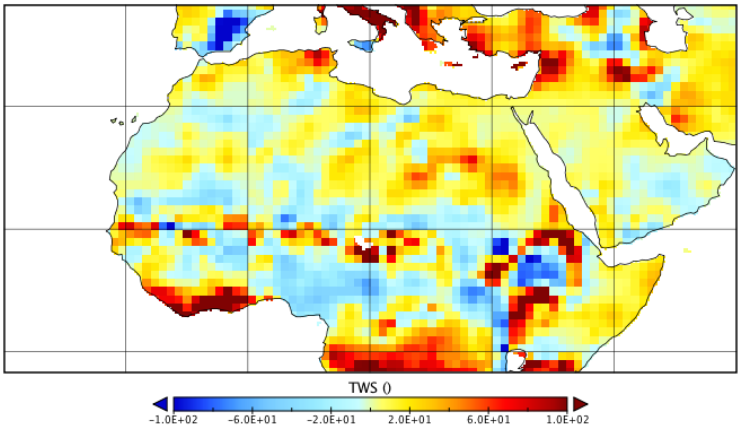

(b) 200 km (0.03 rad) localization radius assimilated results

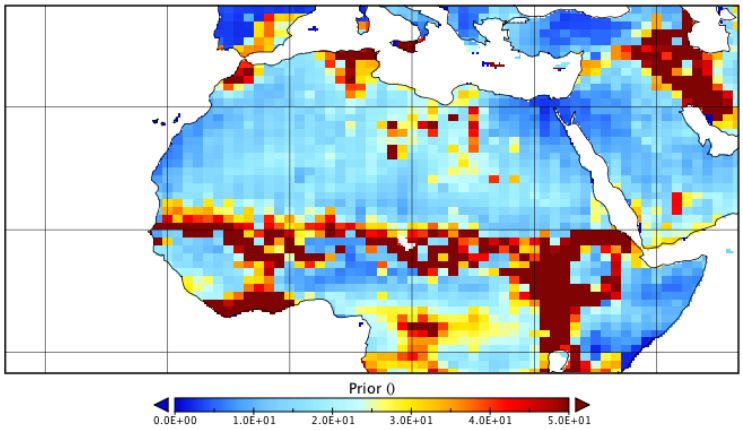

(c) CLM Ensemble Spread

Figure 5.7: Assimilation artifacts in the south Sahara Desert

tial resolution of the assimilated results. The spatial resolution of the land surface model should not be impacted if the assimilation framework appropriately downscales the coarser resolution GRACE RSWM product to the model resolution. The GRACE/CLM assimilated grid should follow the large scale features of the GRACE data and the smaller scale features driven by the high resolution land surface dynamics of CLM. The spatial resolution is assessed through comparison of the degree variance, similar to the analysis in Section 2.4.1, and analysis of the spatial distribution of TWS signals present in the assimilated results.

Each global grid (CLM open-loop, assimilation with 200, 250, 300 km localization radii) was decomposed into the spherical harmonic domain to illustrate the spatial resolution variations via the degree variance. In 5.8 the degree variance of all four fields are seen to be very similar. The assimilation cases show slightly higher power at nearly all frequencies (from assimilation of the higher power RSWM product). Unlike Figure 2.11, where the spatial resolution of the RSWM product was assessed, there is no degree crossover point to identify a lower resolution dataset.

The assimilated results and CLM show nearly identical spatial resolution and thus no evidence of resolution degradation from GRACE assimilation in the degree variance at this global level. Accurately assimilated grids should follow the broad scale features of the RSWM dataset while retaining the higher resolution spatial features driven by the model physics. Figures 5.9 and 5.10 look at the broad and finer signal patterns at a regional scale to better identify if this is accomplished in the assimilation. A comparison of the spatial

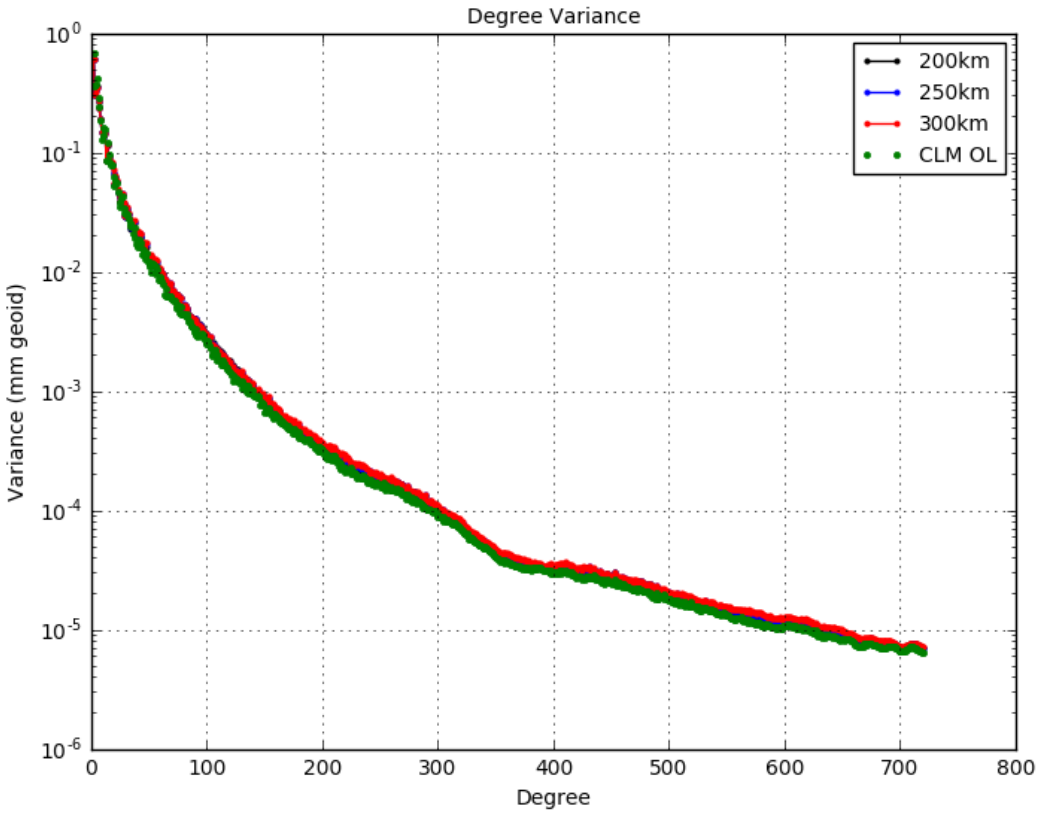

Figure 5.8: Degree variance comparison of the open-loop CLM data and Case 1 assimilation at different localization radii

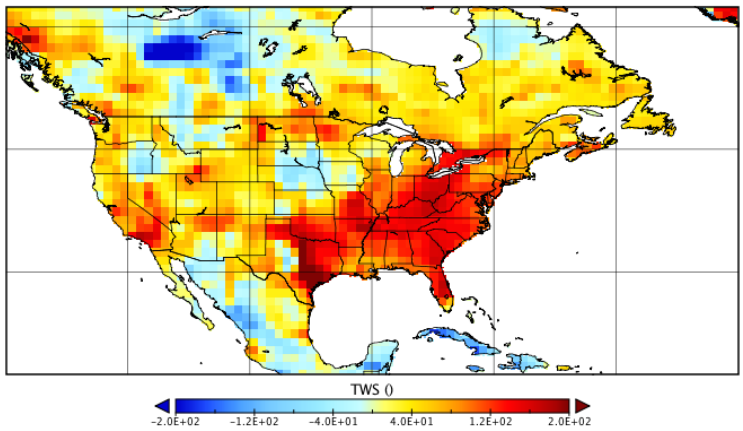

(a) The full TWS signal in the assimilated results

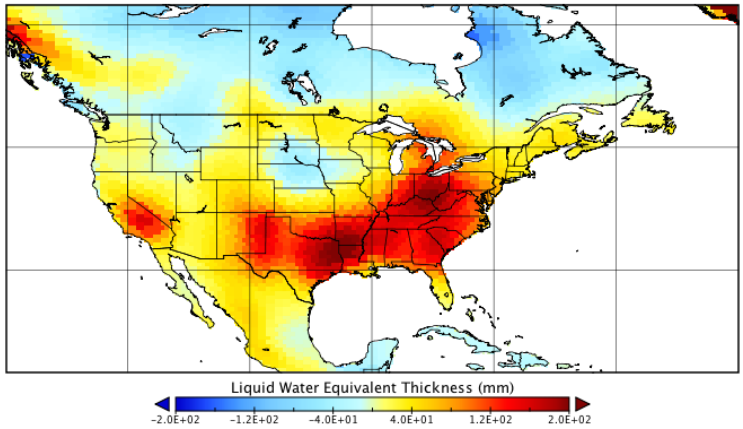

(b) The full TWS signal in the RSWM product

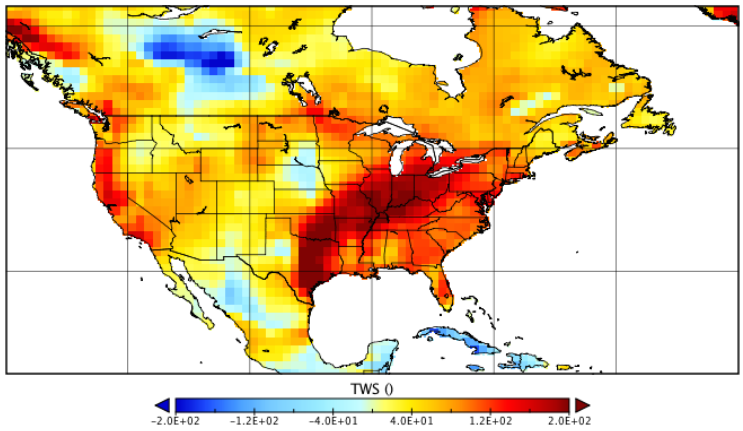

(c) The full TWS signal in an open-loop CLM run

Figure 5.9: Comparison of the large-scale signal profile after a month of GRACE assimilation into CLM (January, 2005)

distribution of the full TWS signal after the assimilation system has reached equilibrium (after a month of assimilation) is shown in Figure 5.9. The assimilated results in (a) follow many of the broad signal patterns of the RSWM dataset (b). The TWS signal is reduced in comparison to CLM (c) in northeastern Canada, the TWS signal in California has been shifted south, and the high (dark red) TWS signal in the midwest has been shifted westward.

To identify the smaller scale features in TWS, an annual, semi-annual, and trend is fit to each gridcell and removed from the RSWM, CLM, and assimilated data. Figure 5.10 plots the residual signal of the three datasets at the same epoch as 5.9 after these large seasonal features have been removed. The assimilated dataset (a) clearly shows more small scale features than the RSWM residual signal in (b). The small scale features change more rapidly in space and have a higher range of variation, similar to the residual CLM signal in (c). There is relatively good agreement between (a) and (c) but the two do not match perfectly - as expected between an open loop and assimilated dataset. The smaller scale features prevalent in the residual assimilated dataset illustrate the accuracy of the assimilation framework in the spatial dimension. The ensemble assimilation system effectively downscales the coarser resolution GRACE TWS data to the higher resolution land surface model domain. The Gaspari-Cohn localization radius of 0.03 radians (200 km) is therefore able to both accurately distribute the magnitude and spatial pattern of the assimilation update.

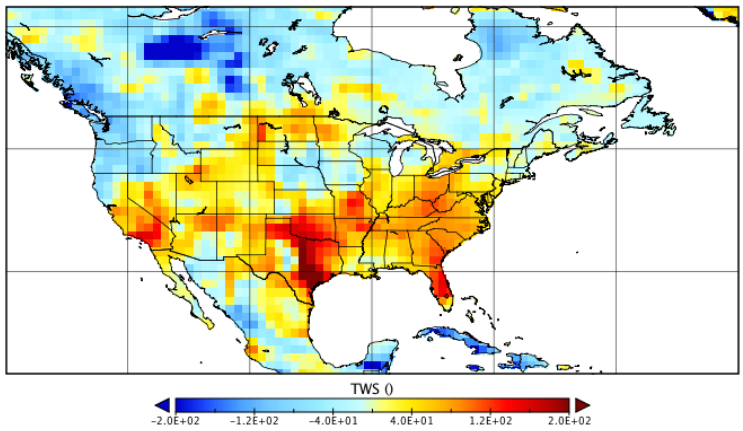

(a) Sub-seasonal TWS signal in the assimilated results

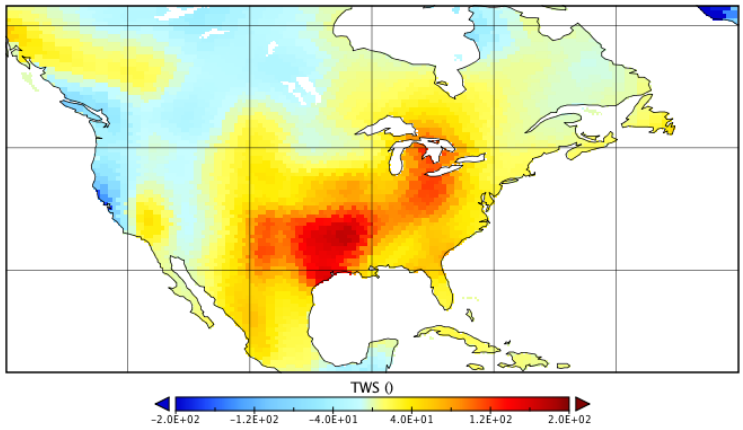

(b) Sub-seasonal TWS signal in the RSWM product

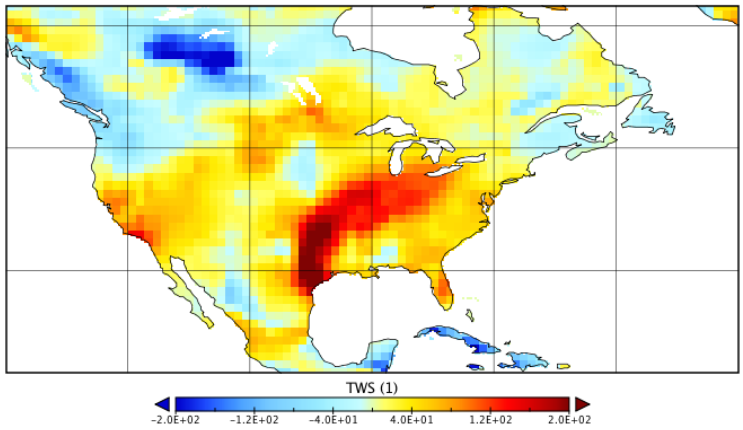

(c) Sub-seasonal TWS signal in an open-loop CLM run

Figure 5.10: Comparison of the small-scale signal profile after a month of GRACE assimilation into CLM (January, 2005)

5.2.2 The GRACE Error Profile in Assimilation

The GRACE data products are characterized by anisotropic and correlated error patterns. As discussed in Chapter 3, the quality of each gravity field estimate is affected by the satellite ground track pattern, spatial coverage, downward continuation, and spatial and temporal aliasing. The newly developed error estimates better represent the magnitude, spatial distribution, and properties of the error in the GRACE data and RSWM product specifically. This section assesses the sensitivity of the assimilation system to the three Assimilation Cases for GRACE error representation outlined in Table 5.1. The first case uses a constant 2cm error estimate for GRACE as has been previously implemented in basin scale assimilation systems. The global 2cm error field is an underestimate of the gridcell level error estimate, but used as a baseline for the assimilation. Case 2 uses the spatially varying GRACE error estimate from Chapter 3 (Figure 5.3). Case 3 implements the error clones via the modified assimilation algorithms.

Figure 5.11 (a) maps the difference in the assimilation update between Cases 1 and 2. The corresponding difference in the error field is shown in (b). The assimilation update variation between the cases generally follows the spatial pattern of the difference in the error estimates in (b): note the larger assimilation update differences in the Amazon, along the Pacific coast of northern Canada and Alaska, etc. The mean difference between the updates is very small, only 0.04 mm, thus roughly the same net amount of TWS is added to the model. The constant 2cm error case, as expected from its lower estimate of the error in GRACE, shows a lower RMSE between the GRACE and CLM

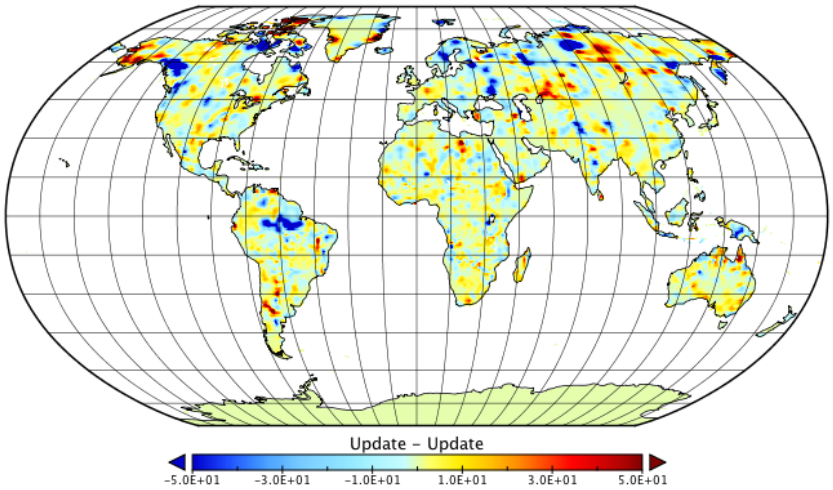

(a) Difference in the Assimilation Update from Case2 - Case1

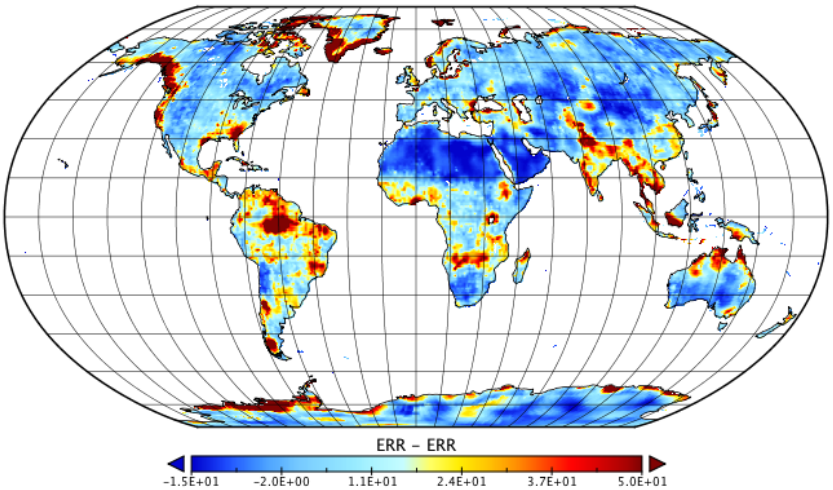

(b) Error estimate difference: Spatially-varying GRACE error - 2cm

Figure 5.11: Comparison of the assimilation update (a) from the different GRACE error estimates (b)

ensemble states post-assimilation by approximately 5 mm comparison to Case 1.

As features of the assimilation are again difficult to examine at the global scale, Figure 5.12 zooms in on the assimilation differences over the US. The Pacific Northwest and Southeast US show the largest differences in the error estimate fed into the assimilation. Additionally, both regions show larger discrepancies between the GRACE and CLM data (Figure 5.5). However, the assimilation update responds differently to the new error information in each region due to the relative size of the GRACE and CLM error estimates. In the southeastern US, CLM has a very low ensemble spread and thus is resistant to any updates from the observational data nearly irregardless of the GRACE error estimate. Differences in this region between Case 1 and 2 assimilation updates are at the millimeter level. In the Pacific Northwest, however, the ensemble spread of CLM is larger and comparable to the error level in the spatially-varying GRACE estimate. The lower 2cm error estimate in Case 1 thus led to a larger assimilation update from the GRACE observational data than from Case 2 assimilation.

The assimilation difference between Cases 1 and 2 was expected to be noticeable. There was a relatively large discrepancy between the error estimates, as seen in Figure 5.11 (b) at values comparable to the ensemble spread in CLM. Even with the relatively large change in the GRACE error estimate the assimilation update was, for most regions of the world, changed by a relatively small amount. The transition from the error representation in Case 2 to Case 3 is more subtle. Both error profiles are informed by the simulation anal-

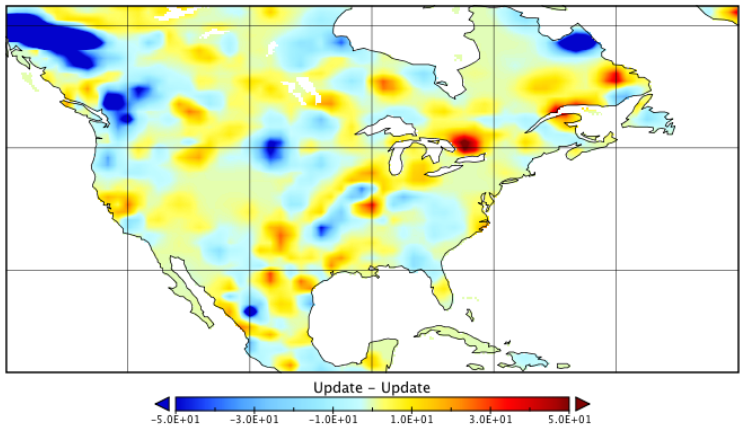

(a) Assimilation update difference: Case2 - Case1

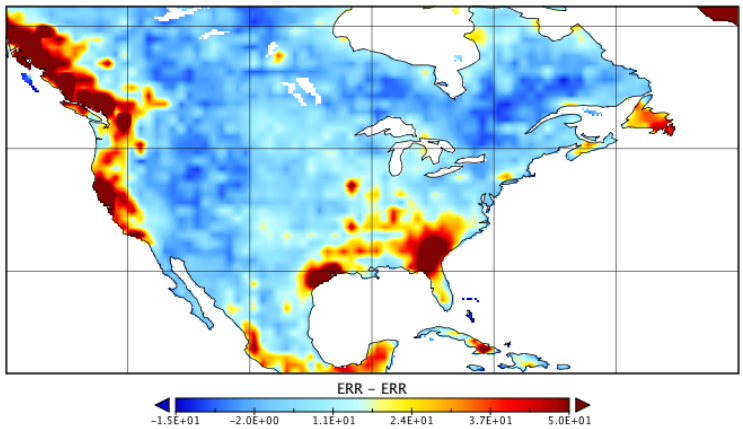

(b) Error estimate difference: Spatially-varying error - constant 2cm

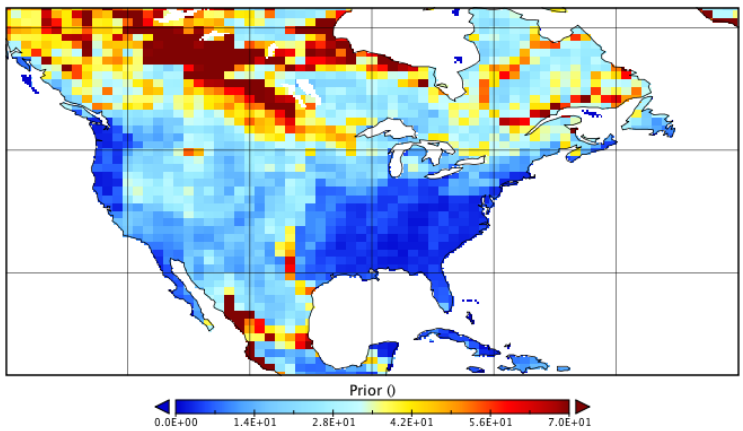

(c) CLM Error representation: Ensemble spread

Figure 5.12: Comparison of the assimilation update (a) from the different GRACE error estimates (b)

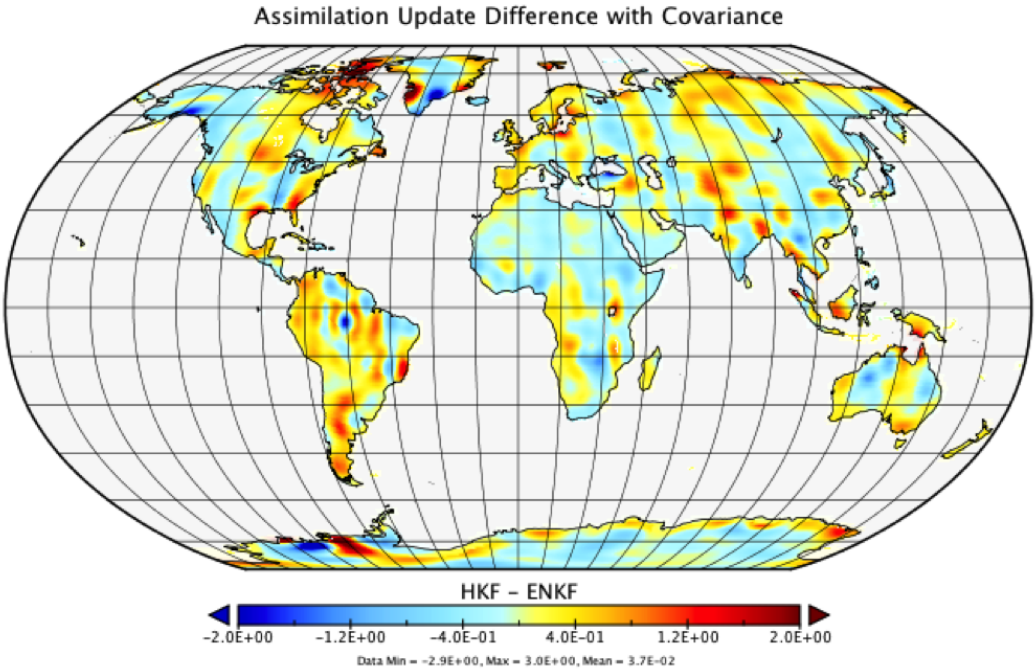

Figure 5.13: Difference in the Assimilation Update from Case3 - Case2

ysis developed in Chapter 3. Case 2 uses the variance of the estimated error in the RSWM product in the Ensemble Adjustment Kalman Filter, while Case 3 incorporates the full covariance information into the assimilation. As described in Section 4.3.2.2, the RSWM covariance is used to create error clones (shown in Figure 3.15) which perturb the ensemble members in the Covariance Ensemble Kalman Filter. The difference in the assimilation update between these two cases is shown in Figure 5.13. Cases 2 and 3 show quite similar assimilated results, varying only at the mm level (Note the scale change from +/- 5cm in Figure 5.11 to +/- 2mm in Figure 5.13). The difference in the GRACE error representation between the cases is very small in comparison to the current overall level of error in GRACE and CLM TWS estimates. The baseline assimilation case for the rest of this chapter implements Case 3 assimilation with a 0.03 rad localization radius. The simulation error information from Chapter 3 best represents the patterns and magnitude of error in the RSWM product, and the 0.03 rad (150km) localization radius best distributed the assimilation update in space.

What have we learned from assimilation of the different GRACE error estimates? The error estimate in Case 1 was known to be unrealistic at the gridcell level. The analysis did, however, show different aspects of the sensitivity of the assimilation system to the GRACE error estimate. If the ensemble spread is very small or very large, the filter is relatively insensitive to the GRACE error profile. Similarly, if the error estimate for the GRACE datasets is very large or small the ensemble spread will have less of an impact upon the assimilated results. This assessment of the spatial dimension of as-

similation highlights the necessity of regional tuning of the error estimates in the observational and land surface model data. Regional analysis of the two datasets is necessary to ensure that the assimilation parameters are tuned to the unique signal and error patterns of each region.

The assimilated results did not respond strongly to the modified assimilation algorithms and inclusion of the GRACE covariance information in Case 3 as the variation in representation of the error in GRACE was below the sensitivity of the filter. At the global scale, the discrepancy between the total error in the CLM and GRACE datasets is much larger than the alterations in the representation of the error in the current GRACE product. Gridded global assimilation has many benefits: it allows the global water balance to be maintained, larger scale interactions to be modeled, and more easily downscales the assimilation updates to the state variables than basin-scale assimilation (less spatial smoothing is required). Future time variable gravity datasets with reduced error levels and finer spatial or temporal resolutions will be more sensitive to these variations. As computational models and observational data evolves, these considerations will be increasingly important and the Covariance Ensemble Kalman Filter offers a relatively simple method to include the error covariance information in data assimilation.

5.3 The Temporal Dimension

The Community Land Model 4.0 simulates land surface dynamics at time scales as short as thirty minutes and reflects seasonal and diurnal cycles, transient events, longer term processes, etc. while maintaining system water

and energy balances [57]. Assimilation of GRACE terrestrial water storage data steers the model states toward the true Earth system state and acts as a boundary condition on the land surface dynamics. The temporal characteristics of the model and GRACE data are analyzed within the assimilation process to ensure appropriate assimilation updates are calculated which best improve the accuracy of the land surface model data at its higher temporal resolution. The updated window design of the RSWM GRACE product significantly reduces the resolution discrepancy between GRACE and CLM leading to more frequent and simpler assimilation. We assess the frequency profile of the assimilated time series and its comparison to the frequency characteristics of the RSWM and CLM input datasets. Considering the necessary sampling rate of the time series, we then establish bounds for a necessary assimilation update rate to balance computational loads and performance of the DA system.

5.3.1 Frequency Profile of the Assimilated Time Series

Analysis of the GRACE RSWM and CLM terrestrial water storage estimates in Chapter 2 showed the two products have similar frequency profiles until the RSWM filter bandwidth of 20 cpy. The RSWM product generally showed higher power in the low frequency range (1-10 cpy) and significant damping above 20 cpy due to the low pass filter effect of the CRN window. A correctly implemented DA framework will fuse the more accurate lower frequency power of the GRACE data with the high resolution, high frequency power of the CLM time series. The resulting time series blends the strengths

of the GRACE and CLM datasets to maintain higher power at all frequencies. This section analyzes the performance of frequency characteristics of the baseline assimilation case within the full DA system. Each RSWM field is assimilated against the CLM daily mean TWS, as the analysis in Section 4.3.4 showed this daily assimilation scheme to better preserve the high resolution model information. The RSWM product was developed to increase the hydrometeorological signal content, and boosts the bandwidth of the GRACE time series from 6cpy to 20cpy. The data assimilation framework is specifically tested for its ability to incorporate the RSWM information in this bandwidth while retaining the higher frequency model resolution in the two focus regions, Texas and Bangladesh.

The TWS time series and associated amplitude spectrum of the CLM/ GRACE assimilated data, GRACE RSWM, and CLM estimates in Texas are shown in Figure 5.14. The RSWM time series shows larger overall signal amplitude changes which vary more smoothly in time than the lower amplitude, more rapidly varying CLM estimates. The assimilated time series, in red, is seen to blend the two characteristics in Figure 5.14 (a). It follows some of the larger scale RSWM variations with more day-to-day variability of CLM. These features are reinforced in the amplitude spectral density of Figure 5.14 (b). Except for the lowest data point on the frequency spectrum, the assimilated time series follows the data source with higher power. In the lower frequency range until 20 cpy the higher power of the RSWM time series is dominant. At frequencies greater than 20 cpy the higher temporal resolution of the CLM product becomes evident, and CLM and the assimilated time series

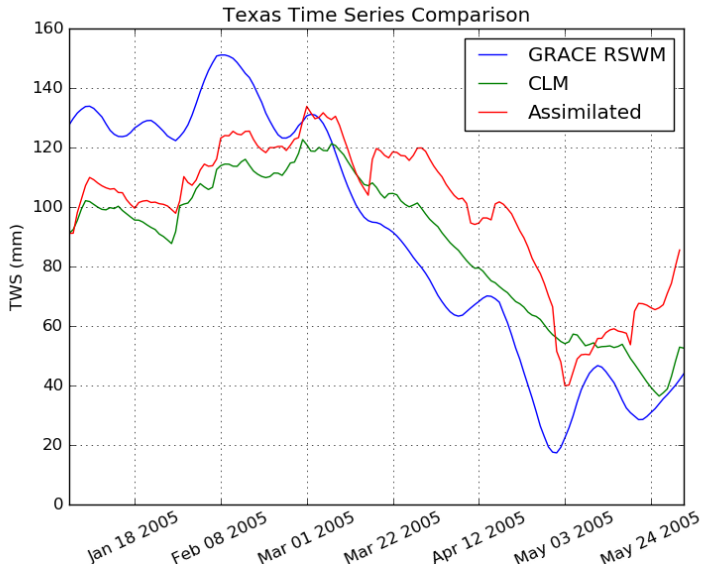

(a) The assimilated time series in Texas

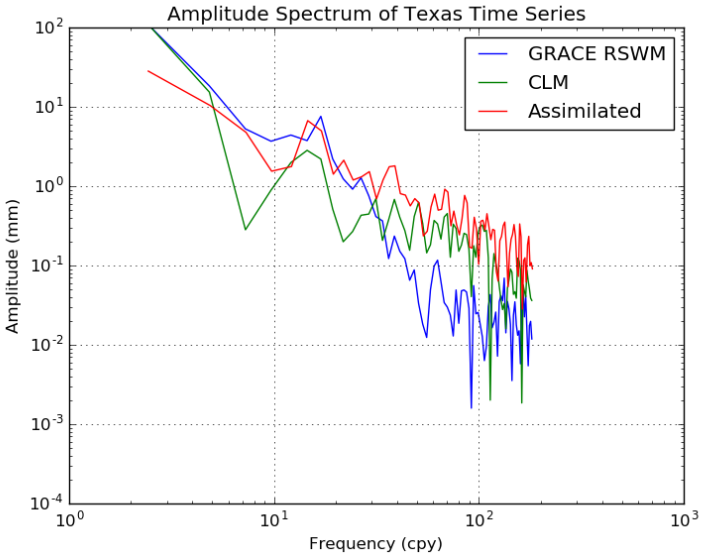

(b) Texas amplitude spectral density

Figure 5.14: Signal and frequency profile comparison of GRACE RSWM, CLM, and the assimilated time series in Texas.

both show higher power.

In Bangladesh, the significantly larger amplitude of the RSWM dataset is immediately evident in Figure 5.15 (a). The assimilated time series follows the RSWM amplitude pattern while still exhibiting the rapid variability evident in the CLM time series. This is again reflected in the ASD of the GRACE, CLM, and assimilated data in Figure 5.15 (b). As the ASD is calculated over only a 6 month period, the larger annual cycle is not present in the frequency spectrum. The seasonal signal has been previously seen to improve with assimilation of monthly GRACE information [95]. In this study we aim to improve the mid-range frequency profile only now available with the RSWM dataset. In the high (> 20 cpy) frequency range the assimilated time series exhibits the higher power of the high resolution CLM variations.

The baseline assimilation case therefore exhibits the desired signal profile in both focus regions: a combination of the higher low frequency (< 20cpy) power of the GRACE RSWM product along with the high resolution land surface dynamics (> 20 cpy) of the Community Land Model. The RSWM product successfully improved the frequency content of the observational data that is available for, and implemented into, the assimilation system. Because the GRACE data primarily affects the assimilated time series in this lower frequency range, we next explore the necessary assimilation rate of the GRACE data. The accuracy and time-evolution of the model time series from this baseline assimilation case will be further explored in Section 4.

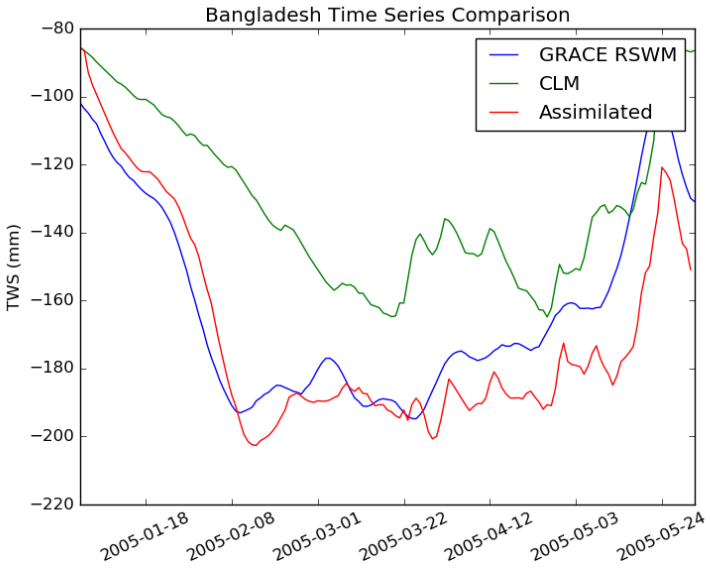

(a) The assimilated time series in Bangladesh

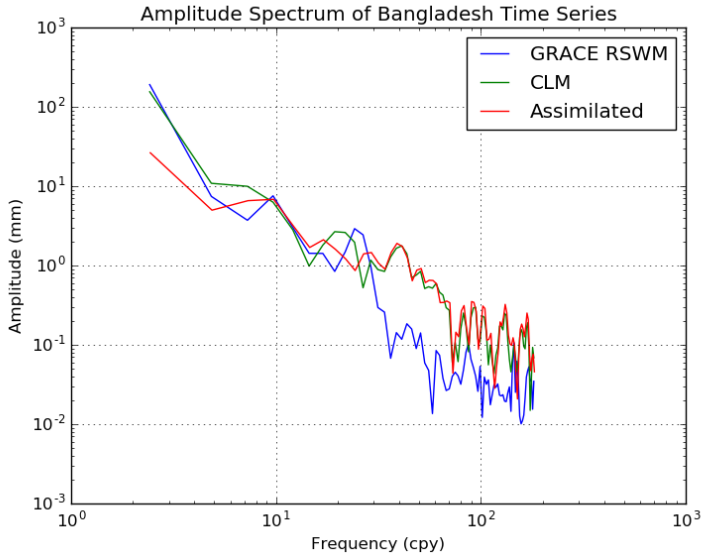

(b) Bangladesh amplitude spectral density

Figure 5.15: Signal and frequency profile comparison of GRACE RSWM, CLM, and the assimilated time series in Bangladesh.

5.3.2 Assimilation Update Rate

The RSWM product offers the ability to assimilate GRACE data every day. However, as was shown in Chapter 2, TWS rarely varies above the precision of the current GRACE mission at time scales of 1-4 days. In addition, the RSWM and CLM TWS time series were shown to be very similarly (highly) temporally correlated over short time scales with similarly sized day to day variations. This raises the question, is daily assimilation necessary? That is, can we reduce the computational burden of assimilation by only assimilating data, for example, every 3, 5, 7, etc. days without significant performance degradation from a daily GRACE assimilation system.

The difference in the purely the RSWM signal content input into the DA system with varying sampling rates is first tested over our two focus regions, Texas and Bangladesh. The power of each time series is estimated as the root mean square of the basin average. As the seasonal cycle dominates the TWS estimate we remove a trend, annual, and semi-annual signal fit from each time series to isolate the high frequency power at these short time scales. The variation in power content is then calculated as the percentage error of the power lost in the differenced (original RSWM time series - RSWM time series at lower sampling rates) and original daily time series. Decreasing the sampling rate can have a significant effect upon the sub seasonal power capture, as shown in Figure 5.16.

For both regions, decreasing the sampling rate from 1 to 14 days continually reduces the overall power capture. Bangladesh shows a greater power

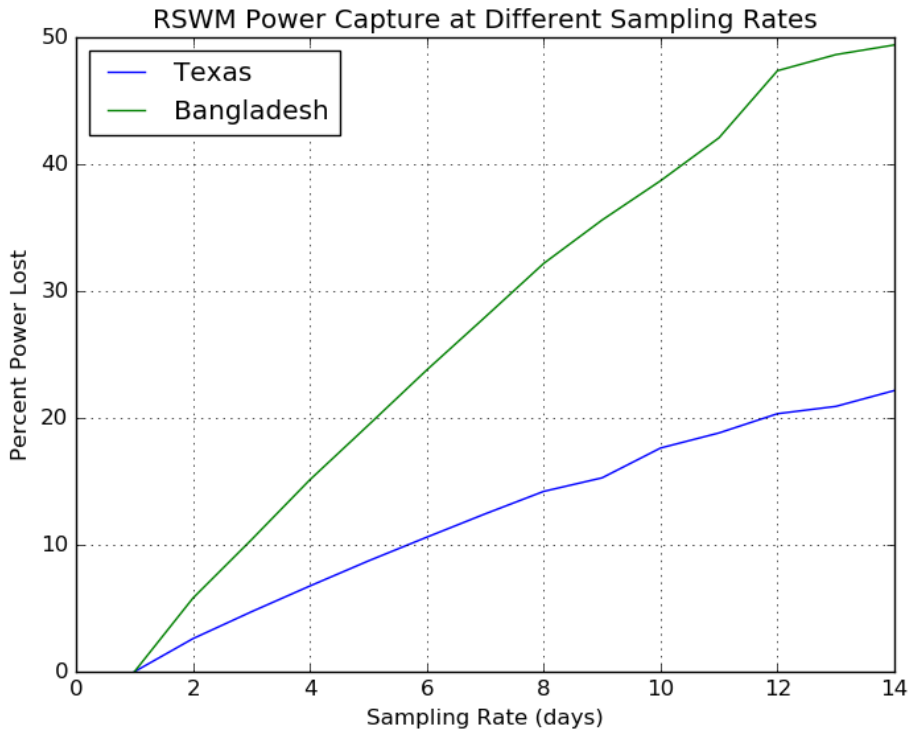

Figure 5.16: Percentage of signal power lost at decreasing sampling rates.

reduction when decreasing the sampling rate in comparison to Texas. This is attributable to the signal profiles of the two regions. The large annual monsoon cycle dominates TWS variation in Bangladesh, and the signal fit is better able to extract this large signal pattern, shown in Figure 5.17 (a). Therefore the residual signal is dominated by high frequency variation which is better captured at a more rapid sampling rate. In contrast, Texas terrestrial water storage has a lower overall signal magnitude, nearly nonexistent annual cycle, and strong inter-annual drift. As shown in Figure 5.17 (b) very little of the signal power follows a seasonal variation and thus the broad structure of the

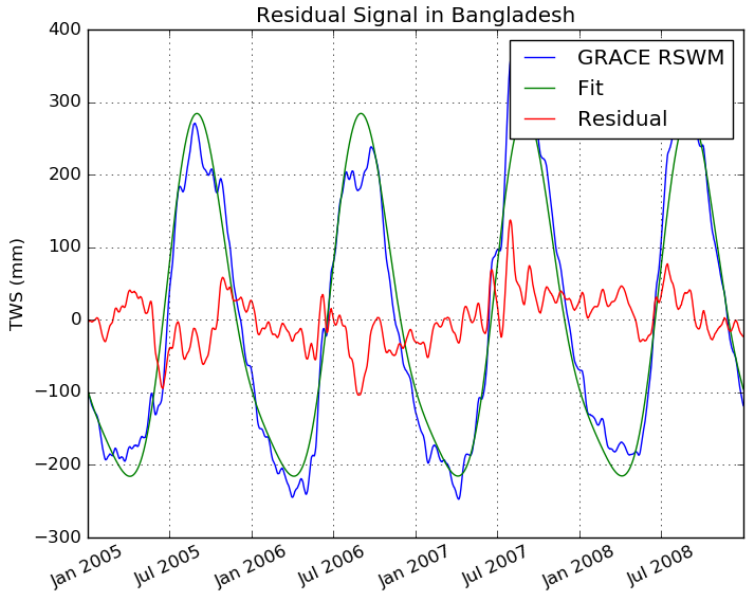

(a) RSWM time series, signal fit, and residual in Bangladesh

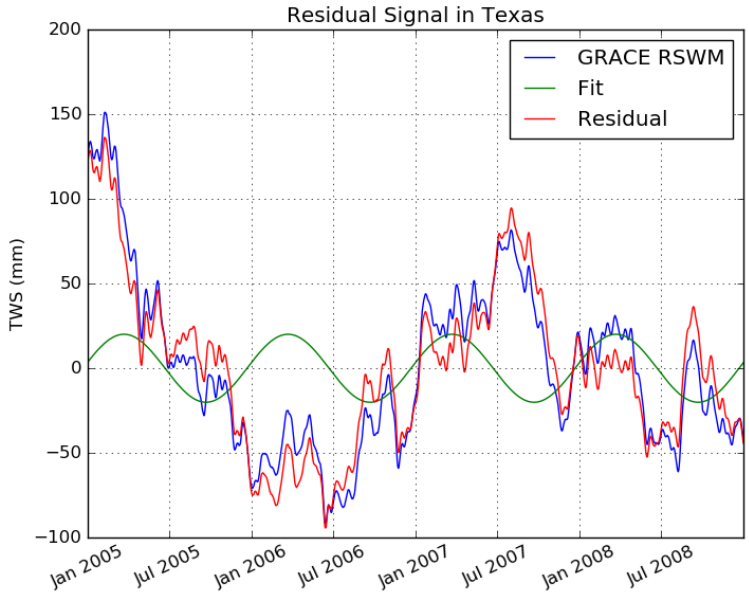

(b) RSWM time series, signal fit, and residual in Texas

Figure 5.17: Residual signal comparison in Texas and Bangladesh

TWS signal is still present. These large amplitude more slowly varying structures are easier to capture at lower sampling rates so less power is lost in this region.

In addition to the input RSWM signal power, other components of the DA system will affect the assimilated results with different assimilation update rates. Each assimilation update is dependent on the RSWM observation and error estimate, the CLM total water column storage, and the spread between the CLM ensemble members. With less frequent assimilation, the model is run freely for longer periods of time and has more freedom to diverge from the RSWM time series. It is also noted that because CLM is run in offline mode in this analysis forward propagation post-assimilation is less sensitive to the updated water column than in a system coupled to atmospheric and other geophysical models.

To test the necessary assimilation rate, we now implement the baseline assimilation case with assimilation update rates of 1, 3, 5, 7, and 14 days. All five cases start with the same initial state on January 1, 2005. The model is then propagated forward for the number of days specified by the update rate, RSWM data is assimilated, and the process is repeated. Analysis of the assimilated results in the two focus regions highlights the additional intricacies of the update rate in a DA system. Each region shows some sensitivity to the varying update rates but in different ways.

In Bangladesh there is a relatively large difference between the CLM and RSWM TWS estimates. CLM tends to underestimate the annual cycle

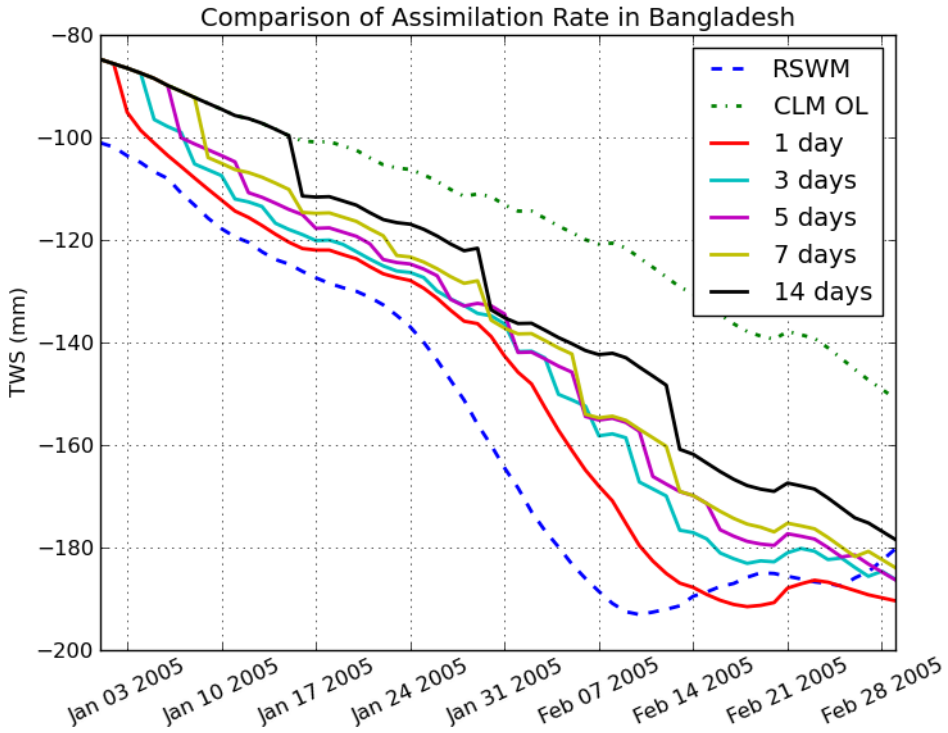

Figure 5.18: Assimilation Method Comparison

- it only captures about 70% of the power of the in situ dataset and 65% of the power of the RSWM series while the RSWM series captures 93% of the power of the in situ dataset. The CLM TWS estimates in Bangladesh also contain more uncertainty in the model states and atmospheric forcing input dataset than in Texas. This leads to a larger ensemble spread and thus larger error variance assigned to the CLM states in the filter. The DA system will be comparatively more responsive to the GRACE observational data. The RSWM data in Bangladesh was additionally shown to be less sensitive to the sampling rate overall. These factors all lead to an effective assimilation system that brings the assimilated time series closer to the RSWM GRACE time series

at all update rates, as shown in Figure 5.18.

There are some noticeable differences between the assimilated time series with different update rates. Daily assimilation, in red, stands out from 3-7 daily assimilation particularly in late January to early February when the RSWM TWS estimate has a steeper slope than the CLM states. Daily assimilation better tracks this variation, and the root mean square error (RMSE) of the daily assimilation from the RSWM time series is 11.7 mm. In comparison, less frequent update rates show RMSE values of 16.8-26.8 mm and greater maximum error values (Table 5.3). Assimilation update rates of 3-7 days show quite similar results, though each decrease in update rate shows a corresponding decrease in agreement to the RSWM data. When the update rate is pushed back to every two weeks the performance degradation can be seen, and the RMSE difference is on the boundary of the GRACE error level.

CLM is much more "certain" of itself in Texas. The model spread - and thus error variance passed to the filter - is relatively small. This lower ensemble spread causes the filter to reject some observations as they are not within 3 standard deviations of the ensemble mean TWS. The overall difference between the GRACE RSWM data and CLM water storage data is much smaller than in Bangladesh as well, so the error bounds of the two datasets will often overlap. Assimilation rates of 1-7 days all show very similar RMSE differences from the RSWM product, and are similar to even bi-weekly assimilation results (Table 5.3). A very slight advantage from daily assimilation over less frequent update rates can be identified due to the lower RMSE and maximum deviation from the RSWM data. However, if computational gains are needed, even bi-

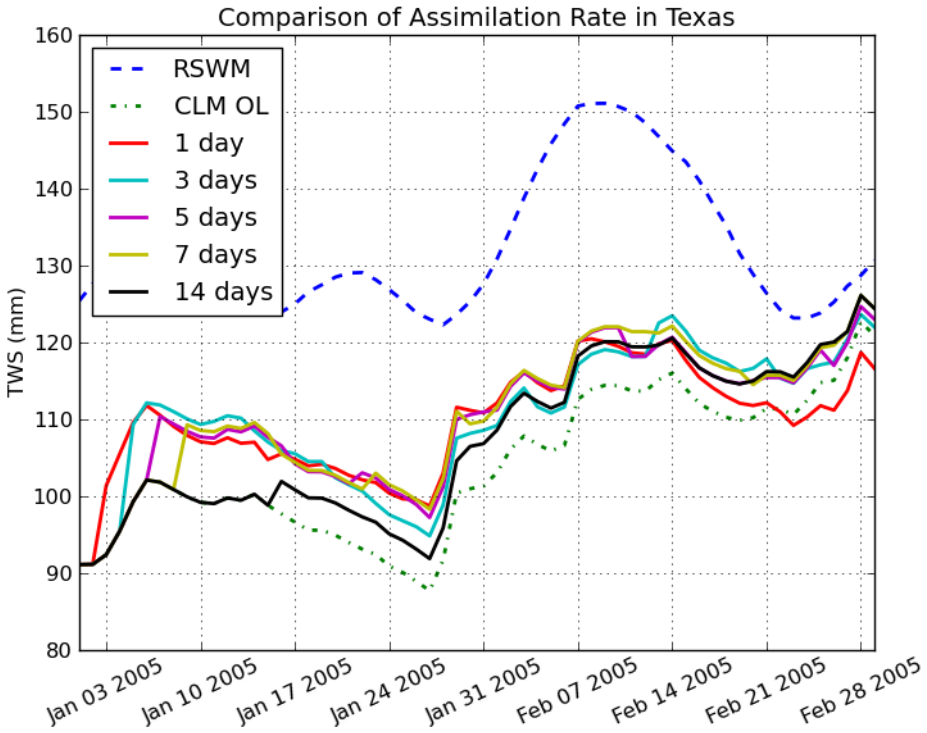

Figure 5.19: Assimilation Method Comparison

weekly assimilation is sufficient for this region if the low model error estimate is trusted.

The recommended assimilation update rate is thus dependent upon the signal profile of the region of interest and the computational limitations of the assimilation system. The most information is naturally passed into the DA system with daily assimilation as was seen in both Texas and Bangladesh. The necessary assimilation update rate in the two regions was dependent upon the quality of the land surface model results, the signal profile of the region of interest, and the regional error assessment of the observational dataset. For a region such as Texas the system was relatively insensitive to small changes

Update Rate	1 day	3 days	5 days	7 days	14 days
Bangladesh RMSE	11.7	16.8	19.1	20.9	26.8
Bangladesh Max	24.9	33.9	37.4	40.9	49.5
Texas RMSE	23.4	23.7	23.6	23.5	26.4
Texas Max	34.0	36.8	34.4	34.3	36.2

Table 5.3: Root mean square error and maximum difference of assimilated time series with varying update rates and the RSWM GRACE product (mm)

in the update rate due to the higher fidelity LSM data, better signal power capture at lower sampling rates, and similar levels of error in the CLM and RSWM data. In Bangladesh, the system was more sensitive to the assimilation update rate due to (i) the larger discrepancy between the CLM and GRACE time series and (ii) more of the RSWM signal is lost in this region at lower sampling rates. The increased information content gained from more frequent assimilation was noticeable and higher assimilation update rates will lead to higher fidelity assimilated results. Regional tuning of this assimilation parameter is therefore necessary to optimize the assimilation system. Assimilation of data from future satellite gravity missions such as GRACE Follow-On with lower levels of observational error will be similarly sensitive to this parameter. Regional error assessments relative to the error profile of the land surface model data, rather than the global covariance, will drive the selection of an efficient and optimal assimilation update rate.

5.4 Effectiveness of the Data Assimilation Framework

The GRACE data assimilation framework was designed to update and optimize existing data assimilation techniques for the unique characteristics

of satellite gravity data. Correspondingly, analysis of land surface model and current data assimilation methods informed the formulation of the GRACE data products themselves. This closed loop design of the data assimilation framework allowed the observational data to respond to the needs of the LSM and DA methods and for the data assimilation system to adapt to the new observational data source. The framework elements for assimilation of GRACE satellite gravity data therefore each address the following component necessary for optimal land data assimilation of the GRACE TWS dataset:

- *Realization of Observations*: Response of the formulation of satellite data products to reduce the resolution discrepancy between the GRACE TWS estimates and the land surface model dynamics.

- *Modified Assimilation Algorithms*: Response of the data assimilation system to incorporate the spatial correlation and error profile of the GRACE data and assimilate on a one-degree grid globally.

- *Gaspari-Cohn Localization Radius*: Tuning of the data assimilation system to the remaining spatial resolution gap between the LSM and GRACE. Appropriately downscale the coarse resolution GRACE data to the high resolution model dynamics.

- *GRACE Assimilation Update Rate*: Tuning of the data assimilation system to regional signal and error profiles for efficient and effective assimilated results.

- *Latency and Open-Loop Error Growth*: Establish the necessary assimilation length for model calibration and open-loop error growth of forecast runs to advise data latency requirements.

This thesis has thus far developed the first four framework elements. The signal amplitude and large-scale spatial patterns of the RSWM dataset was incorporated into the CLM model states and appropriately downscaled to the high spatial and temporal model resolution. This global, gridded assimilation system was tested to determine the appropriate localization radius for the RSWM dataset and recommendations on the necessary assimilation update rate. In this section, we assess the accuracy and evolution of the assimilation system and regional assimilation results over time leading into the final framework element, latency and open-loop error growth. Success for the assimilation framework is not determined by the absolute accuracy of the assimilated results. Rather, the framework success is defined by an assimilation system that represents the strengths and is sensitive to the error profiles of the LSM and observational datasets, that is robust and stable over time, and that is adaptable to new or altered datasets.

We first assess the assimilated results from the baseline assimilation case in the focus regions of Texas and Bangladesh for their ability to combat filter divergence and continually respond to the GRACE observational data. Next the calibration time, the time it takes for the land surface states and observational data to reach an approximate equilibrium, is established. Finally, the rate of departure of model forecast runs from the observational time series

is assessed. The calibration length and error growth of open-loop (forecast) model runs inform the methods and latency requirements for operational data assimilation systems.

5.4.1 Assimilation Efficiency and Filter Divergence

The observational and model datasets must be carefully balanced in an efficient data assimilation system. If the GRACE observational data is weighted too highly in the assimilation process, the independence and higher resolution of the CLM model states could be degraded. In contrast, if the CLM data is weighted too highly the GRACE data is ignored by the filter and cannot improve the model via assimilation. The error profiles of the model and observational data must therefore be well tuned to calculate and downscale the assimilation update. Additionally, if the assimilation system is run freely it is prone to filter divergence. The CLM ensemble spread would continually decrease over time as the updated posterior states, by design, have a smaller distribution than the initial or prior state. This unrealistically small ensemble spread would then reduce the sensitivity of the filter to the GRACE information.

DART has built in tools to address these common sources of error in ensemble data assimilation methods. The error due to sampling a finite number of states (the number of ensemble members used in the study) is referred to as sampling error. To ensure false correlations do not cause unrelated states to be updated, we only update the water storage parameters in this analysis. The sampling error correction tool in DART combines knowledge of the spe-

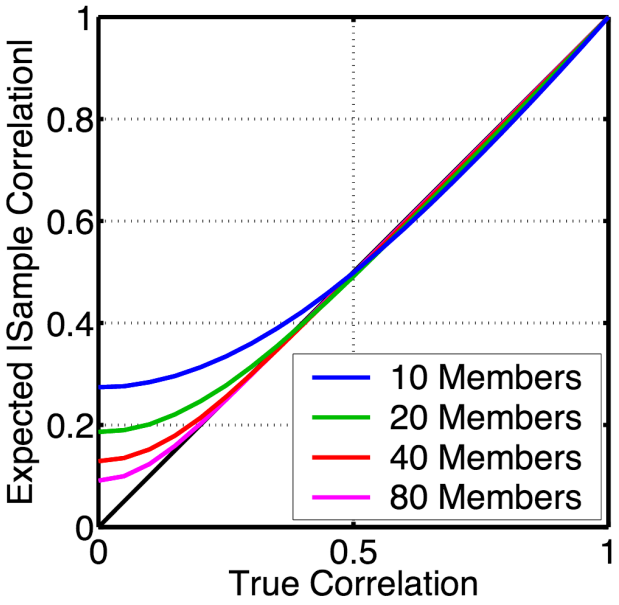

Figure 5.20: Sampling error as a function of number of ensemble members (Source: [55])

cific assimilation system and geophysical model characteristics to add back the expected decrease in ensemble spread [57]. As shown in Figure 5.20 the errors decrease with increasing sample size. After 40 ensemble members, the additional computation load began to outweigh the diminishing accuracy gain so forty ensemble members were used in this study. In addition, to ensure the ensemble spread does not collapse we implement ensemble inflation, another tool in DART, to maintain a reasonable spread in the ensemble TWS estimates. Sampling error correction and ensemble inflation are both run with the recommended parameter setup [55].

At every assimilation epoch, there are over 15,000 observations available for assimilation over the CLM land domain from each RSWM global grid.

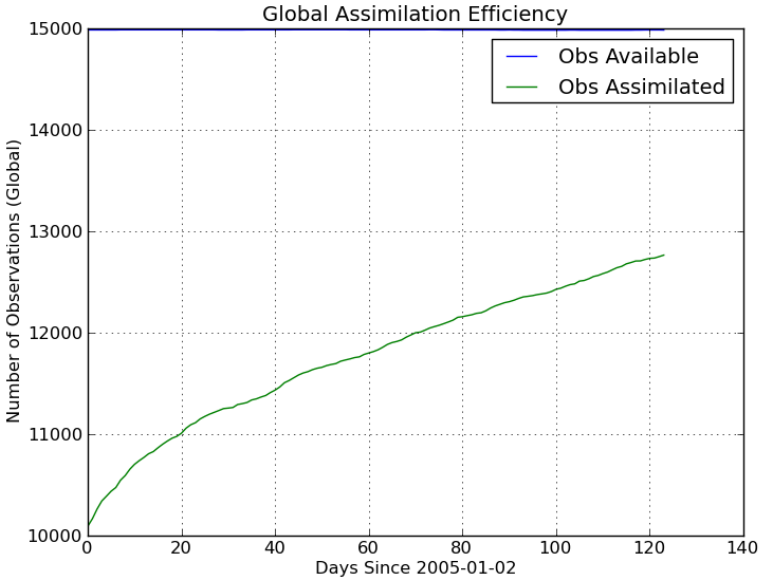

(a) The number of GRACE observations included in data assimilation over time

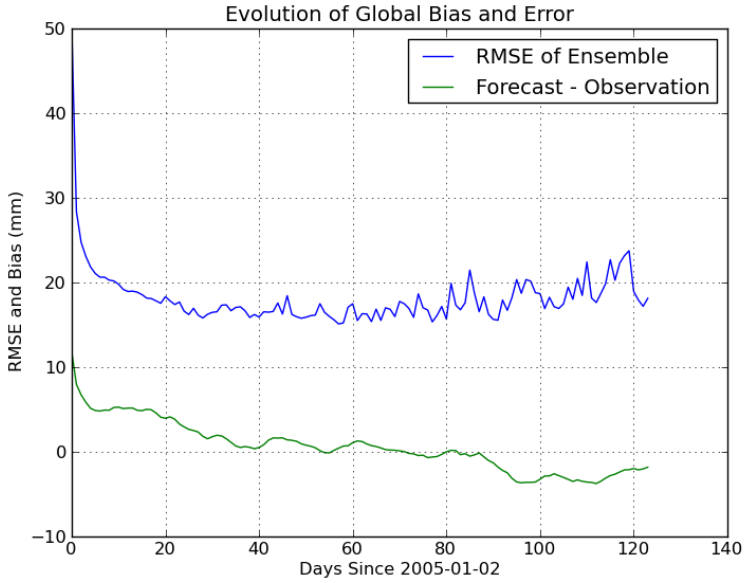

(b) The global RMSE between the CLM ensemble states and GRACE

Figure 5.21: The global assimilation profile

As discussed previously, some of these observations will be rejected as outliers especially at the onset of assimilation with the new data source. Figure 5.21 (a) shows the evolution of the global assimilation "efficiency", defined by the number of observations that are actually used in the filter. Initially around two thirds of the available observations are assimilated into the land surface model. Over time, an increasing number of observations are allowed into the assimilation system while the global root mean square error of the CLM and GRACE TWS estimates remains relatively stable after converging to an equilibrium (Figure 5.21 (b)). Thus at a global scale, the CLM and GRACE states quickly reach an equilibrium around their respective error bounds without disturbing the water balance of the model. Over time, this equilibrium is maintained while more observations are incorporated into the assimilation. The two data sources continue to converge, and the GRACE information continually improves the model accuracy.

This global view shows the CLM/DART assimilation system to behave as designed to incorporate the GRACE TWS information into CLM. However, as we have seen previously in this chapter, the assimilation system may respond quite differently in regions with different signal and error patterns. In Bangladesh, the ensemble spread of CLM is large and all of the GRACE observational data points are included in the assimilation at each epoch. Figure 5.22 shows the assimilated results for two different time periods in comparison to the CLM open-loop model results, the RSWM dataset, and an in situ dataset. First in 5.22 (a) the GRACE data is assimilated into CLM at the beginning of 2005, where the GRACE RSWM better captures the TWS signal than CLM,

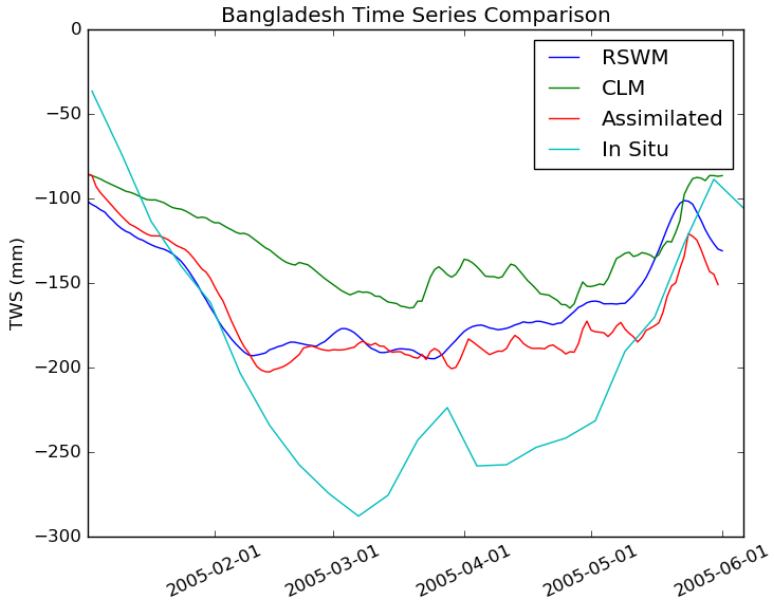

(a) Assimilation in Bangladesh in 2005

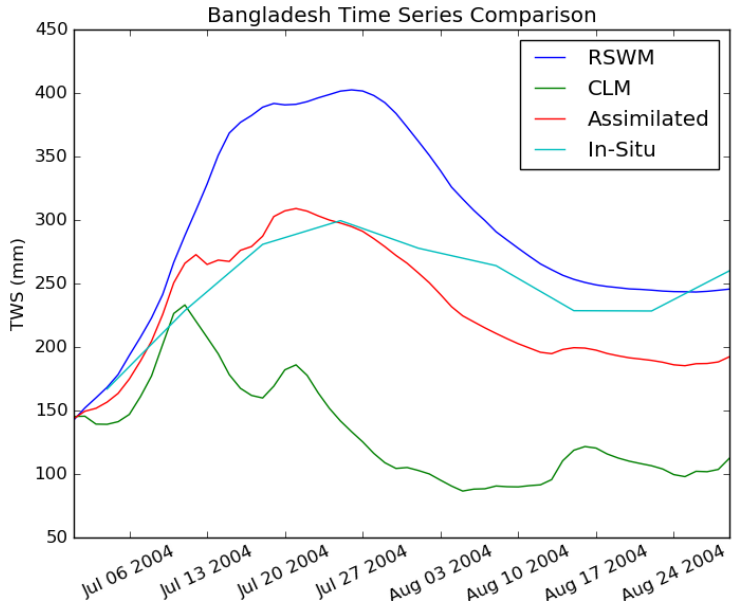

(b) Assimilation in Bangladesh over the July 2004 flood

Figure 5.22: TWS comparison in Bangladesh of GRACE RSWM, CLM, and GRACE/CLM assimilated time series with an in situ dataset

but still underestimates the full amplitude. The assimilated time series much more closely follows the GRACE data than the original CLM open-loop run as the ensemble spread is relatively larger in this region and the GRACE data is more strongly weighted in the filter.

The second assimilation case, Figure 5.22 (b), assimilates the GRACE data over the extreme flooding event identified in Chapter 2 (Figure 2.15). The RSWM dataset captures the peak (July 27) and duration of the flood which is not evident in the CLM time series. The assimilated time series also tracks this flooding event and even best matches the in situ data. The peak of the flood is a bit early in the assimilated time series as CLM greatly underestimates the TWS at that point in time. Many of the smaller scale variations from CLM are evident in the assimilated results, and the assimilated time series thus blends the strength of the GRACE signal with the higher resolution dynamics of CLM.

The assimilation system exhibits a quite different response in Texas than in Bangladesh. The ensemble spread is much lower, and thus initially only 80 of the 146 RSWM observations available in the region are assimilated into CLM. Over time more observations are assimilated as the CLM terrestrial water storage in Texas converges to the GRACE estimated value, shown in Figure 5.23. The assimilated time series, in Figure 5.24, also shows different behavior than in Bangladesh. The assimilated time series does respond to the GRACE data, but clearly still weights the CLM states heavily in the filter. This leads to an interesting evolution in time where the assimilated time series follows many of the large scale features of the RSWM time series, but at a

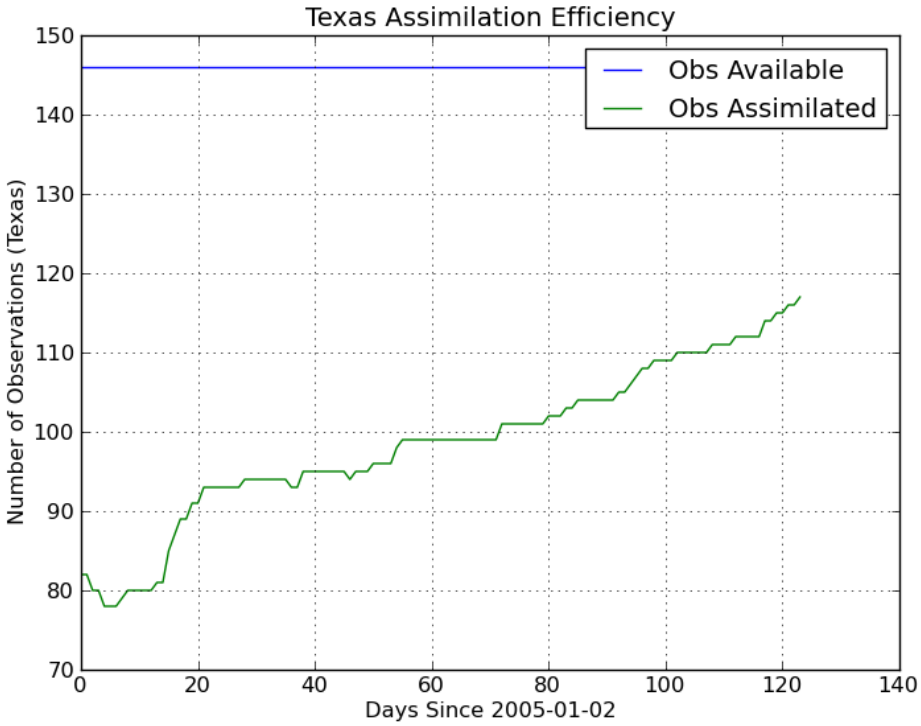

Figure 5.23: The number of GRACE observations included in data assimilation over time

lower accuracy than in Bangladesh.

5.4.2 LSM Conditioning via Data Assimilation

The fundamental nature of the GRACE product makes it impossible to deliver in real time. The global inversion for time-variations in terrestrial water storage requires a sufficient number of observations, geophysical model data, and extensive processing to compute each global gravity field. Tools such as regularization, CRN window functions, and sliding windows allow us to stretch the temporal and spatial resolution available from this data but do

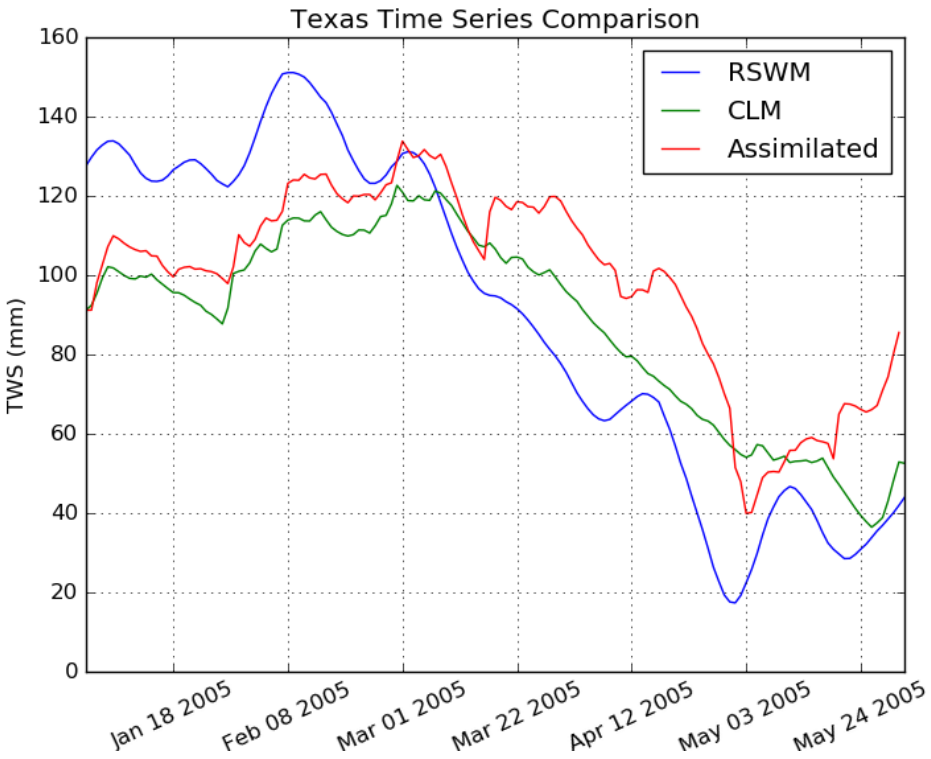

Figure 5.24: TWS comparison in Bangladesh of GRACE RSWM, CLM, and GRACE/CLM assimilated time series with an in situ dataset

not bridge this gap completely. Lower latency products such as the quick look gravity fields will reduce the lag between when the solution is time-tagged and when it is available for assimilation.

In some applications, such as meteorological forecasting, near real-time measurements are incredibly valuable. However, data latency is not as urgent for the GRACE terrestrial water storage measurement [73]. As explored in McMillan et. al. (2012), for parameters such as streamflow, soil moisture, and water table depth assimilation of the observation at its time tag can lead to short-term errors such as spikes or oscillations in the model due to the

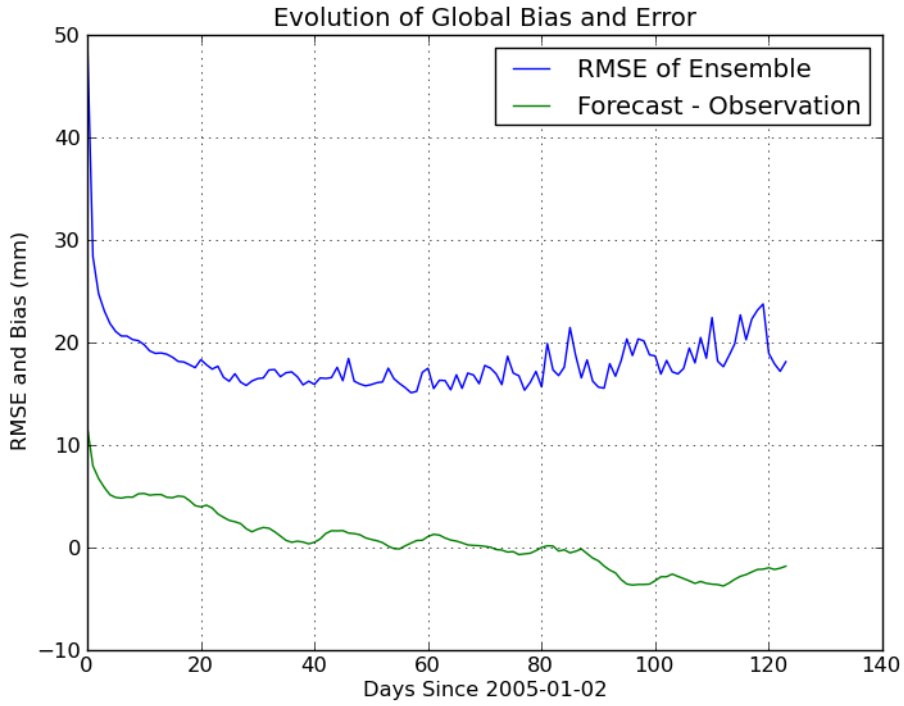

Figure 5.25: The DA spin-up time shown through the global RMSE

natural time lag between catchment state and river flow. Li et al. (2011) found that updating soil moisture states led to a lagged response in discharge - but a slower degradation of forecast accuracy. These two cases for streamflow modeling are representative of the differences in assimilation for land surface processes. Terrestrial water storage has a longer memory and slower response to stimuli and thus can better accommodate a certain amount of data latency than higher frequency systems.

Assimilation acts to calibrate the model and thus improve the initial state of forecast runs. Better conditioned model states from GRACE assimilation have been shown to improve the results of forecast runs [22]. Just as

a “startup” land surface model run requires a certain amount of spin up time for the global states to reach equilibrium, there is a certain amount of assimilation spin-up time until the model and observational data are in equilibrium at global and regional scales. This spin-up time is dependent on the stability of the model after the initial spin-up, the size of the gap between the model and observations, and which state variables are updated [97]. The spin-up can be observed by the global root mean square error (RMSE) between the model ensemble states and the observations, shown in Figure 5.25. To test the limits of the calibration length, the Case 1 setup with a constant 2cm error estimate is implemented. This lower error estimate will cause the model to “travel further” to reach equilibrium with GRACE. The initial RMSE is much higher than the 2cm error level and quickly approaches this baseline error level assigned to GRACE. After approximately 30 days the RMSE is seen to reach an equilibrium while still incorporating more of the GRACE TWS information, as shown in Figure 5.21.

The regional calibration lengths for Bangladesh and Texas, in Figure 5.26 appear to be shorter than for global scale calibration. In Bangladesh, 5.26 (a), the higher weight given to the GRACE data is evident, and the RMSE between the RSWM estimated TWS and ensemble members averages about a centimeter. The larger amplitude signal profile of the region is evident from the relatively large variations between the CLM forecast TWS estimate and GRACE observed value. After twenty days of assimilation this “Forecast - Observation” parameter oscillates around zero bias. The Texas assimilated time series converges even more quickly to an equilibrium state, after approximately

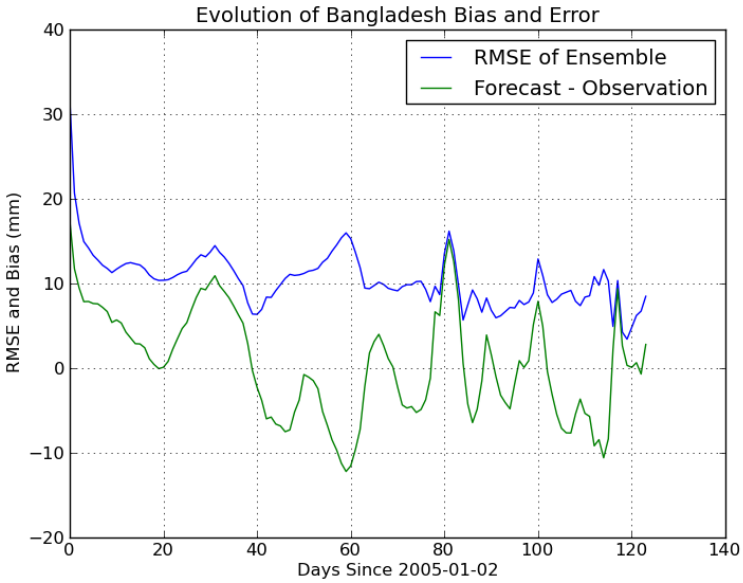

(a)

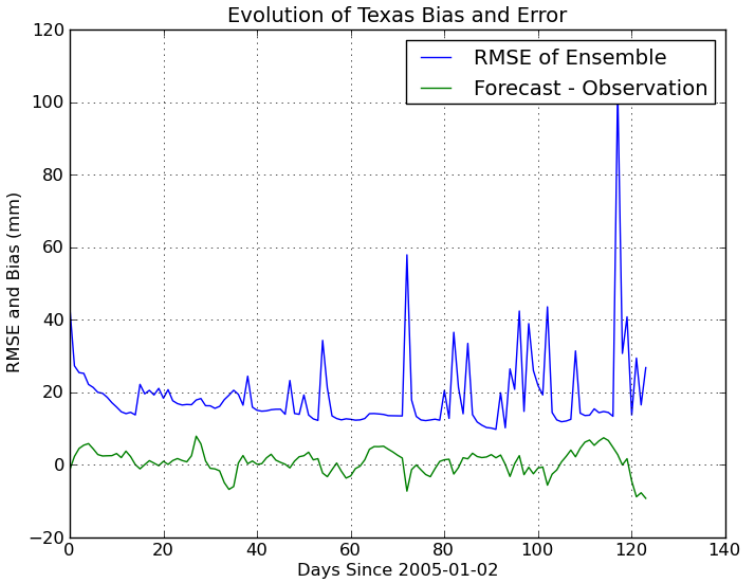

(b)

Figure 5.26: Evolution of the bias and RMSE in Bangladesh and Texas

15 days. The RMSE between the GRACE and ensemble states averages about two centimeters, and this region similarly shows no bias. Texas initially rejects more observations as outliers, as was shown in Figure 5.23, but the initial difference between the GRACE and CLM estimated TWS values are closer so the assimilation system can more easily reach an equilibrium between the two datasets.

5.4.3 Open-Loop Error Growth and Data Latency

After the (regionally defined) spin-up or calibration period the assimilated time series reaches a relative equilibrium between the signal and error profiles of the model and observational data. Smaller assimilation updates are needed to bound the open-loop error growth of the assimilation system from the observational data. The rate at which error increases in forecast runs, model runs without assimilation, determines requirements on the latency of satellite gravity data. Low-latency data is not necessary for a system that stays within the error bounds of the land surface model over long time periods. Rapid error growth, however, necessitates lower latency delivery of the observational data to constrain the system. To test the rate and pattern of open-loop error growth for CLM terrestrial water storage, the model was spun-up with the baseline assimilation case for two months to bring the CLM and GRACE data into equilibrium. Assimilation of the GRACE TWS estimates was then "turned off" and the model propagated forward in time with the atmospheric forcing dataset. Specific regional requirements will undoubtedly be necessary for application in operational systems, so the error growth is

quantified in the two focus regions in Figures 5.27 and 5.28.

The system quickly responds to the GRACE observational data in Bangladesh, Figure 5.27 (a). When assimilation ceases on March 1, 2005 the Assimilated and RSWM datasets show very similar TWS estimates. The forecast run follows the structure of the open-loop CLM run forward in time, but remains quite close to the RSWM basin time series due to the initial state of the assimilated case. Over time, as seen in Figure 5.27 (b), the RSWM and assimilated datasets do start to diverge but for the first two months the calibrated forecast run stays within the basin error bounds (2 cm) of the GRACE dataset.

The Texas case, Figure 5.28 shows a quite different response. Initially, the assimilated time series responds to the GRACE assimilation and moved the CLM TWS estimates closer to GRACE. However, when the assimilation is turned off on March 1, 2005 the RSWM, CLM, and assimilated TWS estimates are all very similar. As the assimilated case does not have a significantly different initial state than the open-loop case it quickly converges within the error bounds of the open-loop CLM run. The GRACE and CLM time series are closer overall in Texas, but there is very little gain from the model calibration. The improvement in open loop error growth is clearly sensitive to the initial state of the model, observational and assimilated time series.

Analysis of the open-loop error growth highlights the need for consideration of the initial state of forecast runs for the model, observational, and assimilated datasets. If all happen to be close, as in the Texas assimilation

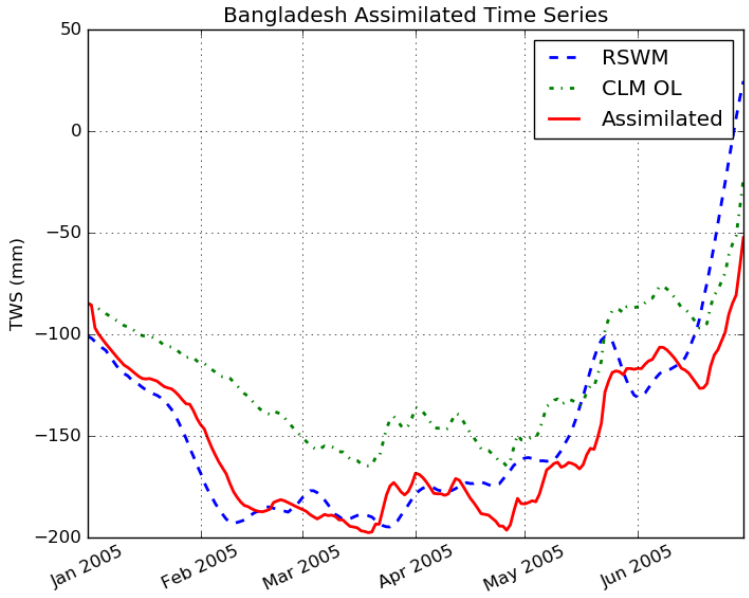

(a)

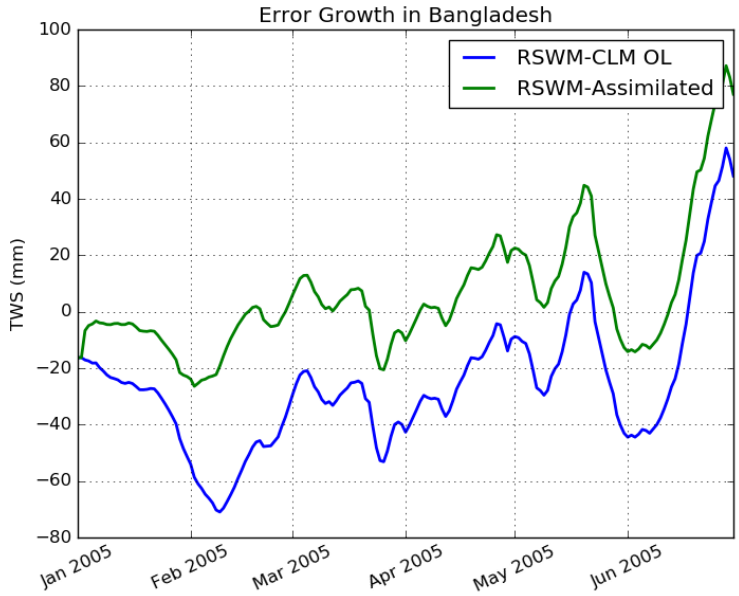

(b)

Figure 5.27: Model calibration and open loop error growth in Bangladesh

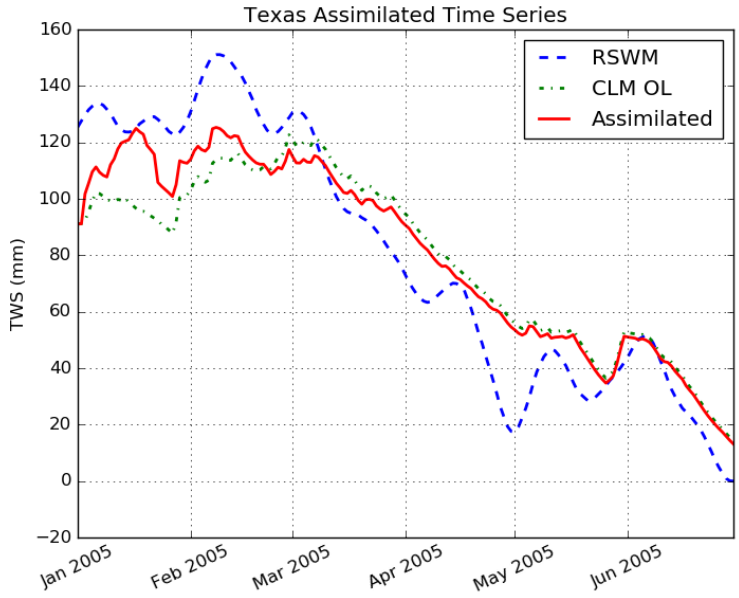

(a)

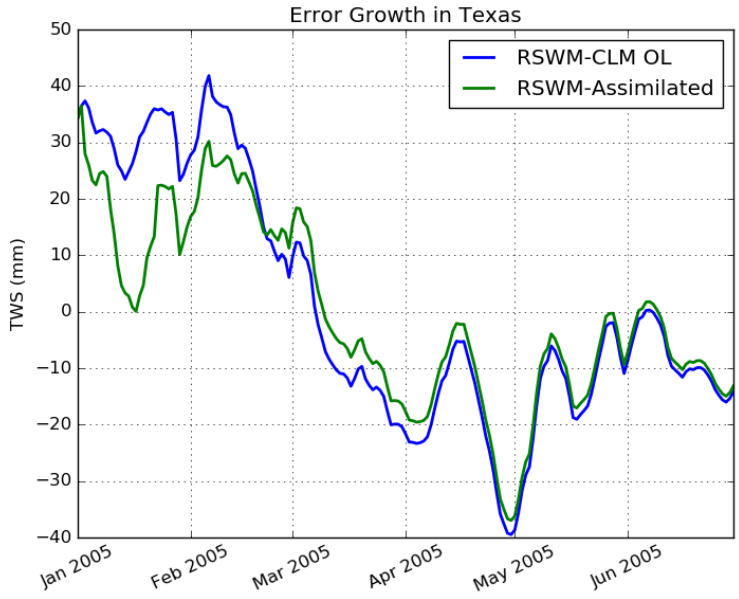

(b)

Figure 5.28: Model calibration and open loop error growth in Texas

case, the calibrated model states will have little impact upon the open-loop error growth. If large differences in these states exist calibration via assimilation creates improved model estimates which persist over longer time scales. The setup of the assimilation system in this study similarly impacts the calibration length. CLM is run in offline mode with a prescribed atmospheric forcing dataset. If it were run coupled to an atmospheric model, the updated land surface states would alter the dynamics and output atmospheric forcing data, and it is reasonable to postulate that a fully coupled system would respond more strongly to the assimilation.

The framework developed and tested in this thesis adapted and specialized the GRACE data and land surface data assimilation methods. Gridded, global assimilation framework effectively and consistently assimilated the RSWM GRACE dataset into the CLM. The strengths of the GRACE (broad scale signal structures and magnitude) and CLM (high resolution land surface dynamics) were fused into the assimilated time series. At a global scale, assimilation of the GRACE data is relatively straightforward but too generic for the current level of error in the GRACE data, the land surface models, and the ensemble assimilation methods. Regional tuning and analysis of the assimilation framework ensures the signal and error profiles of the model and observational datasets are appropriately taken into account. Spatial smoothing of the assimilation update ensures the resolution of GRACE is represented in the assimilation and the assimilation update is not dominated by the LSM ensemble spread. The assimilation update rate and model calibration length are established regionally and adaptable for the land surface model to ensure

efficient, effective assimilation and advise data latency requirements. Each framework element is adjustable and extensible to data from GRACE Follow-On, GRACE-2, and future satellite gravity missions. Future satellite gravity data will further improve the spatial and temporal resolution of terrestrial water storage datasets. Adaptation of the framework elements to the idiosyncrasies of these datasets will further improve assimilated land surface model results.

Chapter 6

Conclusion

Accurate knowledge of terrestrial water storage transport is a critical boundary condition for modeling the global water cycle at both short term (meteorological) and longer term (climate) time scales. The amount and location of water storage regulates the transfer of water and energy between the land surface and atmosphere [78]. Land surface models aim to accurately represent these processes and quantify the transfer of mass, energy, and momentum. The models have limitations due to inaccuracies in parameterization, model physics, and atmospheric forcing data. Accurate, effective assimilation of the GRACE terrestrial water storage information improves the accuracy of land surface models, model conditioning for forecast runs, and identifies deficiencies in the model physics and representation. This analysis advances the signal range and effectiveness of information from the GRACE mission by specializing the data products and methods for land data assimilation of satellite gravity data.

6.1 Summary of Results

This study established a framework for land data assimilation of time-variable gravity field products from GRACE that is flexible to any land surface

model and malleable to future satellite gravity mission data. The GRACE mission has provided a reliable timeline of time-variations in the Earth's gravitational field which will continue in GRACE Follow-On and future satellite gravity missions. The framework developed in this study expands the information available from the current GRACE observations and helps it to be further exploited via data assimilation. The assimilation elements each adapt and expand elements of current GRACE assimilation systems to best form the GRACE terrestrial water storage product and incorporate it into land surface models.

- *Realization of Observations*: The RSWM product expands the range and power of the GRACE data and represents the first daily time series from GRACE created without model or outside information. RSWM boosts increases the frequency range of the GRACE data products to improve hydrometeorological signal capture and the temporal resolution discrepancy with LSMs. The signal and error profile are completely characterized in an end-to-end error analysis of the instrumentation, representation, and omission errors of the GRACE mission. The RSWM error covariance is representative of the magnitude, correlation, and spatial patterns of error in terrestrial water storage.

- *Modified Assimilation Algorithms*: The assimilation algorithms are adapted to include the GRACE covariance information developed from the simulation analysis. The Ensemble Kalman Filter equations use the covariance information to perturb the observation, rather than simply the

variance of the observation, to reduce noise and increase the information content available to the filter. The new GRACE error profile better represents the behavior of the RSWM dataset, and future assimilation systems with higher fidelity observational and land surface model data will be increasingly sensitive to this improved representation.

- *Gaspari-Cohn Localization Radius*: Due to its relatively coarse (200-300 km) spatial resolution it is necessary to spatially smooth the observation space assimilation update to the land surface model state variables within the resolution of the RSWM gridcell. The Gaspari-Cohn localization radius must balance spatial smoothing of the assimilation update so it neither amplifies nor depresses the signal according to the resolution of the observational data source. A Gaspari-Cohn localization radius of 0.03 radians (approximately 200 km) was determined to best distribute the RSWM dataset in space. This will likely be reduced for future higher resolution systems.

- *GRACE Assimilation Update Rate*: Analysis of the model and GRACE temporal profiles showed similarly high levels of correlation over short time scales. To improve computational efficiency it is possible to reduce the assimilation update rate according to regional signal and error properties. Both regions in this analysis were able to incorporate the GRACE information at lower assimilation update rates. In Texas, most of the assimilated signal was sufficiently incorporated into CLM with weekly assimilation. In Bangladesh, sub-weekly assimilation rates are

recommended to keep the assimilated time series in equilibrium with the GRACE and CLM error bounds

- *Latency and Open-Loop Error Growth*: The longer memory of terrestrial water storage processes allow the assimilation system to accommodate latency in the observational data. The two focus regions showed different responses to calibration with the GRACE data. Bangladesh was strongly influenced by the GRACE assimilation and stayed within the error bounds of GRACE for nearly two months, while in Texas the system quickly converged to the open-loop model state. Therefore, specific latency requirements must be tuned to the application, assimilation system, and signal profile of the region of interest.

The framework was developed at a global scale to ascertain all the elements of the data assimilation system which could be improved from or adapted for satellite gravity data. The formulation and motivation for each component of the system - the observational data, the assimilation algorithms, and assimilation methods - was analyzed and the framework designed to be flexible so it may be easily extended to the unique characteristics of other satellite gravity datasets. Many elements, such as the inclusion of covariance in the assimilation algorithms, will become more important as remote sensing technology and geophysical modeling progresses.

The gridded, global assimilation system appropriately downscaled the GRACE information to the CLM state variable level according to the filter parameter definition and error estimates. The success of the assimilation

framework is proven through the sensitivity of the system to the GRACE information over time and the clear blend of large scale spatio-temporal GRACE features and high resolution land surface dynamics in the assimilated results. Global scale assimilation, however, cannot balance both broad scale features and small-scale regional nuances with a single parameter definition. At the current state of development, regional analysis of the relative signal and error profiles of GRACE and LSM data is critical to define many of the framework elements and ensure the accuracy of assimilated results. The assimilation framework thus fully defines the GRACE assimilation problem but must be regionally tuned to exploit the expanded signal range in the RSWM product and account for the improved GRACE error profile.

6.2 Summary of Contributions

The key contributions of this work are a higher frequency GRACE product specialized for use in assimilation, a complete definition of the product's signal and error profile for data assimilation, and specification of the assimilation algorithms and tools to exploit the GRACE TWS information and improved error profile. The daily, regularized sliding window mascon (RSWM) GRACE TWS product was developed to reduce aliasing and signal damping inherent in the operational RL05 GRACE product. The RSWM spatial and temporal properties are enhanced with an improved filter design, regularization within the estimation strategy, and representation in mascon basis functions. The RSWM product is able to bridge much of the gap in temporal resolution between land surface models and GRACE. Assimilation

with RSWM thus eliminates the need to temporally smooth the assimilation update, reducing computational requirements and simplifying the assimilation process.

The signal and error profile of the RSWM product was rigorously assessed in Chapters 2 and 3. The new dataset shows excellent agreement to high-fidelity LSM and in situ datasets, improved amplitude capture, reduced noise, and captures transient events in terrestrial water storage. The end-to-end error simulation study created a realistic covariance for the RSWM data product representative of errors in the satellite instruments, geophysical models, truncation of the gravity field, time-windowing of the observational data, aliasing, etc. Sampling the covariance showed that it is representative of the North-South stripes that afflict the GRACE data as well as regionally specific error patterns. Alteration of the instrument noise parameters, errors in the geophysical models, sampling rate of the gravity field, etc. allow this simulation design to quantify the error in future satellite gravity datasets.

Finally, the assimilation algorithms are adapted for use with the new RSWM data product and error assessments. The full covariance information is used to perturb the observation in the filter. The spatial location and magnitude of the assimilation update is tuned to the satellite gravity data product with the Gaspari-Cohn localization radius. The necessary rate of assimilation must be regionally assessed; daily assimilation will best incorporate the GRACE data into the model, but the assimilation system is still effective if the information is assimilated only weekly. The assimilation system in this analysis is found to allow up to two months of data latency, depending on the

focus region, thus relaxing requirements on product delivery. The data assimilation framework defined in this study thus increases the range and power of the GRACE signal profile and defines the methods to adapt data assimilation methods for new datasets.

This study of daily, global, and gridded GRACE data assimilation both advanced assimilation of satellite gravity information and highlighted deficiencies in the land surface model and current observational datasets. At this time, global assimilation cannot balance both broad scale features and small scale regional nuances. The land surface models, the ensemble perturbation techniques, and the assimilation methods are not capable of accurate, continuous assimilation leading to ensemble spread inaccuracies, assimilation artifacts, and possibly filter divergence if not carefully controlled over time. Regional tuning of the assimilation system is therefore necessary for actionable, meaningful results in operational data assimilation.

Operational data assimilation systems, properly tuned to the unique GRACE signal and error properties, will be able to provide more accurate estimates of current and future land water storage variability. The RSWM product introduces information on an increased range of terrestrial water storage signals. The assimilation system can better use the data as temporal smoothing is not required for the daily product and gridded assimilation reduces spatial smoothing requirements. Due to the longer memory of land surface processes data latency is not as strict as for other applications and future lower-latency GRACE (or GRACE-type) products can meet this need. Future satellite gravity missions will continue the TWS time series and continue to

extend our precise measurement of global water storage and variability. New, innovative instrumentation and mission configurations will expand this signal profile. Higher fidelity satellite gravity data will further advance studies of hydrology, oceanography, etc. and, through data assimilation, our ability to monitor, model, and predict our climate system.

6.3 Future Directions

This thesis developed a data assimilation framework upon which regional tuning and specific applications can be built. The framework is adaptable to future satellite gravity data and enhanced land surface models, and it can be incorporated into larger, multivariate assimilation systems. The GRACE Follow-On mission, to be launched in 2017, will continue the time-variable gravity dataset from GRACE and may increase the accuracy of the results by an order of magnitude. Improvement in the geophysical model data and representation of errors in the estimation strategy can further improve the resolution and accuracy of the GRACE dataset. Even more advanced instrumentation and innovative mission designs in GRACE-2 will further improve the spatio-temporal resolution and overall scientific accuracy of satellite gravity datasets.

The methods and strategies for assimilation of the RSWM product is directly applicable to lower latency operational products such as the quick look dataset from the GRACE Follow-On mission. The RSWM product and current quick-look products use similar window functions and thus have similar signal profiles. Novel methods of forming global or regional scientific products will

expand and adapt specific framework elements. For example, assimilation of low latency swath gravity field solutions, estimated along the satellite ground track, necessitates formation of a new localization function. Rather than uniformly smoothing such a product over a defined radius, the localization function would distribute the TWS estimate across the satellite groundtrack. This and other localization functions can thus be informed by the satellite mission design, the sensitivity of the mission to gravitational perturbations, regional dynamics, etc.

Finally, the RSWM dataset itself offers many avenues for future study. The dataset greatly increases the range and power of signals available from the GRACE observations. The improved window function, regularization and mascon representation combine to create a high-fidelity product representative of hydrometeorological processes in terrestrial water storage. Sub-seasonal signals and transient events are evident in the dataset and further exploration in the scientific community will test the limits of signals that can be observed with the GRACE mission.

Appendices

Appendix A

Representation of the Gravity Signal

The data centers deliver monthly averages of spherical harmonic coefficients. This chapter aims to show what these parameters represent and their derivation. Then the process by which these are converted into estimates of surface mass is presented. It is this surface mass measurement, expressed as equivalent water height, that quantifies mass movement over the surface of the Earth. The notation used in this chapter and throughout the report is given in Table A.1.

A.1 The Earth's Gravitational Potential

The gravitational potential exerted by a body on a point is represented as an integral function of its mass density over its volume in the equation below, where (x,y,z) is the point the at which the potential is being evaluated and (x', y', z') represent the position of the differential mass element:

$$W(x,y,z) = G \int \int \int_v \frac{\rho(x',y',z')dV'}{\sqrt{(x-x')^2+(y-y')^2+(z-z')^2}} \tag{A.1}$$

The gravity vector is the force vector, or the gradient of this gravitational potential:

$$\bar{g} = \nabla W \tag{A.2}$$

Symbol	Meaning
W	Potential
G	Gravitational constant
ρ	Density
(x, y, z)	Reference Position
(x',y',z')	Coordinate of integration
ω	Rotation of the Earth
d	Distance or length of position vector
$\bar{g}$	gravity vector
U	Earths normal potential
T	Earths disturbing potential
H	Height of topography from geoid
h	Height of topography from ellipsoid
N	Height of Geoid from ellipsoid
a_e	Earth radius
θ	Colatitude
ϕ	East longitude
δ_{m0}	delta function of m and 0
l	Spherical harmonic degree
m	Spherical harmonic order

Table A.1: List of Variables Used

A common way to represent the potential is through equipotential surfaces, defined as a surface of constant value of the potential. These surfaces help to visualize the potential and can be defined by any constant value of the potential. The most important of these equipotential surfaces for the Earth is the one which corresponds with the mean sea level if the oceans and atmosphere were in equilibrium and at rest with respect to the rotating Earth, the geoid. The geoid is commonly split into two components, the normal potential, defined as U, and the disturbing potential, T. The normal potential defines the potential of an ellipsoid of revolution, referred to hereafter as simply the ellip-

soid, and the disturbing potential the variations from this ellipsoidal surface. This is illustrated in Figure A.1. N represents the normal height difference of the geoid from the ellipsoid, H shows the normal height of the topography from the geoid, and h is the difference between the ellipsoid and topography, normal to the ellipsoid. It can be seen in Figure A.1 that there is a subtle difference between h and H+ N therefore care must be taken to ensure h and N represent normals to the ellipsoid while H is normal to the geoid.

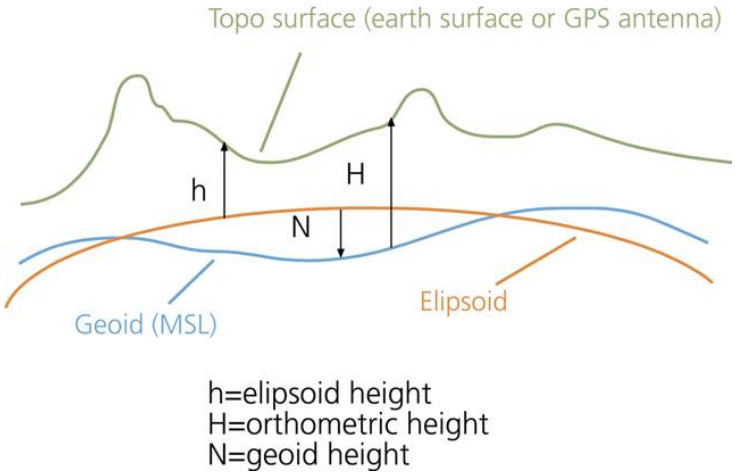

Figure A.1: The ellipsoid, geoid, and topography

A.2 Application to the GRACE mission

A.2.1 Practical Representation of the Gravitational Field

In reality, the gravitational potential cannot be represented as a triple integral as there is no true analytical expression of the Earth's density. Instead, the potential is first represented in spherical coordinates as:

$$W_a = G \int \int \int_M \frac{dm'}{\sqrt{r'^2 + r^2 + 2rr'cos(\psi)}} \tag{A.3}$$

The $\frac{1}{r}$ is then factored out of the denominator and the binomial theorem applied. The resulting expansion terms are then represented by the Legendre polynomials. Following the procedure of Kaula (1966) and transforming the coordinates to latitude and longitude results in the following expression for the potential:

$$\begin{aligned} W_a(r,\phi,\lambda) &= \frac{GM}{r} + \frac{GM}{r}\sum_{l=1}^{\infty}(\frac{a_e}{r})^l P_l(sin(\phi))C_{lm} \\ &+ \frac{GM}{r}\sum_{l=1}^{\infty}\sum_{m=1}^{l}\frac{a_e}{r}^l P_{lm}(sin(\phi))[C_{lm}cos(m\lambda) + S_{lm}sin(m\lambda)] \end{aligned} \tag{A.4}$$

Where the Legendre Polynomials, P_{lm} are given by the equation:

$$P_{lm}(x) = \frac{(1-x^2)^{m/2}}{2^l l!}\frac{d^{l+m}}{dx^{l+m}}(x^2-1)^l \tag{A.5}$$

The expression for the geoid, discussed in the previous section can similarly be expanded as a sum of spherical harmonics by setting the potential, W_a, equal to the corresponding constant value. The variation in geoid height, ΔN, can be solved for for any angular position (ϕ, λ). This expression is commonly given as:

$$\Delta N(\theta,\phi) = a_e \sum_{l=0}^{\infty}\sum_{m=0}^{l}\bar{P}_{lm}(cos\theta)(\Delta C_{lm}cosm\phi + \Delta S_{lm}sinm\phi) \tag{A.6}$$

Where a_e is the mean radius of the Earth, θ is colatitude, and ϕ is east longitude. $\bar{P}_{lm}$ are the normalized associated Legendre functions represented as:

$$\bar{P}_{lm}(x) = \sqrt{(2-\delta_{m0})(2l+1)\frac{(l-m)!}{(l+m)!}}P_{lm} \tag{A.7}$$

Several terms are defined during this process, namely the Legendre Polynomials, P_{lm}, and the Stokes coefficients or spherical harmonic coefficients C_{lm} and S_{lm}. The Legendre Polynomials are defined in the equation above, and are solutions to the Legendre differential equation encountered in the solution process. The Stokes coefficients are dimensionless parameters that ideally extend to an infinite degree (l) and order (m). The sources of error in the GRACE data from instrument noise and interpretation of the data will be further discussed in Section 2.3. The GRACE processing centers return estimates of the Stokes coefficients out to degree and order 50-96. These solutions are referred to as the Level-2 products and encompass 10 or 30 days of data.

A.2.2 Surface Mass Recovery

The Earth's gravitational potential changes over time due to the re-distribution of surface mass and the resulting variations in the solid Earth. In order to isolate this variational component of the gravitational field, the mean or static gravity field must be removed from the data. This variability in the GRACE data is reflected in the variability of the spherical harmonic

coefficients. The Level-2 products are a time series of the full C_{lm} and S_{lm} coefficients. To find the time-varying spherical harmonic coefficients, the mean of each term over the time series is removed. This is shown in the equation below where $\bar{C}_{lm}$ and $\bar{S}_{lm}$ represent the time-averaged parameters.

$$\begin{aligned} \Delta C_{lm} &= C_{lm} - \bar{C}_{lm} \\ \Delta S_{lm} &= S_{lm} - \bar{S}_{lm} \end{aligned} \tag{A.8}$$

The resulting variability in the geoid over time is then found from these coefficients as:

$$\Delta N(\theta, \phi) = a_e \sum_{l=0}^{\infty} \sum_{m=0}^{l} \bar{P}_{lm}(cos\theta)(\Delta C_{lm} cos(m\phi) + \Delta S_{lm} sin(m\phi)) \tag{A.9}$$

The procedure of Wahr et. al. (1998) was followed to find the resulting change in surface mass expressed as equivalent water height (EWH). First, the ΔC_{lm} and ΔS_{lm} are represented in terms of the average (ρ_{ave}) and changing density ($\Delta\rho$), or:

$$\begin{aligned} \Delta C_{lm} &= \frac{3}{4\pi a_e \rho_{ave}(2l+1)} \int \Delta\rho(r,\theta,\phi)\bar{P}_{lm}(cos\theta)(\frac{r}{a})^{l+2} cos(m\phi) sin\theta d\theta d\phi dr \\ \Delta S_{lm} &= \frac{3}{4\pi a_e \rho_{ave}(2l+1)} \int \Delta\rho(r,\theta,\phi)\bar{P}_{lm}(cos\theta)(\frac{r}{a})^{l+2} sin(m\phi) sin\theta d\theta d\phi dr \end{aligned} \tag{A.10}$$

The assumption is made that the $\Delta\rho$ is concentrated near the Earth's surface in a thin layer, and the change in surface density ($\Delta\sigma$) is defined as the radial integral of $\Delta\rho$ through this layer:

$$\Delta\sigma(\theta,\phi) = \int \Delta\rho(r,\theta,\phi) dr \tag{A.11}$$

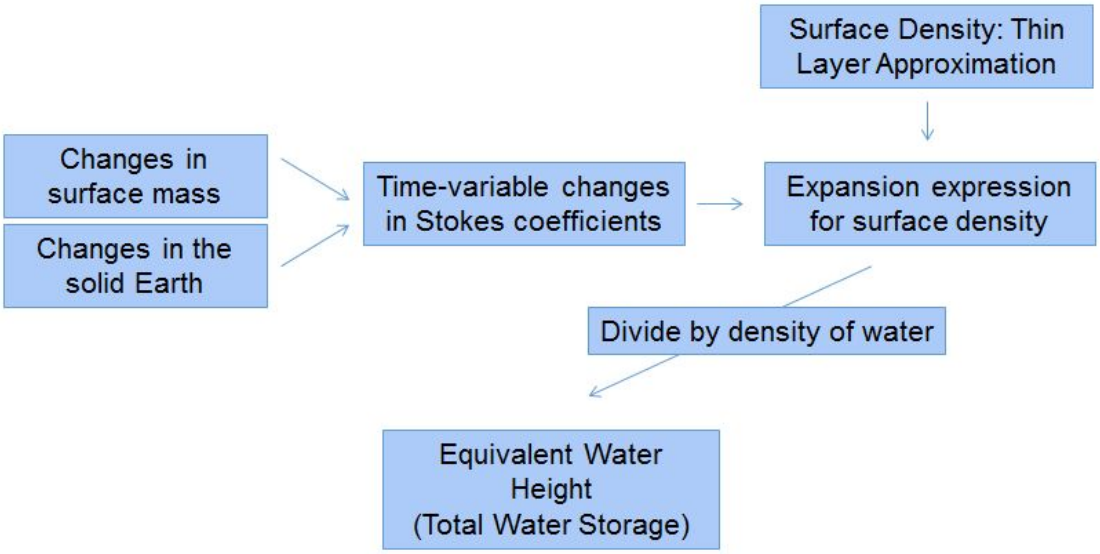

Figure A.2: Surface Mass Recovery Flow Chart

Inputting this into Equation 2.12, simplifying, and taking into account the deformations caused by the loading of the surface mass on the solid Earth results in the following expansion for $\Delta\sigma$:

$$\Delta\sigma(\theta,\phi) = a_e\rho_w \sum_{l=0}^{\infty}\sum_{m=0}^{l} \bar{P}_{lm}(cos\theta)(\Delta\hat{C}_{lm}cos(m\phi) + \Delta\hat{S}_{lm}sin(m\phi)) \quad \text{(A.12)}$$

In this expression, ρ_w represents the density of water, and $\frac{\Delta\sigma}{\rho_w}$ is the equivalent water height (EWH) statistic. The EWH represents the change in surface mass as the change in depth (height) of a thin layer of water across the surface of the Earth. The vertical water height variation found from this analysis is on the order of centimeters [2]. The new harmonic coefficients,

$\Delta\hat{C}_{lm}$ and $\Delta\hat{S}_{lm}$ used in this calculation are found as:

$$\begin{aligned}\Delta\hat{C}_{lm} &= \frac{\rho_{ave}}{3\rho_w}\frac{2l+1}{1+k_l}\Delta C_{lm} \\ \Delta\hat{S}_{lm} &= \frac{\rho_{ave}}{3\rho_w}\frac{2l+1}{1+k_l}\Delta S_{lm}\end{aligned} \tag{A.13}$$

The change in the shape of the elastic Earth is reflected in $(1+k_l)$, the Love number of degree l. These were computed as described by [34] from the numbers in Table A.2 and then numerically interpolated for the intermediate degrees.

l	k_l
0	0.000
1	0.027
2	-0.303
3	-0.194
4	-0.132
5	-0.104
6	-0.089
7	-0.081
8	-0.076
9	-0.072
10	-0.069
12	-0.064
15	-0.058
20	-0.050
30	-0.040
40	-0.033
50	-0.027
70	-0.020
100	-0.014
150	-0.010
200	-0.007

Table A.2: Elastic Love Numbers

This process is illustrated in Figure A.2. The variable Stokes coefficients and Love numbers account for time variable changes in mass and the thin layer approximation makes the connection between these time-variable gravity fields and the movement of water over the surface of the Earth. It is this resulting equivalent water height measure, $\frac{\Delta\sigma}{\rho_w}$ that is as a comparison metric between the different data products and with external models. It represents the change in the vertically integrated total water storage change both over and beneath the surface of the Earth. The six year span of monthly maps of the water height variation allow both seasonal and long-term secular variations of mass transport across the ecosystem to be mapped and analyzed.

Appendix B

List of Acronyms

Acronym	Definition
GRACE	Gravity Recovery and Climate Experiment
DA	Data Assimilation
CSR	University of Texas Center for Space Research
JPL	NASA Jet Propulsion Laboratory
GFZ	GeoForschungsZentrum
TWS	Terrestrial (Total) Water Storage
EWH	Equivalent Water Height
RSWM	Regularized Sliding Window Mascon (GRACE product)
NLDAS	North American Land Data Assimilation System
CLM	Community Land Model
WGHM	WaterGAP Global Hydrology Model
GLDAS	Global Land Data Assimilation System
DART	Data Assimilation Research Testbed
EnKF	Ensemble Kalman Filter
EAKF	Ensemble Adjustment Kalman Filter

Table B.1: Acronyms in this dissertation

Bibliography

[1] Total runoff integrating pathways (trip), April 2011.

[2] Grace tellus, 2013.

[3] J. Anderson. An ensemble adjustment kalman filter for data assimilation. *Monthly Weather Review*, 129:2884–2903, 2001.

[4] V. R. Barletta, L. S. Sorenson, and R. Forsberg. Scatter of mass changes estimates at basin scale for greenland and antarctica. *Cryosphere*, 7:1411–1432, 2013.

[5] Srinivas Bettadpur, editor. *CSR RL05*. European Geosciences Union, April 2012.

[6] Srinivas Bettadpur. *UTCSR Level-2 Processing Standards Document*. The University of Texas at Austin Center for Space Research, May 2012.

[7] Jennifer Bonin. *Improving the Observation of Time-Variable Gravity Using GRACE RL04 Data*. PhD thesis, The University of Texas at Austin, 3925 W. Braker Ln. Austin, TX 78759, August 2010.

[8] S. Bruinsma, J-M Lemoine, R. Biancale, and N. Vales. Cnes/grgs 10-day gravity field models (release 2) and their evaluation. *Advances in Space Research*, 45:587–601, October 2009.

[9] K. Case, Gerhard Kruizinga, and Sien-Chong Wu. Grace level 1b data product user handbook. Technical Report JPL D-22027, Jet Propulsion Laboratory, 2010.

[10] S. Castle and et. al. Groundwater depletion during drought threatens future water security of the colorado river basin. *Geophysical Research Letters*, 41(16):5904–5911, August 2014.

[11] A. Caya, J. Sun, and C. Snyder. A comparison between the 4dvar and the ensemble kalman filter techniques for radar data assimilation. *Monthly Weather Review*, 133:3081–3094, 2005.

[12] D. Chambers and J. Bonin. Evaluation of new grace time-variable gravity data over the ocean. *Geophysical Research Letters*, 33, 2006.

[13] D. Chambers and J. A. Bonin. Evaluation of release-05 grace time-variable gravity coefficients over the ocean. *Ocean Science*, 8(5):859–868, 2012.

[14] Don P. Chambers. Observing seasonal steric sea level variations with grace and satellite altimetry. *Journal of Geophysical Research*, 111:CO3010, March 2006.

[15] J.L. Chen, M. Rodell, C.R. Wilson, and J.S. Famiglietti. Low degree spherical harmonic influences on gravity recovery and climate experiment (grace) water storage estimates. *Geophysical Research Letters*, 32, 2005.

[16] C. Dahle and et. al. Gfz eigen-grace05s weekly gravity field time series. *GRACE science team meeting*, 2008.

[17] Christoph Dahle, editor. *The New GFZ RL05 GRACE Gravity Field Model Time Series*. European Geosciences Union, April 2012.

[18] Christoph Dahle. Gfz grace level-2 processing standards. Technical report, January 2013.

[19] P. Dirmeyer and et. al. The second global soil wetness project (gswp-2): Multi-model analysis and implications for our perception of the land surface. *Bull. Am. Meteorol. Soc.*, 87:1381–1397, 2006.

[20] Bangladesh Disaster and Emergency Response Sub-Group. Bangladesh: Monsoon floods 2004 - post-flood needs assessment summary report. reliefweb.int, October 2004.

[21] C. Dunn and et. al. Instrument of grace: Gps augments gravity measurements. *GPS World*, 14:16–28, 2003.

[22] A. Eicker, M. Schumacher, J. Kusche, P. Döll, and H. M. Schmied. Calibration/data assimilation approach for integrating grace data into the watergap global hydrology model (wghm) using an ensemble kalman filter: First results. *Surv. Geophys*, 35:1285–1309, 2014.

[23] M.H. Eisenbies, W.M. Aust, J.A. Burger, and M.B. Adams. Forest operations, extreme flooding events, and considerations for hydrologic modeling in the appalachians - a review. *Forest and Ecology Management*, 242:7–98, 2007.

[24] J. Famiglietti et. al. Satellites measure recent rates of groundwater depletion in california's central valley. *Geophysical Research Letters*, 38, 2011.

[25] J. Famiglietti. Remote sensing of terrestrial water storage, soil moisture and surface waters. *Geophysical Monograph Series*, 150:197–207, 2004.

[26] F. Flechtner, H. Dobslaw, and E. Fagiolini. Aod1b product description document for product release 05. Technical Report Rev. 4.3, GFZ German Research Centre for Geosciences, April 2015.

[27] R.H. Reichle Forman, B. and M. Rodell. Assimilation of terrestrial water storage from grace in a snow-dominated basin. *Water Recources Research*, 48(W01507), 2012.

[28] F. Frappart and et. al. Surface freshwater storage variations in the orinoco floodplains using multi-satellite observations. *Remote Sensing*, 7:89–110, 2015.

[29] H. Gao, Q. Tang, C. Ferguson, E. Wood, and D. Lettenmaier. Estimating the water budget of major us river basins via remote sensing. *International Journal of Remote Sensing*, 31, July 2010.

[30] G. Gaspari and S. Cohn. Construction of correlation functions in two and three dimensions. *Q.J.R. Meteorol. Soc.*, 125:723–757, 1999.

[31] A. Gunter. Improvement of global hydrological models using grace data. *Surv. Geophys*, 29:375–397, August 2008.

[32] B. Gunter. *Computational methods and processing strategies for estimating Earth's gravity field*. PhD thesis, The University of Texas at Austin, 3925 W. Braker Ln. Austin, TX 78759, 2004.

[33] T. M. Hamill. Interpretation of rank histograms for verifying ensemble forecasts. *Monthly Weather Review*, 129:550–560, August 2000.

[34] D. Han and J. Wahr. The viscoelastic relaxation of a realistically stratified earth, and a further analysis of post-glacial rebound. *Geophys. J. Int.*, 120:287–311, 1995.

[35] S.-C. Han, R. D. Ray, and S. B. Luthcke. One cemtimeter-level observations of diurnal ocean tides from global monthly mean time-variable gravity fields. *Journal of Geodesy*, 84:715–729, 2010.

[36] R. Houburg and et. al. Drought indicators based on model-assimilated gravity recovery and climate experiment (grace) terrestrial water storage observations. *Water Recources Research*, 48(7), July 2012.

[37] C. Jekeli. Alternative methods to smooth the earth's gravity field. Technical Report Report No. 327, Ohio State University, 1981.

[38] E. Kalnay, M. Kanamitsu, R. Kistler, W. Collins, D. Deaven, L. Gandin, M. Iredell, S. Saha, G. White, J. Woollen, Y. Zhu, A. Leetma, R. Reynolds, M. Chelliah, W. Ebisuzaki, W.Higgins, J. Janowiak, K. C. Mo, C. Ropelewski, J. Wang, R. Jenne, and D. Joseph. The ncep/ncar 40-year reanalysis project. *Bullet. Amer. Meteorol. Soc.*, 77, 1996.

[39] W. M. Kaula. *Theory of Satellite Geodesy.* Dover Publications, Inc., 1966.

[40] J-R Kim. *Simulation of a low-low satellite-to-satellite tracking mission.* PhD thesis, The University of Texas at Austin, 3925 W. Braker Ln. Austin, TX 78759, 2000.

[41] S. Klosko, D. Rowlands, S. Luthcke, F. Lemoine, D. Chinn, and M. Rodell. Evaluation and validation of mascon recovery using grace kbrr data with independent mass flux estimates in the mississippi basin. *J Geod*, 83:817–827, January 2009.

[42] E. Kurtenbach, A. Eicker, T. Mayer-Gürr, M. Holschneider, M. Hayn, M. Fuhrmann, and J. Kusche. Improved daily grace gravity field solutions using a kalman smoother,. *Journal of Geodynamics*, 59:39–48, 2012.

[43] J. Kusche. Approximate decorrelation and non-isotropic smoothing of time-variable grace-type gravity field models. *J Geod*, 81:733–739, February 2007.

[44] J. Kusche, R. Schmidt, S. Petrovic, and R. Rietbroek. Decorrelated grace time-variable gravity solutions by gfz, and their validation using a hydrological model. *J Geod*, 83:903–913, March 2009.

[45] F. Landerer and S. Swenson. Accuracy of scaled grace terrestrial water storage estimates. *Water Resources Research*, 48, 2012.

[46] D. Long and et. al. Grace satellite monitoring of large depletion in water storage in response to the 2011 drought in texas. *Geophysical Research Letters*, 40(13):3395–3401, July 2013.

[47] S. Luthcke and et. al. Recent glacier mass changes in the gulf of alaska region from grace mascon solutions. *Journal of Glaciology*, 54(188):767–777, 2008.

[48] F. Lyard and F. Lefvre. Modelling the global ocean tides: a modern insight from fes2004. *Ocean Dynamics*, 56:394–415, 2006.

[49] C. McCullough. Window functions for grace. Technical report, The University of Texas at Austin, 2013.

[50] C. McCullough, S. Bettadpur, and C. McDonald. Numerical accuracy of satellite orbit determination for grace and future geodetic missions. 2015.

[51] N.H. McIntyre, H. Lee, and H. Wheater. Ensemble predictions of runoff in ungauged catchments. *Water Resources Research*, 41:W12434, December 2005.

[52] K. Mitchell and et. al. The multi-institution north american land data assimilation system (nldas): Utilizing multiple gcip products and partners in a continental distributed hydrological modeling system. *Journal of Geophysical Research*, 109(D07S90), 2004.

[53] C. Montzka and et. al. Multivariate and multiscale data assimilation in terrestrial systems: A review. *Sensors*, 12:16291–16333, 2012.

[54] NCAR. The community earth system model, 2014.

[55] NCAR. The data assimilation research testbed, 2014.

[56] Government of Canada. Environment canada, June 2013.

[57] K. Oleson and et. al. Technical description of version 4.0 of the community land model (clm). Technical Report 478, National Center for Atmospheric Research, April 2010.

[58] S. Potempski, S. Galmarini, A. Riccio, and G. Giunta. Bayesian model averaging for emergency response atmospheric dispersion multimodel ensembles. *Journal of Geophysical Research*, 115:D21309, November 2010.

[59] K. Raeder, J. Anderson, N. Collins, T. Hoar, J. Kay, P. Lauritzen, and R. Pincus. Dart/cam: An ensemble data assimilation system for cesm atmospheric modesl. *J. Climate*, 25:6304–6317, 2012.

[60] G. Ramillien, J.S. Famiglietti, and J. Wahr. Detection of continental hydrology and glaciology signals from grace: A review. *Surv. Geophys*, 29:361–374, 2008.

[61] R. Ray. A global ocean tide model from topex/poseidon altimetry: Got99.2. Technical Report 209478, NASA, 1999.

[62] H.J. Rim. *TOPEX orbit determination using GPS tracking system.* PhD thesis, The University of Texas at Austin, 1992.

[63] M. Rodell, P.R. Houser, and et. al. The global land data assimilation system. *American Meteorology Society*, 277:381–394, June 2003.

[64] D. Rowlands and et. al. Global mass flux solutions from grace: A comparison of parameter estimation strategies - mass concentrations versus stokes coefficients. *Journal of Geophysical Research*, 115(B01403), 2010.

[65] H. Save. *Using Regularization for Error Reduction in GRACE Gravity Estimation*. PhD thesis, The University of Texas at Austin, 3925 W. Braker Ln. Austin, TX 78759, 2009.

[66] H. Save and S. Bettadpur. Inversion of grace range-rate data into equal area mass grids using tikhonov regularization. American Geophysical Union, 2014.

[67] H. Save, S. Bettadpur, and B. Tapley. Reducing errors in the grace gravity solutions using regularization. *Journal of Geodesy*, 86:695–711, March 2012.

[68] S. Bettadpur Save, H. Evaluation of global equal-area mass grid solutions from grace. European Geosciences Union, 2015.

[69] R. Schmidt, S. Petrovic, A. Guntner, F. Barthelmes, J. Wunsch, and J. Kusche. Periodic components of water storage changes from grace and global hydrology models. *Journal of Geophysical Research*, 113, August 2008.

[70] A. Shepherd, K. Briggs, D. Bromwich, René Forsberg, N. Galin, M. Horwath, S. Jacobs, I. Joughin, M. King, J. Lenaerts, J. Li, S. Ligtenberg, A. Luckman, S. Luthcke, M. McMillan, R. Meister, G. Milne, J. Mouginot, A. Muir, J. Nicolas, J. Paden, A. Payne, H. Pritchard, E. Rig-

not, H. Rott, L. Sandberg Sørensen, T. Scambos, B. Scheuchl, E. J. O. Schrama, B. Smith, A. V. Sundal, J. H. van Angelen, W. J. van de Berg, M. R. van den Broeke, D. G. Vaughan, I. Velicogna, J. Wahr, P. L. Whitehouse, D. J. Wingham, D. Yi, D. Young, and H. Zwally. A reconciled estimate of ice-sheet mass balance. *Science*, 338(6111):1183–1189, 2012.

[71] R. Shumway and D. Stoffer. *Time series analysis and its applications*. Springer, 2000.

[72] M. Steckler and et. al. Modeling earth deformation from monsoonal flooding in bangladesh using hydrographic, gps, and gravity recovery and climate experiment (grace) data. *Geophysical Research Letters*, 115(B08407), 2010.

[73] G. Stephens and et. al. Dreary state of precipitation in global models. *Journal of Geophysical Research*, 115(D24211), 2010.

[74] H. Su and et. al. Multisensor snow data assimilation at the continental scale: The value of gravity recovery and climate experiment terrestrial water storag information. *Journal of Geophysical Research*, 115(D10), May 2010.

[75] S. Swenson and J. Wahr. Methods for inferring regional surface-mass anomalies from gravity recovery and climate experiment (grace) measurements of time-variable gravity. *Journal of Geophysical Research*, 107, September 2002.

[76] S. Swenson and J. Wahr. Post-processing removal of correlated errors in the grace data. *Geophysical Research Letters*, 33, April 2006.

[77] S. Swenson, J. Wahr, and P.C.D Milly. Estimated accuracies of regional water storage variations inferred from the gravity recovery and climate experiment (grace). *Water Recources Research*, 39, August 2003.

[78] Richard Swinbank, editor. *Data Assimilation for the Earth System*, volume 26 of *NATO Science Series*. Kluwer Academic Publishers, 2002.

[79] B. Tapley, S. Bettadpur, and J. Ries. The gravity recovery and climate experiment: Mission overview and early results. *Geophysical Research Letters*, 31, 2004.

[80] B. Tapley, S. Bettadpur, J. Ries, P. Thompson, and M. Watkins. Grace measurements of mass variability in the earth system. *Science*, 305:503–505, 2004.

[81] B. Tapley, B. Schutz, and G. Born. *Statistical Orbit Determination*. Elsevier Academic Press, 2004.

[82] J. B. Thomas. An analysis of gravity-field estimation based on intersatellite dual-1-way biased ranging. Technical Report 98-15, Jet Propulsion Laboratory, 1998.

[83] V.M. Tiwari, J. Wahr, and S. Swenson. Dwindling groundwater resources in northern india, from satellite gravity observations. *Geophysical Research Letters*, 36, September 2009.

[84] P. Touboul and et. al. Accelerometers for champ, grace and goce space missions: synergy and evolution. *Boll Geof Teor Appl*, 40:321–327, 1999.

[85] P. Tregoning, K. Lambeck, and G. Ramillien. Grace estimates of sea surface height anomalies in the gulf of carpentaria. *Earth and Planetary Science Letters*, 271:241–244, July 2008.

[86] USGS. Groundwater atlas of the united states, 2015.

[87] I. Velicogna. Increasing rates of ice mass loss from the greenland and antarctic ice sheets revealed by grace. *Geophysical Research Letters*, 36(L19503), 2009.

[88] F. Vivier and C. Provost. Direct velocity measurements in the malvinas current. *Journal of Geophysical Research*, 104:21083–21103, 1999.

[89] J. Wahr and M. Molenaar. Time variability of the earth's gravity field: Hydrological and oceanic effects and their possible detection using grace. *Journal of Geophysical Research*, 103:30,205–30,229, December 1998.

[90] J. Wahr, S. Swenson, and I. Velicogna. Accuracy of grace mass estimates. *Geophysical Research Letters*, 33(6), March 2006.

[91] F. Wang. Grace simulation noise models. Technical report, The Center for Space Research, The University of Texas at Austin, 2013.

[92] M. Watkins. JPL Level-2 Processing Standards Document. Technical report, May 2012.

[93] S. Werth, A. Guntner, S. Petrovic, and R. Schmidt. Integration of grace mass variations into a global hydrological model. *Earth and Planetary Sciences*, pages 166–173, October 2008.

[94] T. Yokohata, J. D. Annan, M. Collins, C. Jackson, M. Tobis, M. Webb, and J. Hargreaves. Reliability of multi-model and structurally different single-model ensembles. *Climate Dynamics*, 39:599–616, August 2012.

[95] B. Zaitchik, M. Rodell, and R. Reichle. Assimilation of grace terrestrial water storage data into a land surface model: Results for the mississippi river basin. *Journal of Hydrometeorology*, 9:535–548, 2008.

[96] Y.-F. Zhang, T. Hoar, Z.-L. Yang, J. Anderson, A. Toure, and M. Rodell. Assimilation of modis snow cover through the data assimilation research testbed and the community land model version 4. *Journal of Geophysical Research*, 119(12):7091–7103, 2014.

[97] M. Zupanski, S. J. Fletcher, I. M. Navon, B. Uzunoglu, R. P. Heikes, D. A. Randall, T. D. Ringler, and D. Daescu. Initiation of ensemble data assimilation. *TELLUS*, 58A:159–170, 2006.